Universidad Autónoma de Madrid

Facultad de Medicina

Departamento de Bioquímica

Mitochondrial respiration fuels adaptive immune responses: from immune synapse formation to T cell differentiation

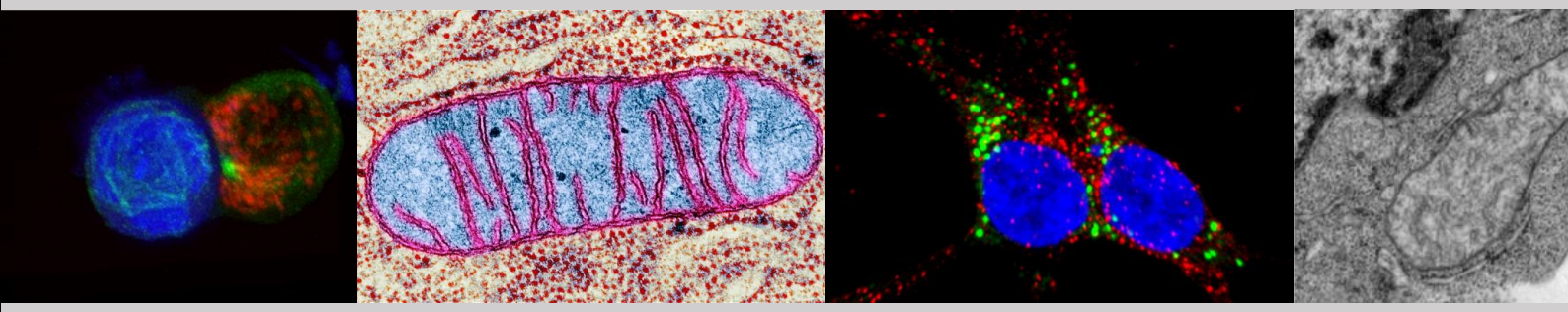

Tesis doctoral

Francesc Baixauli Celda

Madrid, 2016

Universidad Autónoma de Madrid

Facultad de Medicina

Departamento de Bioquímica

Mitochondrial respiration fuels adaptive immune responses: from immune synapse formation to T cell differentiation

Tesis doctoral

Francesc Baixauli Celda

Madrid, 2016

Departamento de Bioquímica

Facultad de Medicina

Universidad Autónoma de Madrid

Mitochondrial respiration fuels adaptive immune responses: from immune synapse formation to T cell differentiation

Memoria presentada por el licenciado en Bioquímica:

Francesc Baixauli Celda

para optar al título de Doctor por la Universidad Autónoma de Madrid

Directores de Tesis:

Dr. Francisco Sánchez Madrid

Dra. María Mittelbrunn Herrero

Este trabajo ha sido realizado en el laboratorio de Comunicación intercelular, en el Centro Nacional de Investigaciones Cardiovasculares (CNIC)

Madrid, 2016

Francisco Sánchez Madrid, Doctor en Ciencias Biológicas y Catedrático de Inmunología de la Universidad Autónoma de Madrid, y Maria Mittelbrunn Herrero, Doctora en Ciencias Biológicas,

CERTIFICAN:

Que Francesc Baixauli Celda, Licenciado en Bioquímica por la Universitat de València, ha realizado bajo nuestra dirección el trabajo de investigación correspondiente a su Tesis Doctoral con el título: **Mitochondrial respiration fuels adaptive immune responses: from immune synapse formation to T cell differentiation.**

Revisado este trabajo, los que suscriben consideran el trabajo realizado satisfactorio y autorizan su presentación para ser evaluado por el tribunal correspondiente.

Y para que así conste y a los efectos oportunos, firmamos el presente certificado en Madrid a 15 de Febrero de 2016

Vº Bº directores

Prof. Francisco Sánchez-Madrid **Dra. Maria Mittelbrunn Herrero**

This work has been performed at the Prof. Francisco Sánchez-Madrid's laboratory in the Hospital Universitario de la Princesa and Centro Nacional de Investigaciones Cardiovasculares (CNIC) in Madrid. This study was funded by grants SAF 2008-02635, SAF2011-25834 and ERC-2011-AdG 294340-GENTRIS to Francisco-Sánchez-Madrid and by Contrato de Investigadores SNS Miguel Servet I (CP14/00219 and MS14/00219) from the Instituto de Salud Carlos III to Maria Mittelbrunn. Francesc Baixauli was supported by a PhD fellowship from the Spanish Ministry of Economy and Competitiveness (FPI Program, BES-2007-14884) and ERC-2011-AdG 294340-GENTRIS.

A la meua familia; Fina, Violeta i Andrea,

i al meu pare,

que el seu record sempre m'acompanya

Summary

Summary

Defense against pathogenic microorganisms requires extensive communication between cells of the innate and adaptive immune system. T cell recognition of an antigen in the surface of an antigen-presenting cell (APC) leads to the formation of a specialized membrane-based structure at the interface of the APC and the T lymphocyte that favor transient cell-cell communication. This molecular assembly, termed immune synapse (IS) is a highly dynamic structure where polarized macromolecular components such as T cell receptors, adhesion molecules, cytoskeletal components and related organelles, orchestrate the early events of T cell activation. Following IS formation and T cell activation, T cells undergo a process of rapid clonal expansion and differentiation that give rise to the different types of effector and memory T cells. Immune signals and key metabolic cues present in the inflammatory milieu drive the expression of 'lineage-specific' transcription factors that ultimately guide the development of the different effector T cell subsets, which produce a specific repertoire of cytokines that determine the nature of the immune response and avoid autoimmune diseases.

In this work, we have addressed the role of mitochondria in the regulation of adaptive immune responses. Our results uncover a fundamental role of mitochondria in almost every step of T cell function, starting with the control of IS organization and early TCR signaling to T cell differentiation, cytokine production and regulation of the outcome of immune responses. By regulating IS organization and the balance between OXPHOS and glycolysis, mitochondria provide a metabolic context appropriate for efficient regulation of inflammatory responses. In addition, we demonstrate a functional crosstalk of mitochondria and the biogenesis and function of endolysosomal compartment, linking for the first time mitochondrial deficiencies with lysosomal storage disorders.

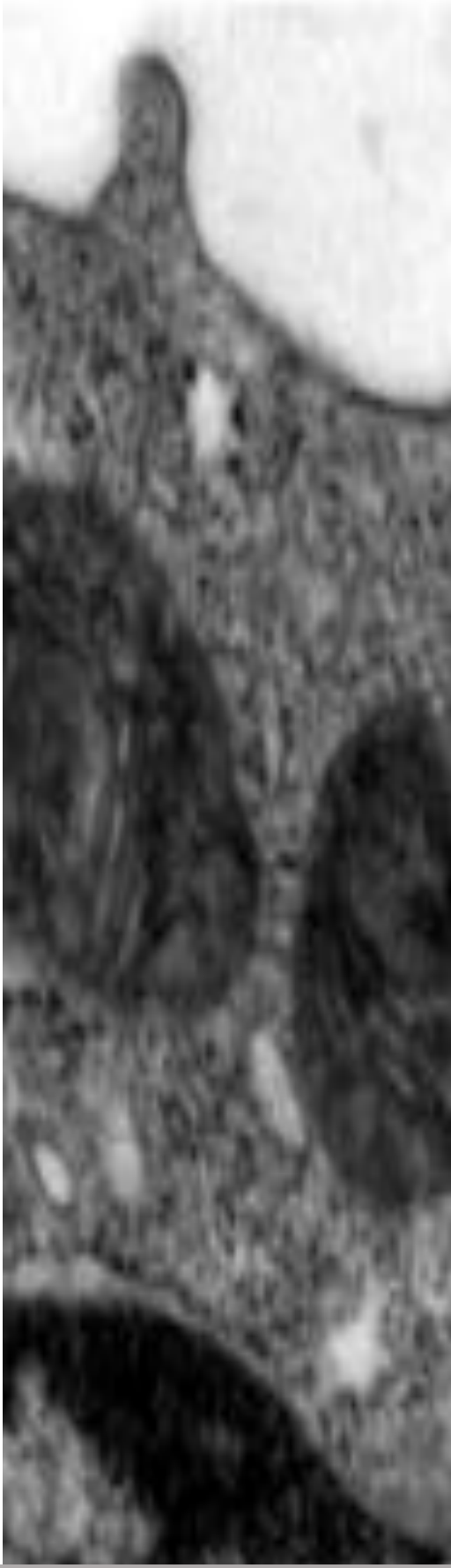

Resumen

Resumen

La defensa contra los microorganismos patógenos requiere una amplia comunicación entre las células del sistema inmune innato y adaptativo. El reconocimiento por parte de las células T de un antígeno en la superficie de una célula presentadora de antígeno promueve la formación de una estructura altamente especializada que favorece la comunicación transitoria célula-célula. Este conjunto, denominado sinapsis inmune, es una estructura altamente dinámica donde se polarizan diversos componentes macromoleculares; como los receptores de células T (TCR), moléculas de adhesión, componentes del citoesqueleto y orgánulos contiguos, orquestando así los primeros acontecimientos de la activación de la célula T. Posteriormente a la formación de la sinapsis inmune y la activación de las células T, estas experimentan un proceso de rápida expansión clonal y diferenciación, dando lugar a los diferentes tipos de células T efectoras y de memoria. Las distintas señales inmunes y metabólicas presentes en el nicho inflamatorio promueven la expresión de factores de transcripción específicos de los diferentes linajes celulares Estos factores de transcripción guían el desarrollo de los diferentes subconjuntos de células T efectoras, productoras de un repertorio de citoquinas que determinan la naturaleza de la respuesta inmune y evitan la aparición de enfermedades autoinmunes.

En este trabajo hemos abordado el papel de la mitocondria en la regulación de la respuesta inmune adaptativa. Nuestros resultados revelan un papel fundamental de las mitocondrias en casi todos los pasos de la función de las células T, comenzando con el control de la organización de la sinapsis inmune y la señalización temprana del TCR, hasta su diferenciación, la producción de citoquinas y el control final de la respuesta inmune. Mediante la regulación de la sinapsis inmune y del balance entre la fosforilación oxidativa y la glicólisis, las mitocondrias proporcionan un contexto metabólico adecuado para la regulación eficaz de la respuesta inflamatoria. Además, demostramos la existencia de una comunicación funcional entre las mitocondrias y la biogénesis y función del compartimento endolisosomal, relacionando por primera vez deficiencias mitocondriales con los trastornos de depósito lisosomal.

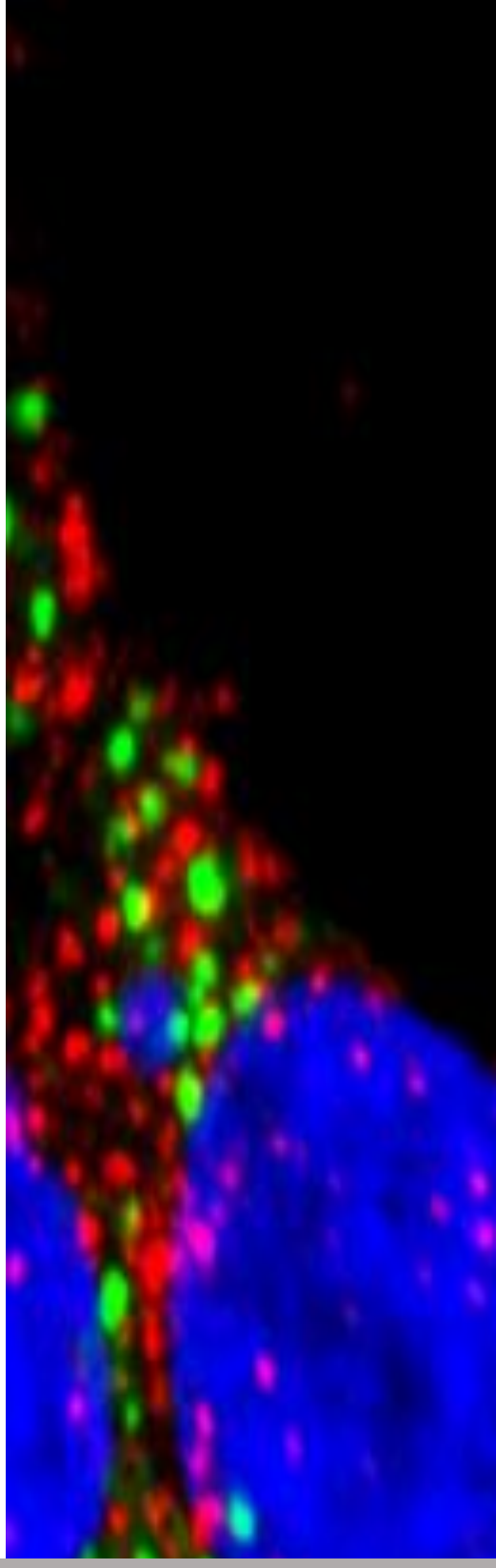

Index

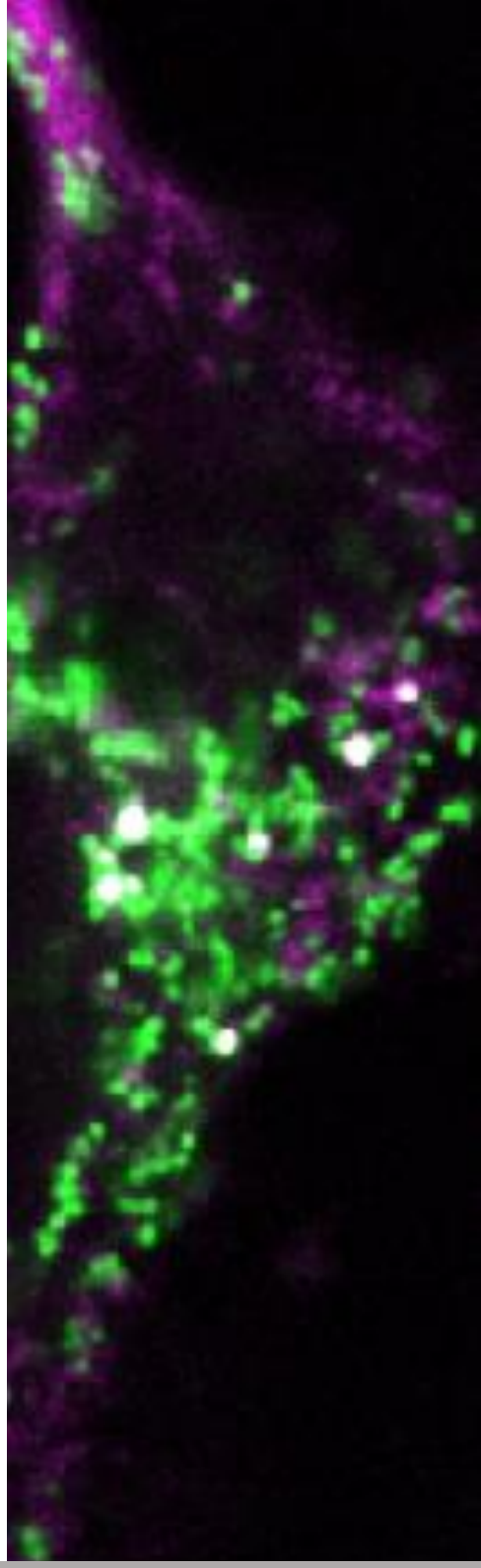

Abbreviations

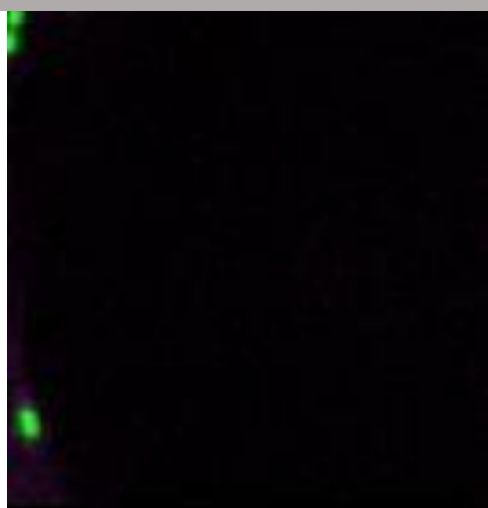

List of Abbreviations

Ab	antibody
Acacb	acetyl-CoA carboxylase 2, beta
ADPGK	ADP-dependent glucokinase
AKT	RAC-alpha serine-threonine-protein kinase, protein kinase B
AMP	adenosine monophosphate
AMPK	AMP-activated protein kinase
AP-1	activator protein 1
APC	antigen presenting cell
ASM	acid sphingomyelinase
ATAD-3	ATPase family AAA domain-containing protein 3
ATP	adenosine triphosphate
ATP6V0	ATPase, H+ transporting, lysosomal 16kDa, V0 subunit c
Bcl-xL	B-cell lymphoma-extra large
BNGE	blue native gel electrophoresis
C/EBP	CCAAT/enhancer binding protein
Ca2+	calcium
CD25	IL-2Ralpha
CD69	very early activation antigen
CH7C17	HA-specific, Vb3+ Jurkat T cell clone
CHS	contact hypersensitive response
CI	mitochondrial complex I
CLEAR	coordinated lysosomal expression and regulation
CMA	chaperone-mediated autophagy
CMAC	7-amino-4-chloromethylcoumarin
Myc	Myc protooncogene transcription factor
ConA	concanavalin A
Core 1	cytochrome b-c1 complex subunit 1, mitochondrial
CRAC/ORAI1	calcium release-activated calcium channel protein 1

cSMAC	central supramolecular activation complex
CtsB	cathepsin B
Cyp4a10	cytochrome P450, family 4, subfamily a, polypeptide 10
CytC	cytochrome C
DCA	dichloroacetate
DCFDA	2',7' –dichlorofluorescin diacetate
DGK	diacylglycerol kinases
DMSO	dimethyl sulfoxide
DNA	deoxyribonucleic acid
DP	double positive
Drp1	dynamin related protein-1
DSS	dextran sodium sulfate
EAE	experimental autoimmune encephalomyelitis
ECAR	extracellular acidification rate
EDTA	ethylenediaminetetraacetic acid
EEA1	early endosome antigen 1
ER	endoplasmic reticulum
ERMs	ezrin-radixin-moesin
ERRα	estrogen-related receptor α
ESCRT	endosomal sorting complexes required for transport
ETC	electron transport chain
EVs	extracellular vesicles
FABP3	fatty acid binding protein 3
FADH2	flavin adenine dinucleotide
FAO	fatty acid oxidation
FAs	fatty acids
FBS	fetal bovine serum
FCCP	fluoro-carbonyl cyanide phenylhydrazone
FIS1	mitochondrial fission 1 protein
FN	fibronectin
Foxp3	forkhead box P3 transcription factor
FpSDH	succinate dehydrogenase [ubiquinone] flavoprotein subunit

GA	Golgi apparatus
GFP	green fluorescent protein
GPD	glycerol-3-phosphate dehydrogenase
GPI	glycosylphosphatidylinisotol
H58	Hoechst 58
HA	influenza hemagglutinin peptide
HBSS	Hanks' balanced salt solution
Hepes	4-(2-hydroxyethyl)-1-piperazineethanesulfonic acid
HIF-1	hypoxia inducible factor-1
HIV-1	human immunodeficiency virus
ICAM-1	intercellular adhesion molecule-1
IFN-γ	interferon-gamma
IL-1β	interleukin-1 beta
IL-6R	interleukin-6 receptor
ILN	inguinal lymph node
ILVs	intraluminal vesicles
IMM	inner mitochondrial membrane
IS	immune synapse
J77	Vb8+ Jurkat T cell clone
JC-1	5,5’,6,6‘-tetrachloro-1,1’,3,3‘-tetraethylbenzimidazolcarbocyanine iodide
LAMP	lysosome associated membrane protein
LBPA	lysobiphosphatidic acid
LSDs	lysosomal storage diseases
m.f.i.	mean fluorescence intensity
mdivi-1	mitochondrial division inhibitor 1
MDVs	mitochondrial derived vesicles
MFF	mitochondrial fission factor
Mfn	mitofusin
MID49	mitochondrial dynamic protein of 49 kDa
MID51	mitochondrial dynamic protein of 51 kDa
miRNA	microRNA; small non-coding RNA
Miro	mitochondrial Rho-like GTPase

MLC	myosin light chain
MLN	mesenteric lymph node
MnSOD	manganese superoxide dismutase
mRNA	messenger RNA
mROS	mitochondrial reactive oxygen species
mtCO1	mitochondrial cytochrome c oxidase subunit 1
mtDNA	mitochondrial DNA
mtND1	mitochondrial-encoded NADH dehydrogenase 1
mtND6	mitochondrial-encoded NADH dehydrogenase 6
MTOC	microtubule-organizing center
mTOR	mammalian target of rapamycin
MTSSB	mitochondrial single-stranded DNA-binding protein
MVB	multivesicular bodies
NAC	N-acetylcysteine
NADH	nicotine adenine dinucleotide
NADPH	nicotinamide adenine dinucleotide phosphate
NAM	nicotinamide
NDUFA9	NADH dehydrogenase (Ubiquinone) 1 alpha subcomplex, 9,
NF-κB	nuclear factor kappa-light-chain-enhancer of activated B cells
NPA	Niemann Pick disease type A
nSMase2	neutral sphingomyelinase 2
NTA	nanoparticle tracking analysis
OCR	oxygen consumption rate
OMM	outer mitochondrial membrane
Opa1	optic atrophy 1
Oxazolone	4-Ethoxymethylene-2-phenyl-2-oxazolin-5-one
OXPHOS	oxidative phosphorylation
PI3K	phosphoinositide 3-kinase
P2X	purinergic receptors
PDH	pyruvate dehydrogenase
PDHK1	pyruvate dehydrogenase kinase-1
PGC1-α	peroxisome proliferator-activated receptor gamma coactivator 1-alpha

PHA	phytohemagglutinin
PLL	poly-L-lysine
PMA	phorbol-12-myristate-13-acetate
pMLC	phospho-myosin light chain
POLGA	mitochondrial DNA polymerase gamma A
POLGB	mitochondrial DNA polymerase gamma B
PPP	pentose phosphate pathway
pSMAC	peripheral supramolecular activation complex
R5P	ribose-5-phosphate
RFP	red fluorescent protein
RNA	ribonucleic acid
RORγT	RAR-related orphan receptor gamma T
ROS	reactive oxygen species
rRNA	ribosomal RNA
SDH	succinate dehydrogenase
SEE	*Staphylococcus enterotoxin* E
SEM	standard error of the mean
shRNA	small hairpin RNA
SM	sphingomyelin
SP	single positive
TAGs	triacylglycerides
T-bet	T-box transcription factor TBX21
TCA	tricarboxylic acid cycle
TCR	T cell receptor
Teff	effector T cell, activated T cell
TFAM	mitochondrial transcription factor A
***Tfam*$^{-/-}$**	CD4Cre+/-Tfamfl/fl, CD4 specific Tfam flox mice
TFBM	mitochondrial transcription factor B
TFEB	transcription factor EB
Th	helper T cell
Th1	T helper 1
TIRFM	total internal reflection fluorescence microscopy

TLR4	toll-like receptor 4
TLR9	toll-like receptor 9
Tm	memory T cell
TMRM	tetramethylrhodamine methyl ester
Tn	naive T cell
Tom20	translocase of outer mitochondrial membranes 20 kDa
Treg	regulatory T cell
tRNA	transfer RNA
TSG101	tumor susceptibility gene 101
Uqcrfs1	ubiquinol-cytochrome c reductase
VS	virological synapse
WB	western blot
WT	wild-type
α-KG	alpha-ketoglutarate
Δψm	mitochondrial membrane potential

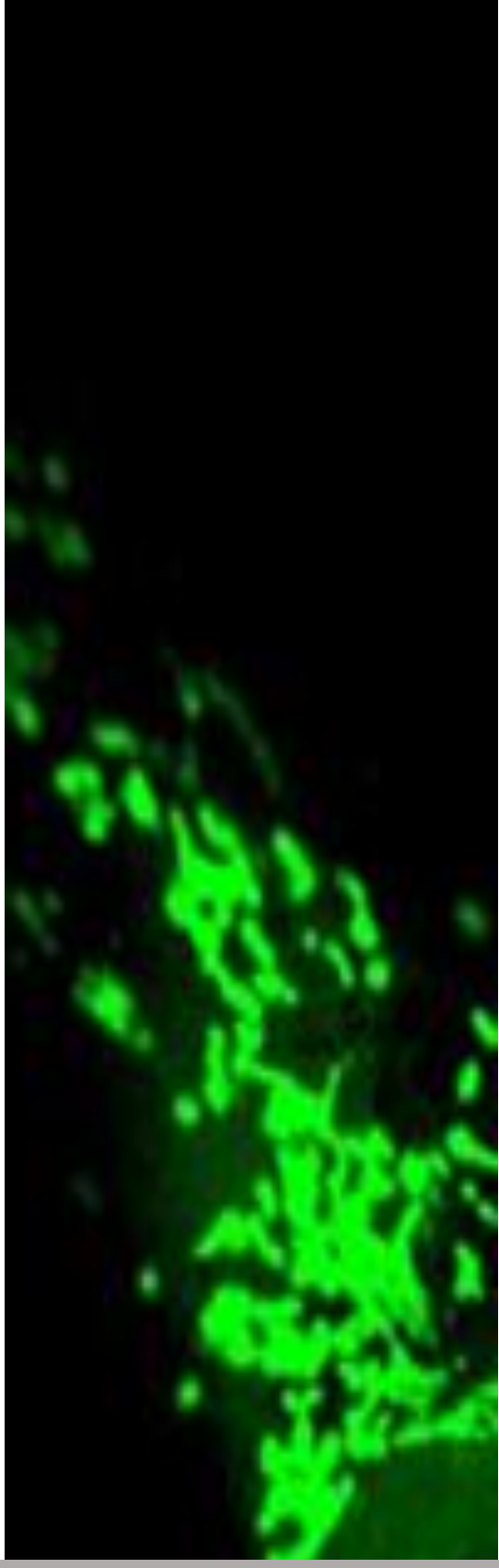

List of Figures

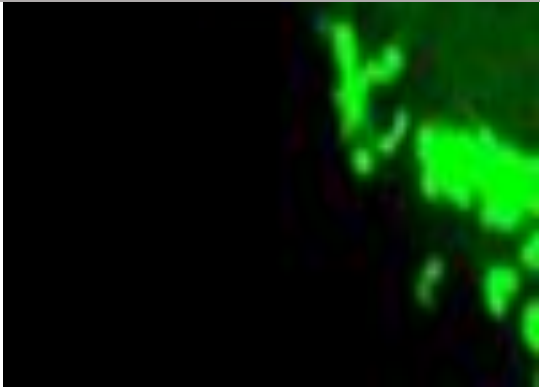

Introduction

Results

Discussion

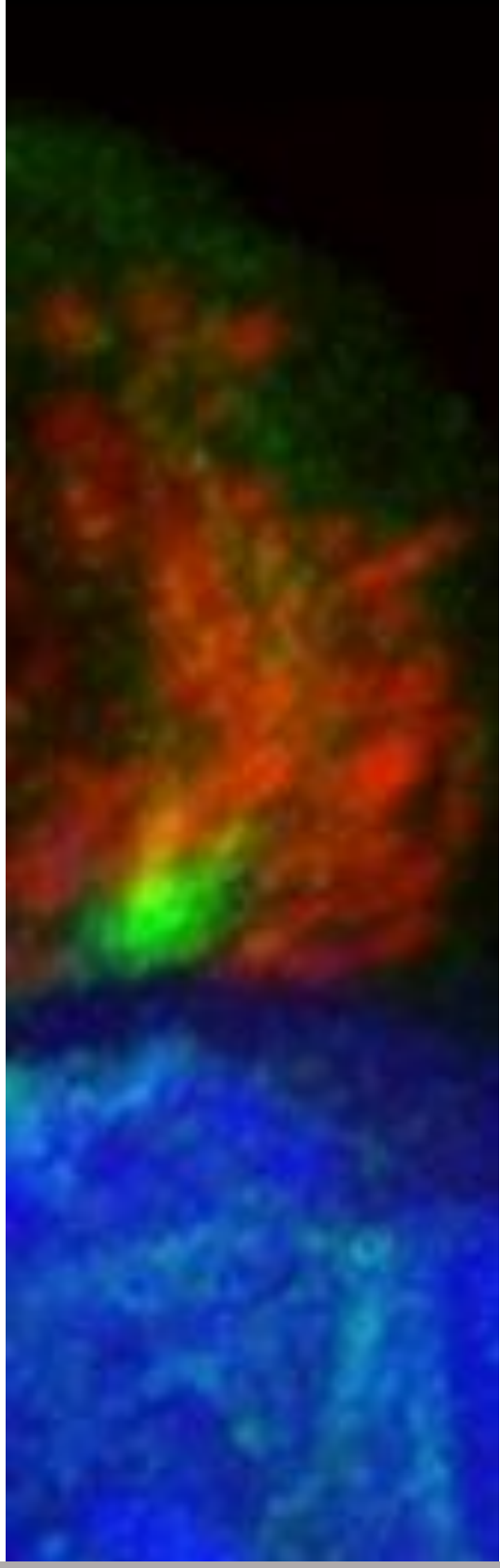

Introduction

1. Introduction

Organelles are a distinguishing feature of eukaryotic cells. Among them, mitochondria are exceptional organelles that maintain features of their ancestral origin besides the billion years of endosymbiotic co-evolution. Mitochondria contain their own genome and maintain an electrochemical gradient that empowers organelle functions and sustains cell homeostasis. More importantly, mitochondria turned out to be central hubs of the signaling cascades that sense situations of cellular stress, inflammation and cell death (Galluzzi et al., 2012).

Mitochondria are multifunctional organelles that regulate many cell processes, including calcium signaling, apoptosis and cell metabolism. A key function of mitochondria is the control of ATP production through oxidative phosphorylation (OXPHOS), the tricarboxylic acid cycle (TCA), and fatty acid ß-oxidation (FAO); however, mitochondria also modulate amino acid metabolism and supply metabolic intermediates needed to sustain cell growth, proliferation and differentiation (Friedman and Nunnari, 2014; McBride et al., 2006). Defects in mitochondrial homeostasis are closely linked to the development of cancer, inflammation, neurodegenerative diseases and metabolic disorders (Taylor and Turnbull, 2005), and are also a hallmark of aging (Lopez-Otin et al., 2013). However, the molecular mechanisms by which mitochondria contribute to human diseases remain far from being resolved.

1.1 Mitochondria: form and function

Mitochondria are double-membrane organelles consisting of an outer membrane surrounding an inner membrane of greater surface area. The space between the two membranes is termed the intermembrane space. Because of its greater surface area, the inner mitochondrial membrane (IMM) folds back on itself, creating compartments termed cristae. These cristae membranes concentrate the oxidative phosphorylation respiratory chain complexes, whereas the smooth mitochondrial outer membrane (OMM) encapsulates the inner membrane and an intermembrane space (Figure I1a). Functioning together with the Krebs' cycle in the mitochondrial matrix, the complexes I, III and IV of the respiratory chain pump protons from the matrix to the intermembrane space through the coupled transfer of electrons to oxygen. The electrochemical gradient generated across the inner membrane is used to power ATP production by complex V (ATP synthase) in a process referred as oxidative phosphorylation (OXPHOS). Then, the ATP–ADP translocase exports the ATP into the intermembrane space, where it freely diffuses out of the outer membrane into the cytosol for fueling cellular processes (Figure I1b). The electrochemical potential is used for additional crucial mitochondrial functions, such as

buffering the signaling ion calcium (Ca^{2+}) through uptake by a uniporter in the inner membrane. Interestingly, a reduction in the electrochemical potential has evolved as a read-out for mitochondrial functional status, which creates signals to activate pathways that repair and/or eliminate defective mitochondria (Galluzzi et al., 2012).

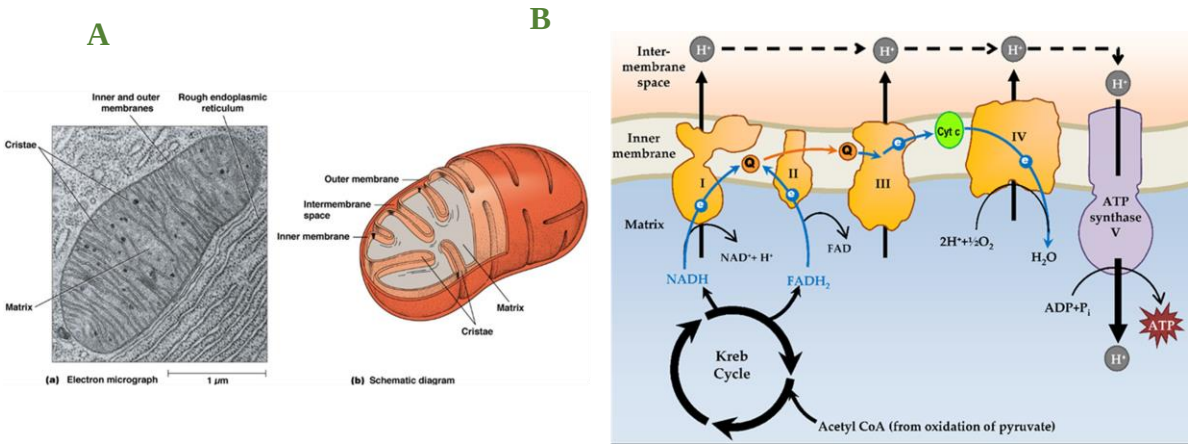

Figure I1

(A) Electron microscopy image and representation of mitochondrial compartments. (B) The transfer of electrons through the electron transport chain (ETC) is used to pump protons (H^+) from the mitochondrial matrix into the intermembrane space, creating an electrochemical proton gradient across the IMM called mitochondrial membrane potential ($\Delta\Psi$). The $\Delta\Psi$ allows ATP synthase (complex V) to use the flow of H^+ through the enzyme back into the matrix to generate ATP from ADP and inorganic phosphate. Complex I (NADH coenzyme Q reductase) accepts electrons from the Krebs cycle electron carrier NADH, and passes them to coenzyme Q (ubiquinone), which also receives electrons from complex II (succinate dehydrogenase). Ubiquinone passes electrons to complex III (cytochrome bc_1 complex), which passes them to cytochrome *c* (cyt *c*). Cyt *c* passes electrons to Complex IV (cytochrome *c* oxidase), which uses the electrons and hydrogen ions to reduce molecular oxygen to water.

Mitochondria are metabolic hubs within the cell that alter their function to meet cellular needs. This implies that mitochondria receive signals to change their function, but more importantly, accumulating evidence suggests that mitochondrial pathways provide signals back to the nucleus creating a crosstalk that integrate cell-fate decisions such as metabolic adaptation, proliferation, differentiation and cell death with metabolic capacity dependent on the cellular environment (Weinberg et al., 2015). Recent studies emphasize how mitochondrial activity, shape and localization appear as direct players in cell differentiation and developmental processes by

regulating signaling pathways such as the Notch or the Nf-kB pathways or the antiviral innate immune response (Kasahara and Scorrano, 2014).

Several signal transduction mechanisms between mitochondria and the rest of the cell have been described. Anterograde signaling is the signal transduction from the cytosol to mitochondria. The best known example is the entrance of calcium into mitochondrial matrix upon elevations on cytosolic calcium concentrations (Rizzuto et al., 2012), which results in activation of multiple enzymes of the TCA cycle and the electron transport chain (ETC). The retrograde signaling is the signal transduction from mitochondria to the cytosol. Mitochondrial products such as mitochondrial ROS (mROS) regulate the activation of the hypoxia-inducible factor (HIF-1) (Chandel et al., 1998), whereas superoxide can induce thiol oxidation of proteins and modify their function (Murphy, 2009). Mitochondria can also impact signaling by altering the availability of TCA cycle intermediates such as acetyl-CoA, succinate, fumarate, and a-ketoglutarate, which modify and alter protein function or act as important signaling molecules (Boland et al., 2013; Buck et al., 2015) (Figure I2). In addition, mitochondrial bioenergetics status can also influence signaling pathways. The decrease in mitochondrial ATP production increases the concentration of AMP, causing a shift from an anabolic state to a catabolic state to sustain ATP-coupled reactions. The increase in AMP/ATP ratio triggers the activation of AMP-activated protein kinase (AMPK) that decreases mammalian target of rapamycin (mTOR) activity reducing anabolic reactions and increasing autophagy and FAO to increase metabolic supply by providing nutrients to mitochondria for generation of ATP (Pearce et al., 2013). Other example of retrograde signaling is the change in mitochondrial membrane potential that is sensed as readout of the functionality of mitochondria to activate processes such as mitophagy or apoptosis (Kasahara and Scorrano, 2014). Finally, the OMM, serves as a signaling platform to allow coordinated interaction of proteins and signaling pathways (Weinberg et al., 2015).

Glossary

Oxidative phosphorylation (OXPHOS); A two-step metabolic pathway that produces ATP from oxidation of nutrients and the transfer of electrons. First, pyruvate and fatty acids (FAs) are converted into acetyl-CoA, which enters the TCA cycle, producing free electrons carried by NADH and $FADH_2$. Second, the electrons enter the electron transport chain, resulting in the movement of electrons out of mitochondrial matrix and the synthesis of ATP.

Tricarboxilic Acid Cycle (TCA, Krebs cycle); acetyl-CoA derived from pyruvate and FAs is shuttled through eight enzymatic reactions in the mitochondria to generate the reducing equivalents NADH and $FADH_2$ that fuel ATP production during OXPHOS. In addition, the cycle provides metabolites and NADH that function as aminoacid precursors, signaling molecules, or as substrates in other biochemical reactions.

Fatty acid oxidation (FAO); metabolic process used to derive energy from the mobilization and oxidation of FAs, mainly in the mitochondrial matrix.

Glycolysis; involves the enzymatic breakdown of glucose to pyruvate in the cytoplasm generating ATP and NADH.

Glutaminolysis; a series of biochemical reactions in which the amino acid glutamine is degraded to glutamate and then to a-ketoglutarate for further metabolism in the TCA cycle.

Pentose Phosphate Pathways and Serine biosynthesis pathway; utilizes the six carbons of glucose to generate ribose-5-phosphate (R5P) and glycine for the synthesis of the nucleotides and reducing equivalents in the form of NADPH for reductive biosynthesis reactions.

Figure I2

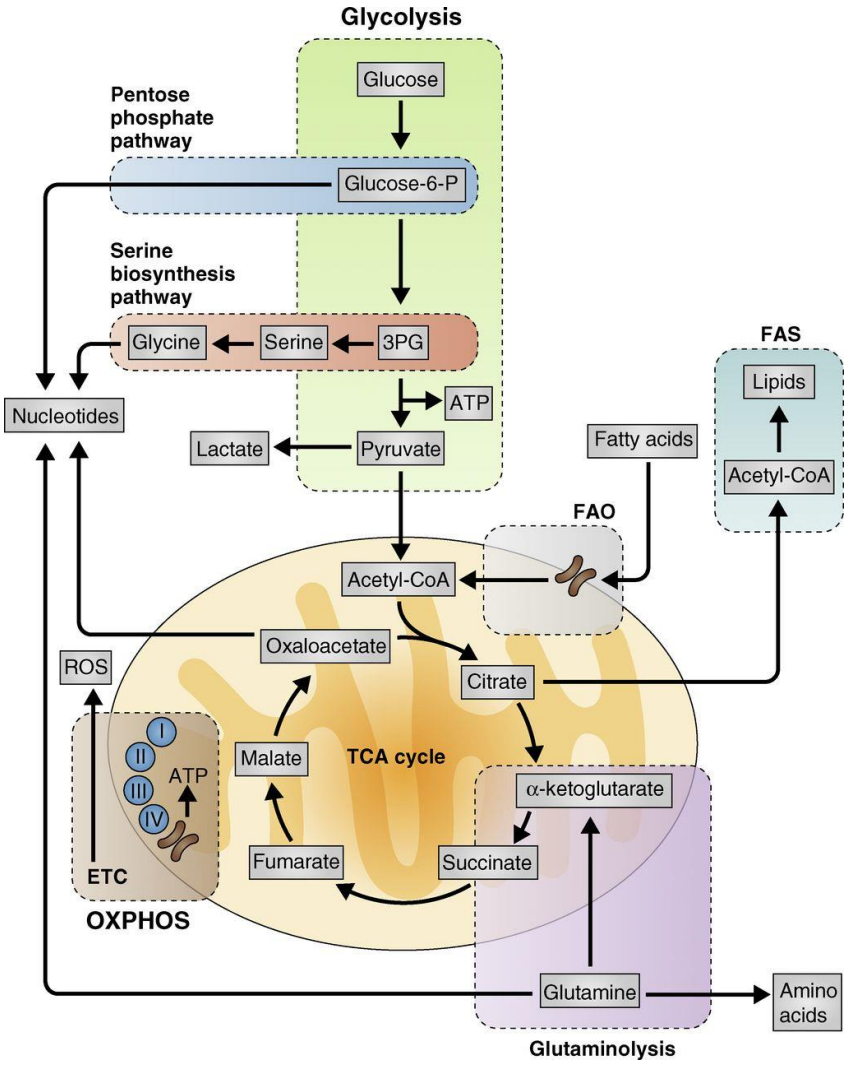

Cytosolic metabolic pathways converge on mitochondria where they constantly replenish the TCA cycle. TCA cycle intermediates can be further oxidized to generate ATP or they can be shuttled out of mitochondria into subsidiary pathways to generate cellular building blocks such as fatty acids (FAs). TCA cycle metabolites, in addition to other byproducts of mitochondrial metabolism, such as ROS, function as important signaling molecules that control cellular functions (Buck et al., 2015).

1.1.1The mitochondrial genome

Mitochondria have their own small circular genomes, encoding selected subunits of ATP synthesis and electron transport proteins that form the OXPHOS complexes, as well as transfer and ribosomal RNAs (tRNAs and rRNAs) (Figure I3A). The mitochondrial genome is ~16.6 kilobases in length and contains 37 genes encoding 13 proteins, 2 ribosomal RNAs and 22 tRNAs. The 13 polypeptides are distributed among the OXPHOS protein complexes I, III, IV and V whereas complex II is entirely encoded by the nuclear genome (Figure I3B). The 2 rRNAs and 22 tRNAs encoded by the mitochondrial DNA (mtDNA) are essential for the mitochondrial translational machinery that is used to generate the 13 polypeptides. The remaining proteins (>1,000) in the mitochondrial proteome are encoded by the nuclear genome, synthesized in the cytosol and imported into the mitochondria. Since the subunits of the respiratory complexes are encoded by nuclear and mtDNA, communication among both genomes is critical to maintaining

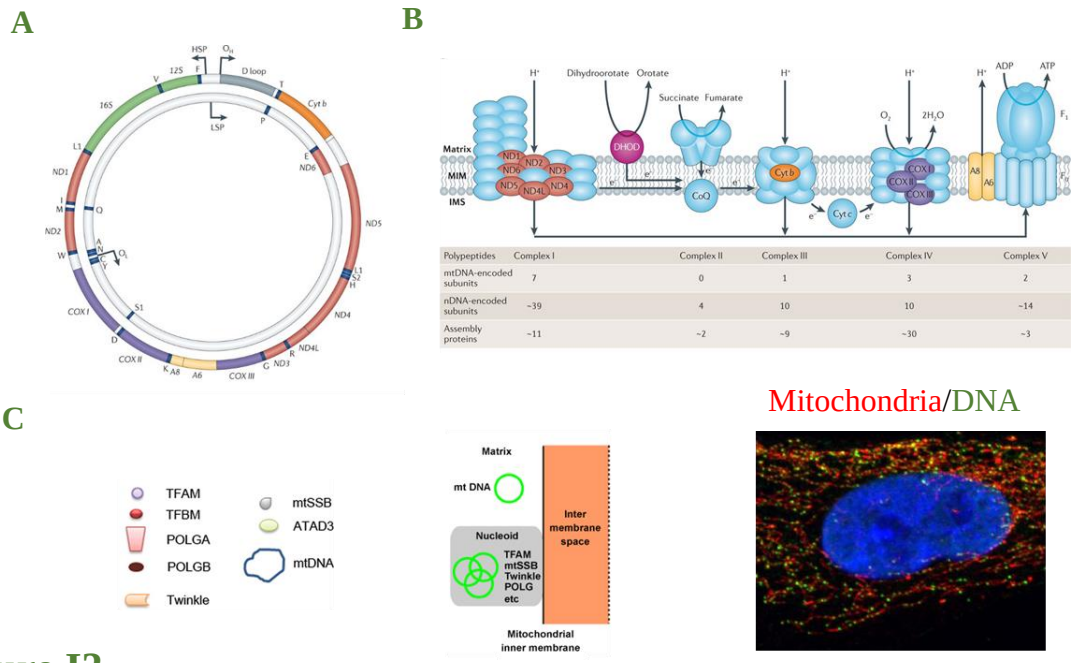

Figure I3

The mitochondrial genome resides within the inner membranes of the mitochondrion. It consists of a heavy (H) and a light (L) strand, coding regions that contain no introns and the displacement loop (D-loop), where transcription and replication factors interact. (B) The mtDNA encodes 13 polypeptides contributing to complexes I, III, IV and V of the ETC, whereas the remaining subunits are encoded by the genomic DNA. Of note, mutations in the mitochondrial genome are usually associated to Complex I deficiency since seven of its subunits are encoded by mtDNA. (C) mtDNA replication is mediated by several nuclear-encoded transcription and replication factors, which along with mtDNA are packaged forming the mitochondrial nucleoid. The number of mitochondrial nucleoids per mitochondrion ranges from 1 to 10 (Satoh and Kuroiwa, 1991) and contain proteins involved in mtDNA replication, translation and protein assembly (TFAM, TFBM, POLGA, POLGB, MTSSB, Twinkle and ATAD) (Legros et al., 2004).

the function of the electron transport chain and is associated with organism life-span (Feng et al., 2001; Gomes et al., 2013; Houtkooper et al., 2013).

A typical human cell contains hundreds of copies of mtDNA, which are grouped in protein-rich complexes called nucleoids, with between one and eight genome copies per nucleoid (Legros et al., 2004) (Figure I3C). The nuclear-encoded mitochondrial transcription factor A (Tfam) is the most abundant mtDNA-associated protein in mammalian cells (Friedman and Nunnari, 2014). This factor plays a crucial role in mtDNA transcription, and its expression controls mtDNA copy number in cells, thus being an essential player in the maintenance, transcription, and replication of mtDNA (Ekstrand et al., 2004; Larsson et al., 1998; Ngo et al., 2011; Rubio-Cosials et al., 2011). Global deletion of Tfam causes embryonic lethality (Larsson et al., 1998), but tissue-specific ablation of this factor disrupts respiratory chain function in selected cell populations and generates a variety of alterations that recapitulate important phenotypes of human mitochondrial diseases (Ekstrand et al., 2007; Hansson et al., 2004; Vernochet et al., 2012; Viader et al., 2013; Wang et al., 1999).

1.2 Mitochondrial dynamics

The activity of mitochondria is regulated by their number, shape and positioning, features that are modified in response to changing circumstances such as oxygen availability or stress (Acin-Perez et al., 2014; Detmer and Chan, 2007; Lapuente-Brun et al., 2013). Our view on how mitochondria are organized within cells and function has changed since the description of the machinery involved in their fusion and fission (Chen and Chan, 2005). Mitochondria are no longer considered discrete organelles. Instead, mitochondria form a highly dynamic tubular network that is continuously remodeled by opposing processes of fusion and fission (Chan, 2006). During mitochondrial fusion, two mitochondria merge their outer and inner membranes, resulting in a single, larger mitochondrion. Mitochondrial fission is the opposite process, whereby a mitochondrion divides into two organelles (Figure I4).

Mitochondrial fission and fusion is controlled by a family of dynamin related GTPases highly conserved between yeast, flies, and mammals (Hoppins, 2014). Their combined actions divide and fuse the two lipid bilayers that surround mitochondria. Constriction and fission is driven by the dynamin-related protein 1 (Drp1) (Smirnova et al., 2001). In the cytosol, Drp1 is activated and recruited to the OMM and form spirals that constrict inner and outer membranes to induce division of the organelle into two separate entities. The activity of Drp1 is highly regulated by post-translational modifications (Cereghetti et al., 2008; Guo et al., 2013; Harder et al., 2004).

To date, four Drp1 receptors located in the outer mitochondrial membrane have been described in mammals; mitochondrial fission 1 (FIS1), mitochondrial fission factor (MFF), mitochondrial dynamics protein of 49 KDa (MID49) and MID51, which promote Drp1 recruitment often at sites where mitochondria contact with the endoplasmic reticulum (ER) (Friedman et al., 2011).

Mitochondrial fission and fusion

Figure I4

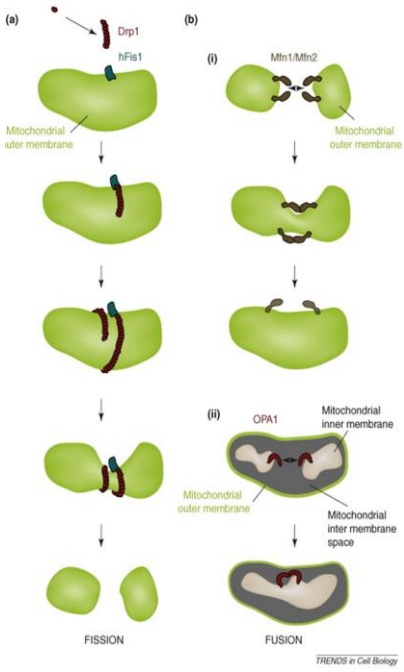

Mitochondrial fusion consists of two sequential steps; first, the outer membranes of two mitochondria fuse; second, the inner membranes fuse. Tethering and fusion between mitochondrial outer membranes is mediated by membrane-anchored dynamin family members named mitofusin 1 (Mfn1) and Mfn2 in mammals (Santel and Fuller, 2001), whereas fusion between mitochondrial inner membranes is mediated by a single dynamin family member called optic atrophy 1 (Opa1) in mammals. Although Mfn1 and Mfn2 are highly homologous to one another, they have different roles in cell physiology. Mfn2 is the more versatile and participates in cell metabolism, tethering the ER to mitochondria and cell proliferation (de Brito and Scorrano, 2008). Moreover, mutations in the *MFN2* gene are associated with the peripheral neuropathy Charcot–Marie–Tooth disease type 2A (Zuchner et al., 2006). Interestingly, OPA1 has other non-fusogenic functions: regulates apoptosis by controlling the structure of cristae and the release of cytochrome *c* (Frezza et al., 2006), and regulates mitochondrial cristae shape, critical in respiratory chain supercomplex assembly and respiratory efficiency (Cogliati et al., 2013).

Although the precise function of mitochondrial dynamics is still obscure, recent evidence suggests that fission and fusion are critical for maintaining a healthy mitochondrial population (Figure I5A, B). Complete deficiency in any of these proteins is embryonically lethal in mice, and mutations in some of these proteins are associated with neuromuscular disease in humans (Chen et al., 2003; Ishihara et al., 2009; Wakabayashi et al., 2009). But, how fusion and fission maintain the proper function in mitochondria? Cells lacking MFNs or OPA1 show heterogeneity among mitochondria in protein content, mtDNA nucleoid content and membrane potential, that results in defects in respiratory chain function and accumulation of mtDNA deletions (Chen and Chan, 2005; Chen et al., 2007; Chen et al., 2010). Thus, cycles of fusion and fission facilitate the exchange of molecules such as metabolites, DNA and enzymes from healthy to dysfunctional

mitochondria (Chen et al., 2005). Fusion between mitochondria can also rescue two mitochondria with mutations in different genes by cross-complementation to one another, and it can mitigate the effects of environmental damage through the exchange of proteins and lipids with other mitochondria (Mishra and Chan, 2014). Interestingly, although functional mitochondria continually mix their contents, quality control mechanisms prevent dysfunctional mitochondria from fusing with healthy mitochondria, for instance by promoting the proteolytic inactivation of OPA1 (Ishihara et al., 2006). Mitochondrial fission allows the selective targeting of damaged mitochondria for degradation via macroautophagy (Twig et al., 2008). Additionally, fission is also required for the proper distribution of mitochondria to daughter cells during mitosis (Taguchi et al., 2007), essential for growing and dividing cells to populate them with adequate numbers of mitochondria, and the asymmetric partitioning of mitochondria during stem cell division (Campello et al., 2006; Kanfer et al., 2015; Katajisto et al., 2015; Li et al., 2004; Varadi et al., 2004).

Figure I5

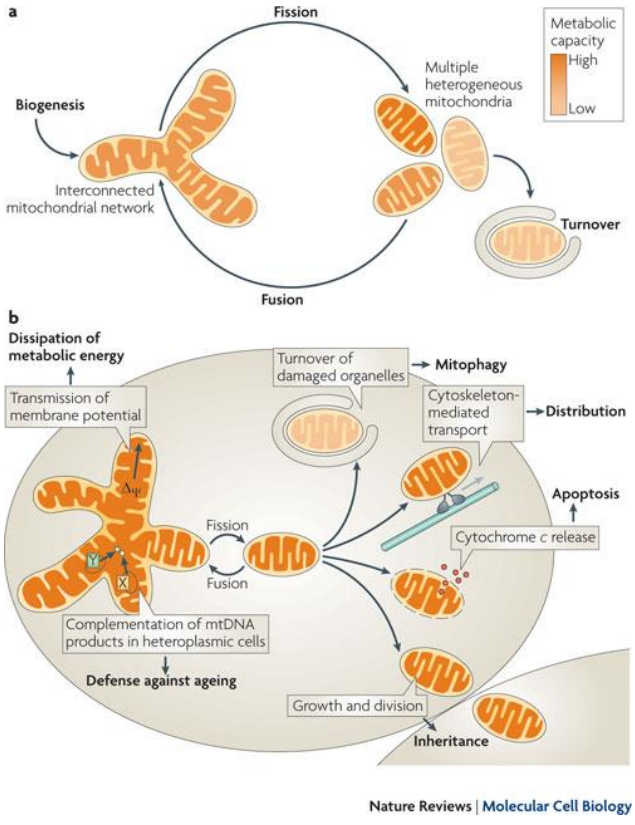

(A) Life cycle of mitochondria. Growth and division of mitochondria ends with the degradation of impaired or excess organelles by mitophagy. Mitochondrial dynamics remodels constantly the mitochondrial network and generate multiple heterogeneous mitochondria and segregate "dysfunctional" mitochondria that can be eliminated by selective autophagy.

(B) Proposed functions of mitochondrial dynamics. Fusion of mitochondria allows the complementation of mtDNA gene products in heteroplasmic cells to counteract the decline of respiratory functions in aging and the transmission of membrane potential within the mitochondrial network. Mitochondrial fission is involved in mitochondrial inheritance during cell division, the release of pro-apoptotic factors, the cellular positioning to specific sites by cytoskeleton-mediated transport and the turnover of damaged organelles by mitophagy (Westermann, 2010).

1.3 Positioning mitochondria to specific subcellular locations

The cytosolic localization of mitochondria is not random: these organelles accumulate where high amounts of ATP are required, or where Ca^{2+} signaling needs to be regulated. Mitochondrial movement is highly coordinated with changes in organelle shape in order to produce mitochondria whose size is compatible with their movement. Mitochondrial distribution within the cell depends on mitochondrial trafficking along the cytoskeleton. For example, the expression of pro-fusion shaping proteins decreases mitochondrial movement along axons and dendrites and consequently reduces the number of dendritic spines and synapses (Li et al., 2004), the formation or maintenance of which require local levels of high mitochondrial ATP production. Similarly, mitochondria cluster at many sites of high ATP demand in different cell types. In *Drosophila* neuromuscular junctions, synaptic mitochondria are required to fuel the myosin ATPase that mobilizes a reserve pool of vesicles (Verstreken et al., 2005). Mitochondria specifically redistribute to and accumulate at the uropod during directed leukocyte migration to provide ATP, thus regulating the cell motor of migrating lymphocytes (Campello et al., 2006). The accumulation of mitochondria at the uropod requires their fission since promoting mitochondrial fusion blocks mitochondria and cell polarization in response to chemokines and prevents the migration of T lymphocytes. The inhibition of mitochondrial transport reflects an inability of the cytoskeleton to transport organelles that are too large or, alternatively, altered interaction between mitochondria shaping proteins and the components of the mitochondria transport machinery, such as the kinesin and dynein motors or the adaptor Miro–Milton complex (Liu et al., 2009). In this sense, disruption of the dynein-dynactin complex results in mitochondrial elongation caused by Drp1 blockage (Varadi et al., 2004), whereas MFN2 binding to Miro-Milton complex coordinate axonal transport of mitochondria (Misko et al., 2010). Similarly, Miro-1 links mitochondria to dynein complex and regulates mitochondrial positioning necessary for cell polarization and migration during lymphocyte adhesion to the endothelium (Morlino et al., 2014), which supports a model whereby the machinery that transports mitochondria is coordinated with mitochondrial shaping proteins.

1.4 Communication between mitochondria and other intracellular organelles

The crosstalk of mitochondria with other intracellular organelles is crucial during cell adaptation to stresses and for the preservation of organelle functionality (Klecker et al., 2014). Mitochondria interact with peroxisomes, lipid bodies or the plasma membrane, and these contacts are involved in lipid metabolism and regulation of calcium signaling (Naon and Scorrano, 2014). Mitochondria and the ER, form critical hubs implicated in the regulation of mitochondrial fission, calcium homeostasis, ATP production, apoptosis and lipid metabolism (de Brito and Scorrano,

2008; Osman et al., 2011; Rowland and Voeltz, 2012), and deregulation of these contacts can lead to disease (Area-Gomez et al., 2012; Arruda et al., 2014; Tubbs et al., 2014). Mitochondrial contacts with the lysosome-related vacuole in yeast (Elbaz-Alon et al., 2014; Honscher et al., 2014) and with melanosomes in melanocytes (Daniele et al., 2014), have been shown to modulate lipid homeostasis and organelle function. Defining the intricate communication of mitochondria with other intracellular organelles is thus critical for understanding essential physiological processes and how their dysfunction might contribute to the development of human disease.

The **endolysosomal system** is a dynamic compartment in which endosomes, lysosomes and multivesicular bodies (MVBs) mediate signaling, degradation and exosome secretion. Early endosomes regulate receptor signaling and direct endocytosed receptors back to the plasma membrane for repeated receptor signaling, or sort them for lysosomal degradation and signal termination. The maturation of early endosomes and the production of MVBs is a multistep process that includes changes in lipid composition and acidification of the endosomal compartment. Part of the MVB specific components traffic from the trans Golgi network (TGN), and may finally form part of the lysosomes. Therefore, MVB can be seen as an intermediate compartment where different compounds can be sorted for recycling instead of being directed to degradative pathways.

During maturation of endosomes, inward budding of the limiting membranes of MVBs forms small intraluminal vesicles (ILVs). These vesicles can be secreted into the extracellular environment as **exosomes** and mediate cell-to-cell communication (Mittelbrunn and Sanchez-Madrid, 2012) or, alternatively, are directed to the lysosome for degradation. Contrary to other types of extracellular vesicles, exosomes have endocytic origin (Raposo and Stoorvogel, 2013). Their secretion occurs in a constitutive manner although cellular stress or activation signals modulate their secretion (Villarroya-Beltri et al., 2014). Exosomes carry specific repertoires of proteins and nucleic acids that can transferred to neighboring cells and regulate at a distance the properties of receptor cells (Mittelbrunn and Sanchez-Madrid, 2012). Consequently, exosomes play a role in intercellular communication in several physiological processes, and contribute to organism development, immune responses, neuronal communication, and tissue repair (Yanez-Mo et al., 2015). However, exosomes may participate in some pathological disorders, favoring tumor progression, virus dissemination and the spreading of toxic forms of aggregated proteins in neurodegenerative diseases (Bellingham et al., 2012).

Loading of proteins into exosomes is controlled through a variety of pathways (Figure I6). The endosomal sorting complexes required for transport (ESCRT) machinery is essential for the sorting of ubiquitinated membrane proteins and for the formation of ILVs in the MVB compartment. ILVs budding and protein sorting depend also on tetraspanin and lipid-dependent

interactions. The most abundant RNA species in exosomes are small rRNAs, fragmented tRNAs, and structural RNAs and are also highly enriched in specific set of microRNAs and mRNAs (Nolte-'t Hoen et al., 2012). An active sorting mechanism participates in RNA targeting into exosomes, which allows some RNA species to be particularly enriched in exosomes, whereas other RNAs are barely detected (Villarroya-Beltri et al., 2013). Although a great deal of effort has been placed on understanding the mechanisms of exosome cargo loading, less is known about the signals and the metabolic clues that coordinate the fate of MVBs between exosome secretion or their integration with the degradative and recycling pathways of the cell (Figure I7).

Figure I6

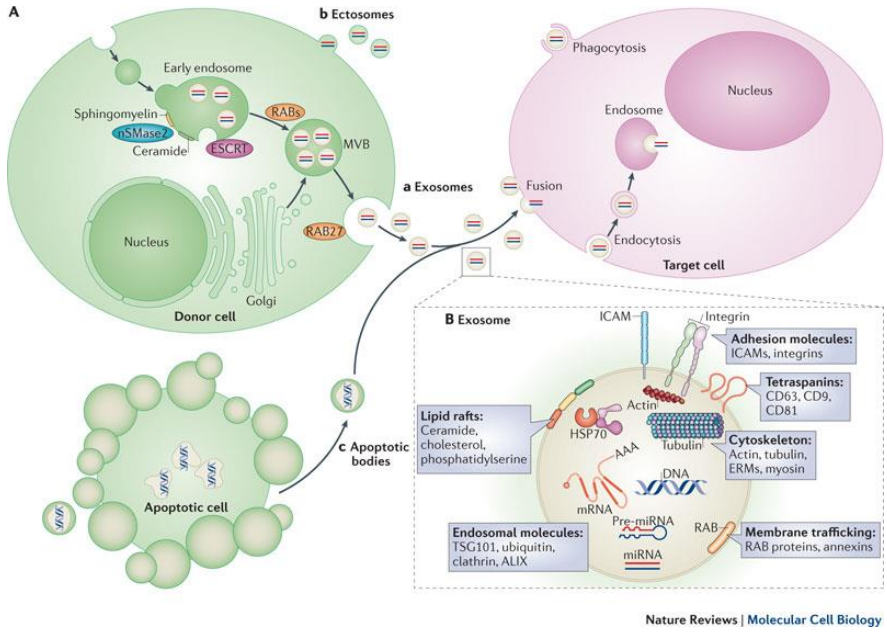

Biogenesis and composition of Extracellular Vesicles (EVs). Blebbing of the cellular plasma membrane generates ectosomes whereas breakdown of dying cells forms apoptotic bodies. Exosomes derive from endosomal compartments through fusion of MVBs with the plasma membrane. Neutral sphingomyelinase 2 (nSMase2), ESCRT complex and RABs participate in ILV formation, protein sorting and exosome secretion, respectively. EVs, contain functional mRNA, microRNA (miRNA) and DNA molecules that can be taken up by recipient cells through mechanisms including fusion with the plasma membrane, phagocytosis and endocytosis. Exosomes contain proteins involved in membrane transport and fusion (such as RAB proteins and annexins), cytoskeletal proteins, adhesion molecules and tetraspanins. Exosome membranes are enriched in raft lipids such as cholesterol, ceramide and sphingolipids (Mittelbrunn and Sanchez-Madrid, 2012).

Lysosomes are recognized as the main degradative compartment of the cell. First described by the Nobel laureate Christian de Duve in the 1950s, lysosomes are responsible for proteolytic degradation and recycling of functional and damaged proteins and organelles. Lysosomes ensure continuous renewal and recycling of cellular constituents avoiding accumulation of harmful components. In addition to the catabolic function of lysosomes, these organelles participate in a range of physiological processes such as plasma membrane repair, bone and tissue remodeling, cell signaling, energy metabolism, immune response and cell death (Cuervo, 2013; Settembre et al., 2013b). Lysosomes contain a single-lipid bilayer membrane in which are located proteins involved in the acidification of the lysosomal lumen, fusion of the lysosome with other cellular structures such as late endosomes, autophagosomes and the plasma membrane, and transport of degradation products into and out of lysosomes (Saftig and Klumperman, 2009). The most important biochemical feature of the lysosome is its acidic lumen (pH 4.5-5.0), which allows higher enzymatic activity of the resident acidic hydrolases, and facilitates partial unfolding of the substrate proteins allowing endoproteases to gain access to internal peptide bonds. The generation of the lysosomal pH gradient is maintained by the lysosomal membrane (Mindell, 2012). The proton-pumping v-type ATPase, uses the energy of ATP hydrolysis to pump protons from the cytosol to the lumen creating a H+ concentration in the lysosome that is about 100-fold higher than that of cytosol. Lysosome biogenesis and function are subject to transcriptional regulation by the transcription factor EB (TFEB), which allows adaptation of lysosomal function to different physiological conditions (Medina et al., 2015; Sardiello et al., 2009; Settembre and Ballabio, 2011). Alterations to lysosome function and endolysosomal trafficking pathways are mostly found in lysosomal storage disorders (LSDs). LSDs are caused either by deficiency of lysosomal proteins or by changes in non-lysosomal proteins that result in the accumulation of undegraded substrates in lysosomes and abnormal storage of lipids such as sphingomyelins, triacylglycerides, glycosphingolipids or sphingosines (Boustany, 2013; Futerman and van Meer, 2004). Remarkably, lysosomal dysfunction in Gaucher disease blocks mitochondrial turnover by mitophagy (Osellame et al., 2013), thus connecting the lysosome degradation capacity to the maintenance of a healthy mitochondrial repertoire. However, whether mitochondria regulate the biogenesis and function of the endolysosomal compartment is still unknown.

Figure I7

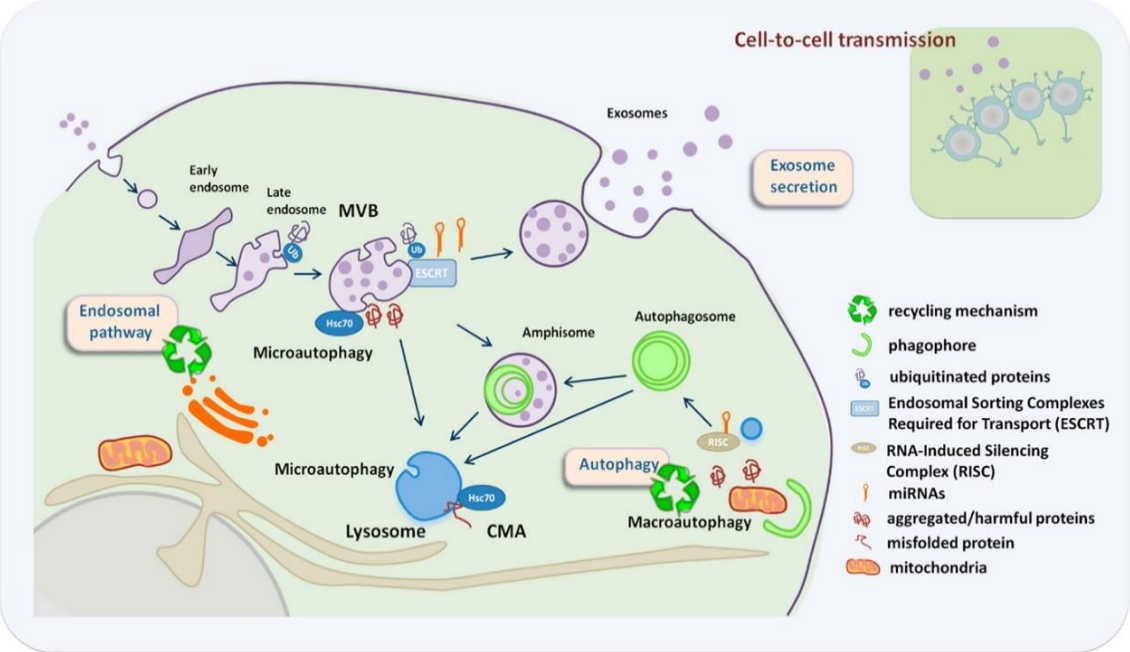

Crosstalk of the endolysosomal compartment in the maintenance of cellular homeostasis. Recycling mechanisms relay on endosome/autophagy and lysosomal function. Recycling pathways include: macroautophagy where whole cytosolic regions are sequestered inside autophagosomes that fuse either with MVBs or lysosomes, chaperone-mediated autophagy (CMA) where LAMP-2A acts as a receptor for hsc70 on the lysosome to deliver unfolded proteins into the lysosomal lumen, and microautophagy that involves engulfment of small cytoplasmic components by inward invagination of the lysosomal or endosomal membrane. Exosome secretion is an alternative way to alleviate stress when recycling pathways are compromised, with an impact in neighboring cells (Baixauli et al., 2014)

1. 5 Mitochondrial function during adaptive immune responses

The role of mitochondria in T cell function has been historically neglected because of the glycolytic nature of T lymphocytes. Recent observations, however, have elucidated the requirement for mitochondrial oxygen consumption, ATP and mROS in fueling many if not all the steps of T cell function; ranging from early T cell activation, survival and proliferation, to the final events leading to T cell differentiation and effector function (Chang et al., 2013; Gill and Levine, 2013; Kaminski et al., 2012; Sena et al., 2013; Yi et al., 2006).

1.5.1 Immune synapse formation and early T cell activation

T cell recognition of an antigen in the surface of an antigen-presenting cell (APC) leads to the formation of a specialized membrane-based structure at the interface of the APC and the T lymphocyte that favor transient cell-cell communication (Figure I8). This assembly, termed immune synapse (IS) because of its similarity to the neurological synapse, is a highly dynamic structure where polarized macromolecular components orchestrate the early events of T cell activation (Grakoui et al., 1999; Monks et al., 1998; Wulfing and Davis, 1998). T cell relocates adhesion and activating receptors, cytoskeletal components and secretory organelles to the contact site with the APC. T cell receptors (TCRs) gather at this site, and form the central supramolecular activation cluster (cSMAC), which also includes CD3 and co-stimulatory receptors. The cSMAC is surrounded by a ring of adhesion receptors that form the peripheral SMAC (pSMAC) (Dustin et al., 1998; Mittelbrunn et al., 2004). Polarization of the cytoskeleton toward the IS involves polymerization of actin, which, together with myosin, forms a contractile ring that is important for the correct concentration of the TCR complex at the cSMAC (Ilani et al., 2009). The tubulin cytoskeleton also reorganizes, and the microtubule-organizing center (MTOC) is re-orientated toward the IS through the activity of dynein/dynactin molecular motors (Martin-Cofreces et al., 2008). Under these circumstances, the cytoskeleton guides the redistribution of the secretory and Golgi apparatus (GA) toward the IS, which favors the polarized secretion and endocytic recycling of receptors at the IS (Martin-Cofreces et al., 2014). The MVB polarize toward the IS (Alonso et al., 2011; Calabia-Linares et al., 2011; Mittelbrunn et al., 2011).

The localization of the MVB at the IS organize a dense actin network through interaction with the clathrin adaptor and Hrs at the lamella-like structure beneath the plasma membrane (Calabia-Linares et al., 2011). Synaptic MVBs support the active secretion of microRNA-loaded exosomes towards contacting APCs (Alonso et al., 2011; Calabia-Linares et al., 2011; Mittelbrunn et al., 2011). This unidirectional transference of functional microRNA mediated through exosomes appears as a novel mechanism of cell-to-cell communication and immune modulation (Mittelbrunn and Sanchez-Madrid, 2012). The release of miRNA-enriched exosomes from MVB to the intercellular space would be facilitated by the skeleton and proteins involved in fusion of membranes, such as the SNARES (Mittelbrunn et al., 2015). Additionally, the lipid composition of the limiting membrane of the MVB may act as a sensor to enhance or decrease the secretion of exosomes. Lack of diacylglycerol kinases (DGK) increases exosome secretion by stimulated T cells (Alonso et al., 2011) and prevents T cell anergy upon CD3 stimulation without costimulation (Joshi and Koretzky, 2013). In addition, lysobiphosphatidic acid (LBPA), a lipid

present in MVBs, is found at the cSMAC plasma membrane (Varma et al., 2006), which support the exocytic process from the MVB at the IS.

Figure I8

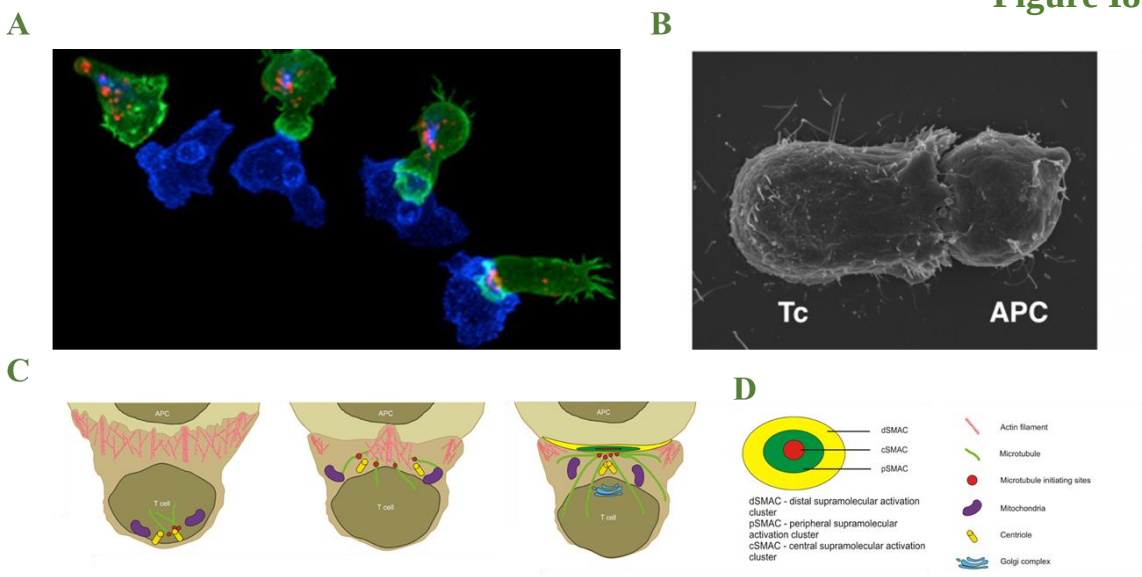

The early steps of T cell activation, polarization and IS formation: after initial engagement of the TCR with its cognate peptide–MHC complex, the T cell stops migrating, polarizes and the MTOC is reoriented from the uropod to beneath the IS together with its associated organelles and vesicles (A-C). TCR molecules are recruited into the synapse whereas other cell-surface molecules are excluded (D). The sequential states in the assembly of the IS provide a framework for establishing checkpoints for cellular activation. In addition, the IS can regulate the initiation, balance and termination of signaling by accumulation of proteins at the IS to increase the rate of TCR triggering and the downregulation and degradation of TCR. (A) Confocal images from a T cell immune synapse formation between T cell and an APC (Ritter et al., 2015), (B) Transmission electron microscopy image show the extensive polarization of T cells upon IS formation, (C) diagram representing the polarization of cytoskeleton and related organelles towards the IS, and (D) IS architecture (Piragyte and Jun, 2012).

T cell mitochondria relocate toward the IS during T cell activation (Abarca-Rojano et al., 2009; Kummerow et al., 2009; Quintana et al., 2007). Mitochondria are required for efficient T cell activation by regulating calcium signaling and by producing ROS and ATP. Mitochondria act as efficient Ca^{2+} buffers and their translocation towards the IS is essential to maintain Ca^{2+} influx upon TCR stimulation by preventing the premature Ca^{2+}-dependent inactivation of CRAC/ORAI1 channels at the plasma membrane and calcium flux across plasma membrane (Kummerow et al., 2009; Quintana et al., 2011). Mitochondrial ROS generated at mitochondrial complexes III and I triggers an oxidative signaling indispensable for full antigen-specific T cell activation. T cells deficient for ubiquinol-cytochrome c reductase (Uqcrfs1), a component of complex III of the ETC, display impaired TCR-dependent ROS production and defects in antigen-

specific proliferation. These cells, which are not bioenergetically compromised, can undergo homeostatic proliferation but they lack ROS-dependent signaling mechanisms needed for antigen-specific T cell activation and subsequent clonal expansion (Sena et al., 2013). By regulating ROS levels, the mitochondrial antioxidant enzyme manganese superoxide dismutase (MnSOD/SOD2), modulates NF-κB- and AP-1-mediated transcription (Kaminski et al., 2012). The regulation of the mitochondrial oxidative signal required for full T cell activation is also regulated by the ADP-dependent glucokinase (ADPGK). Its activation deviates glycolytic metabolism toward mitochondrial glycerol-3-phosphate dehydrogenase (GPD) shuttle, resulting in hyperreduction of ubiquinone and ROS release from mitochondria which is required for NF-κB-dependent gene expression (Kaminski et al., 2012).

Mitochondria play another critical role in T cell activation by producing ATP. ATP released from stimulated cells fuel autocrine purinergic signaling processes required for a successful immune response (Ledderose et al., 2014). TCR stimulation initially triggers the uptake of Ca^{2+} by mitochondria, which stimulates Ca^{2+}-dependent dehydrogenases of the TCA cycle, driving mitochondrial ATP production by OXPHOS. Increased oxidative synthesis of ATP upon T cell activation is followed by its release through pannexin 1 channels to the extracellular space to stimulate purinergic P2X receptors that function as ATP-gated Ca^{2+} channels that facilitate Ca^{2+} influx. Besides the increasing appreciation on the role of mitochondria in the early steps of T cell activation, the molecular mechanisms driving mitochondrial positioning at IS and their role in IS organization and TCR signaling have not been elucidated.

1.5.2 The metabolic switch of T cell activation

Following the early events of IS formation upon antigen recognition, T cells undergo a developmental program characterized by rapid growth, proliferation, and acquisition of specialized effector functions. This process is tightly controlled by the coordinated activity of immune cell-specific cytokines and transcription factors. Activation of T cells is an energetically demanding process, and naive $CD4^+$ T cells must reprogram their metabolism to meet the costly biosynthetic and bioenergetic demands of T cell activation and proliferation (Pearce et al., 2013; Pollizzi and Powell, 2014). Immune cells transform from a state of relative metabolic quiescence or catabolic state to a highly active metabolic or anabolic state during the activation phase.

Resting naïve T cells maintain low rates of glycolysis and predominantly oxidize glucose-derived pyruvate via OXPHOS or engage FAO to make ATP. In this catabolic state, macromolecules are completely degraded and shuttled to energy-generating pathways to produce

ATP to maintain cellular homeostasis and allow long term survival during quiescence. However, upon T cell activation, cellular metabolism is reorganized to an anabolic state that balances the need for ATP with the need for metabolic intermediates that are required for the novo synthesis of macromolecules (Figure I9).

Figure I9

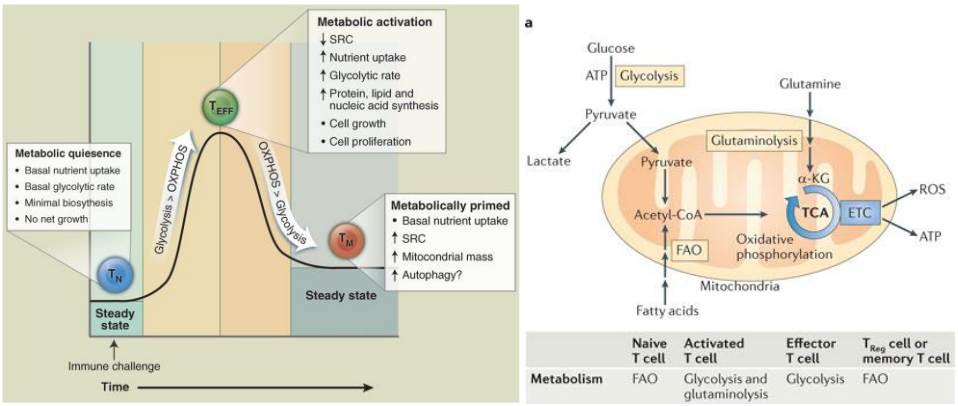

Different metabolic hallmarks of resting T cells (Tn), activated T cells (Teff) and memory T cells (Tm) (Pearce et al., 2013).

The cytokines and transcription factors that act in the regulation of immune cell differentiation and function are closely linked to the metabolic reprogramming of T cells. T cell receptor (TCR) signaling directs this metabolic reprogramming of naïve T cells. TCR activation promotes the coordinated up-regulation of glucose and amino acid transporters (Pollizzi and Powell, 2014), that fuel glutaminolysis and glycolysis during T cell blastogenesis. Activation of T cells rapidly switches metabolic programs from FAO and pyruvate oxidation via the TCA cycle to aerobic glycolysis, the pentose phosphate pathway (PPP), and glutaminolysis (Wang et al., 2011). This metabolic reprogramming in T cells is associated with a global change in the transcriptome linked to the up-regulation of the transcription factors c-Myc (Wang et al., 2011), estrogen-related receptor α (ERRα) (Michalek et al., 2011b) and Hif-1α activation, and which seems very similar to that described in cancer cells (Gordan et al., 2007; Shi et al., 2011; Wang et al., 2011). This process, also known as the Warburg effect from earlier work in cancer biology, is a common trait of actively proliferating cells and is characterized by the conversion of glucose-derived pyruvate to lactate despite the availability of oxygen for complete glucose oxidation. It is important to note that OXPHOS is still engaged in activated T cells (Chang et al., 2013), although the production of lactate from pyruvate by aerobic glycolysis is the dominant pathway of glucose

metabolism in T cells. Oligomycin, a specific inhibitor of mitochondrial ATP synthase, can block the expression of early activation markers after TCR ligation and blunts subsequent T cell proliferation (Chang et al., 2013), suggesting that the naive-to-effector transition requires either de novo production of ATP by mitochondria or specific signals generated during OXPHOS function such as mROS (Kaminski et al., 2012; Sena et al., 2013; Weinberg et al., 2015).

1.5.3 Metabolic reprogramming in T cell differentiation and effector function

Despite their diverse functions, T cell populations largely arise from the same pool of precursor naive $CD4^+$ T cells upon antigen stimulation in the context of immune signals and key metabolic cues present in the inflammatory milieu (Pollizzi and Powell, 2014). Specific cytokines or combination of cytokines induce the expression of 'lineage-specific' transcription factors that ultimately guide the development of the different Th effector cell subsets (Figure I10). These include the pro-inflammatory T helper 1 (Th1), Th17, Th2, and regulatory T cells (T_{reg}) that restrain inflammatory responses. Upon pathogen clearance, most T_{eff} cells die, leaving behind a small population of long-lived antigen-specific memory T cells (T_m) that can be reactivated into rapidly expanding T_{eff} cells if a similar infection occurs to quickly restrain the infection. The balance among the distinct functional effector and regulatory T cell subsets is thus decisive to determine the nature of the immune response and avoid autoimmune diseases.

Similar to what was observed in the resting and activated state, a different T cell metabolic signature has been observed in T effector populations. Th1, Th2, and Th17 T cells specifically rely on glycolysis rather than mitochondrial metabolism, while Tregs show a requirement for lipid metabolism, glycolysis, and OXPHOS (Gerriets et al., 2015; Michalek et al., 2011a). Nutrient sensing and canonical signaling pathways such as mammalian target of rapamycin (mTOR), phosphoinositide 3-kinase (P13K), and AKT, link immune signals and metabolic cues for the activation, development, function and differentiation of T cells (Chi, 2012; van der Windt and Pearce, 2012; Waickman and Powell, 2012). The mTOR pathway integrates diverse environmental inputs, including immune signals and metabolic cues that direct T-cell fate decisions between effector and regulatory T cell lineage commitment (Chi, 2012; Zeng et al., 2013). mTORC1 signaling promotes Th1 and Th17 differentiation whereas mTORC2 signaling promotes Th2 differentiation (Chi, 2012). In addition, $CD4^+$ T cells that lack mTOR fail to differentiate into effector cells under appropriate skewing conditions and become Foxp3+ regulatory cells (Delgoffe et al., 2011).

Tregs have elevated levels of OXPHOS and decreased glycolytic flux compared to Th17 cells (Michalek et al., 2011a). The increased mitochondrial metabolism of Tregs is due to increased AMPK-dependent FAO since etomoxir, which inhibits FAO, impairs Treg differentiation (MacIver et al., 2011; Michalek et al., 2011a). Th17 cells, in contrast, show increased glycolytic metabolism which appears to be important to maintaining their Th17 lineage state. The increase in glycolysis observed in Th17 cells is due to increased HIF-1α stabilization. HIF-1α, an oxygen sensitive transcription factor, regulates glycolytic gene expression in Th17 cells and the balance between regulatory T cell and Th17 differentiation (Dang et al., 2011; Shi et al., 2011) by targeting Foxp3 for proteosomal degradation under normoxic and hypoxic conditions (Dang et al., 2011).

Figure I10

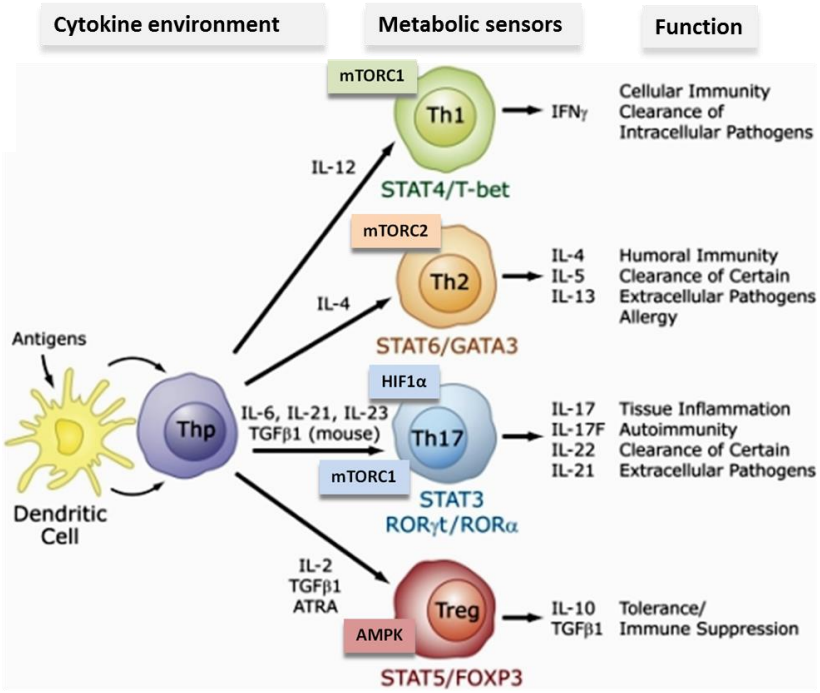

Host defense against pathogenic microorganisms requires extensive communication between innate and adaptive arms of the immune system. Signals from innate immune cells, induced by pathogens and inflammatory stimuli, drive naive CD4+ T cells to differentiate into one of several effector fates, including Th1, Th2, and Th17 cells and Treg cells, which dampen immune responses. The main signaling pathways activated and the master transcriptional factors driving each lineage are indicated. The cytokine products of differentiated T cells subsequently tailor immune responses to effectively eliminate intracellular and extracellular pathogens.

Th17 cells are important in responses mounted against extracellular bacterial infections of the intestine and the airways (Korn et al., 2009). Despite providing a benefit in these settings, Th17 can play a pathologic role in the induction of several autoimmune diseases, including collagen-induced arthritis, experimental autoimmune encephalomyelitis (EAE), inflammatory bowel diseases, and inflammation-induced carcinogenesis (Bedoya et al., 2013). Mice with T cells deficient in HIF-1α show reduced Th17 cells, increased Treg cells, and resistance to Th17-dependent EAE. The HIF-1α target pyruvate dehydrogenase kinase 1 (PDHK1) is expressed in Th17 cells, but not in Treg cells, and diminishing PDHK1, the negative regulator of pyruvate dehydrogenase (PDH) suppresses Th17 formation and increases Treg formation (Gerriets et al., 2015). PDH converts pyruvate to acetyl-CoA in mitochondrial matrix and increasing PDHK1 reduces PDH activity thus limiting acetyl-CoA availability. Pharmacologic inhibition of PDHK by dichloroacetate (DCA) in mice diminishes Th17 and promotes Tregs resulting in inhibition of Th17 dependent colitis and EAE pathologies (Gerriets et al., 2015).

Memory T cells have a different metabolism from their activated effector T cell counterparts, and they do not use aerobic glycolysis but rely on mitochondrial FAO for development and long-term survival (van der Windt et al., 2012). Memory T cells maintain greater mitochondrial mass which is required to support their oxidative metabolism and mitochondrial respiratory capacity required for increased cellular longevity, allowing CD8 T memory cells to respond more rapidly upon secondary exposure to the antigen. Although still not fully understood, all these metabolic studies suggest that mitochondrial metabolism dictates the different inflammatory and suppressive T helper lineages.

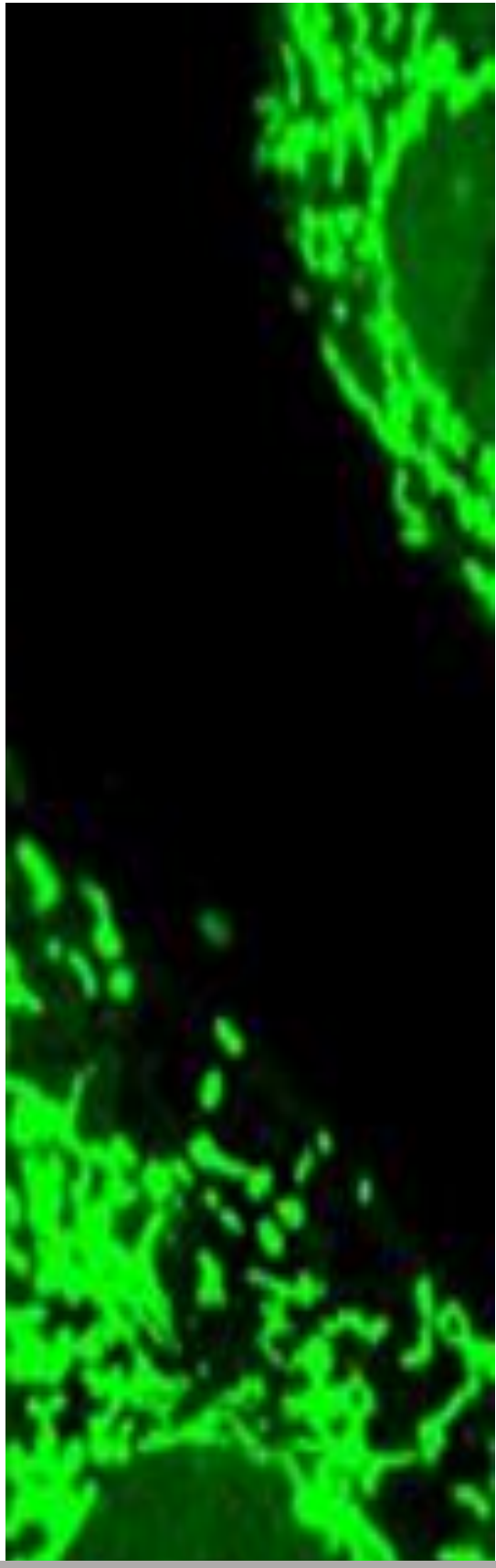

Objectives

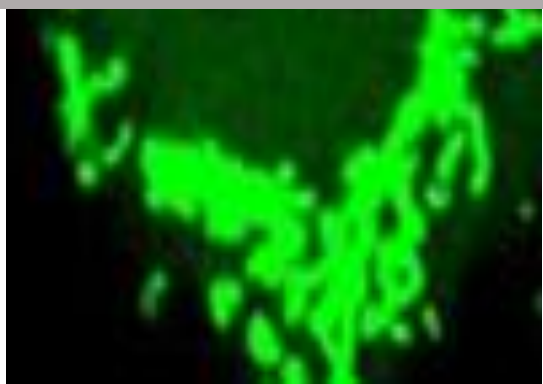

2. OBJECTIVES

Based on the previous studies and background knowledge on mitochondrial function we postulate the following hypothesis; ***mitochondria regulate the activation, proliferation and differentiation of T lymphocytes through (1) their active relocation and activity at the IS mediated by mitochondrial shaping proteins and (2) by integrating cellular metabolism and the function of the endolysosomal compartment***.

In order to challenge our hypothesis, we have addressed 3 main objectives;

1) Dissect the molecular mechanisms driving mitochondrial positioning at IS and determine the role of mitochondria in IS organization and early TCR signaling.

2) Define the requirements of mitochondrial metabolism in T cell activation and differentiation *in vitro* and *in vivo*.

3) Assess the crosstalk of mitochondria with the endolysosomal compartment and its impact on intracellular homeostasis and T cell function.

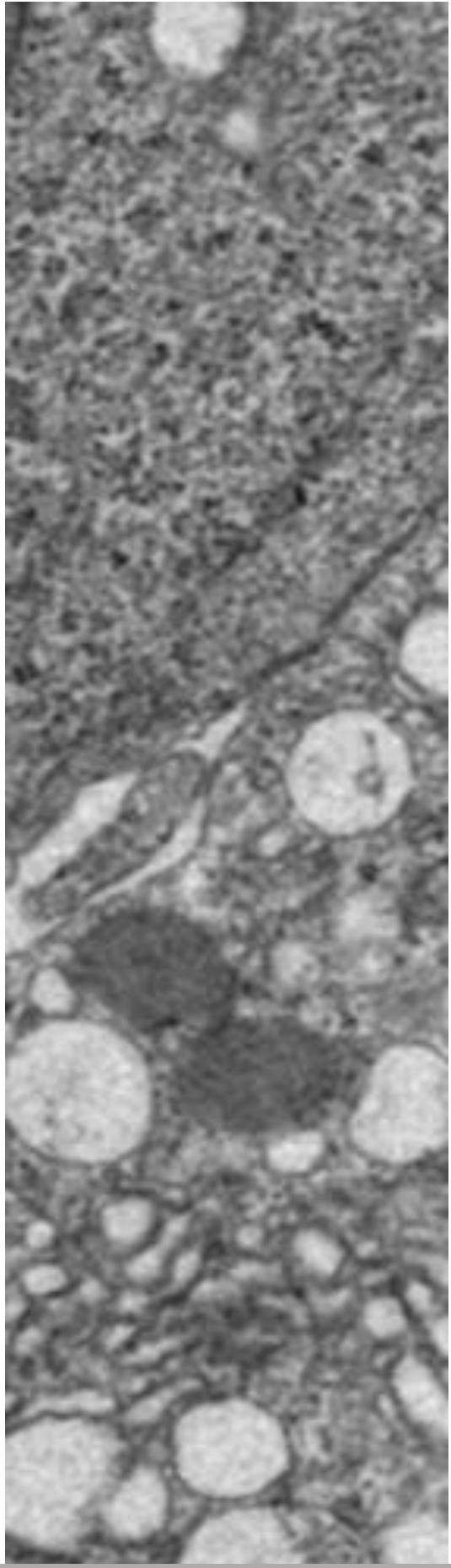

Materials and Methods

3. Materials and methods

3.1. Reagents and antibodies

Fibronectin (FN), poly-L-lysine (PLL), tetramethylrhodamine methyl ester (TMRM), 5,5',6,6'-tetrachloro-1,1',3,3'-tetraethylbenzimidazolcarbocyanine iodide (JC-1), carbonyl cyanide 4-(trifluoromethoxy)phenylhydrazone (FCCP), RU360, influenza hemagglutinin (HA) peptide, and FITC-conjugated or unconjugated anti-α-tubulin and anti-γ-tubulin were from Sigma-Aldrich (St. Louis, MO). *Staphylococcus enterotoxin* E (SEE) was from Toxin Technology (Sarasota, FL). Antibodies for western blot and immunofluorescence were as follows: the antibody T3b (anti-human-CD3), anti-human CD81, anti-ERMs, and anti-human CD63 (Tea3/18) were produced in our laboratory; Erk1/2 and p74-dynein Abs were from Millipore (Billerica, MA); anti-phospho-Erk1/2, anti-phospho-PLC-γ1 (Y783), anti-PLC-γ1, anti-p-AMPK (Thr172), anti-AMPK, and anti-HisH4 from Cell Signaling Technology (Denver, MA); monoclonal Drp1 Ab and anti-p150 from BD Biosciences (Lexington, KY); polyclonal Drp1, phospho-specific Ser-19 myosin regulatory light chain (MLC), anti-MLC2; anti-EEA1, anti-CD63, anti-CD81 (5A6) and anti-TOM20 Abs from Santa Cruz Biotechnology (Santa Cruz, CA); anti-MnSOD from Rockland (Gilberstsville, PA); anti-tubulin, anti-flotillin and anti-p62 from Sigma-Aldrich (St Louis, MO); anti-TFAM, anti-CD63 (NKI/C-3), anti-HRS, anti-CO1, anti-NDUFA9, anti-Core-1, anti-SDHA (FpSDH) and anti-TSG101 from Abcam; anti-TFEB from Bethyl Laboratories; anti-LAMP1 from Biolegend; anti-LBPA from Tebu-Bio; and anti-MnSOD from Enzo Life Sciences. Alexa 488-, 647-, and 568-labeled secondary antibodies, phalloidin 488, cell tracker 7-amino-4-chloromethylcoumarin (CMAC), INDO-1, Fluo4-AM, Lysotracker Green, LysoSensor™ Yellow/Blue DND-160 and Mitotracker Orange were from Invitrogen (Carlsbad, CA). Goat anti-mouse peroxidase and goat anti-rabbit peroxidase were from Thermo Scientific. Hoechst 42 and 58 was from Molecular Probes. Leupeptin and sphingomyelin were from Sigma.

3.2. Cells, plasmids and cell transfection.

Human T lymphoblasts were obtained from human peripheral blood lymphocytes (PBLs) by treatment for 48 h with 1 μg/ml PHA, followed by 50 U/ml IL-2 in complete RPMI 1640 medium until day 11. SEE-specific human T lymphoblasts were obtained as described (Ibiza et al., 2006). Vβ8+ Jurkat T cell clones (J77) and the lymphoblastoid Raji and Hom2 B cell lines were cultured in complete medium. HA-specific, Vβ3+ Jurkat T cells (CH7C17) were supplemented with 400 μg/ml hygromycin B and 4 μg/ml puromycin.

The human Jurkat T cell line and the oligodendroglia Oli-neu cell line were cultured in RPMI (Sigma) containing 10% fetal bovine serum (Invitrogen). FBalb/cJ and mt-ND6 (FG23-1) mutant cell line were grown in DMEM and supplemented with 10% fetal bovine serum (Invitrogen) (Acin-Perez et al., 2014). Human fibroblasts (control patient, a patient with a point mutation in the complex I subunit mt-ND5 gene (m.13513G>A), and a patient with a point mutation in the mt-tRNA^{Asn} gene (m.5658T>C) were obtained from skin biopsies for research purposes after written informed consent in accordance with the Helsinki declaration. Fibroblasts were grown in DMEM and supplemented with 10% fetal bovine serum (Invitrogen).

Plasmids encoding mtRFP, mtYFP, Drp1wtYFP, Drp1S647AYFP, Drp1S647DYFP were previously described (Cereghetti et al., 2008), and generously provided by Dr L Scorrano (University of Geneva, Switzerland). LC3-GFP-RFP tandem construct was a gift from Tamotsu Yoshimori (Addgene plasmid # 21074). pEGFP-parkin WT was a gift from Edward Fon (Addgene plasmid # 45875). T cell lines and human T lymphoblasts were transfected with DNA plasmids or with specific Drp1 double-stranded siRNAs against human Drp1 (GGUGCCUGUAGGUGAUCAA) or negative control (Eurogentec) using the Gene Pulser II electroporation system (Bio-Rad Laboratories) or the Nucleofector system (Amaxa Biosystems, Gaithersburg, MD).Tfam-silenced Jurkat and Oli-Neu cells were generated by lentiviral infection. Briefly, HEK293T cells were co-transfected with Lipofectamine2000 (Invitrogen) with pCMV-ΔR8.91-(Delta 8.9), pMD2.G-VSV-G and plasmids encoding shRNAs against Tfam (Open biosystems), and the corresponding control shRNAs pLKO.1 (Open Biosystems). Supernatants were collected after 48–72 h and filtered (0.45 μm). Oli-neu cells or Jurkat T cells were subsequently transduced with lentiviral vectors encoding shRNA targeting Tfam or with negative control pLKO.1 shControl and selected with RPMI medium containing puromycin (4 μg ml^{-1}). Stable cell lines with downregulated Tfam were grown in the presence of 0.25 mM uridine and 1 mM sodium pyruvate.

3.3. Mice

All animal experiments were performed in the specific pathogen-free facilities at the Centro Nacional de Investigaciones Cardiovasculares (CNIC) in accordance with European Union recommendations and institutional guidelines. *Tfam*$^{fl/fl}$ mice were kindly provided by N.G. Larsson (Larsson et al., 1998) and CD4^{+}Cre$^{+/wt}$ mice were purchased from the Jackson Laboratory. Double heterozygotes (*Tfam*$^{+/fl}$, CD4^{+}Cre$^{+/wt}$) were obtained and backcrossed to the *Tfam*$^{fl/fl}$ strain to generate tissue specific knockouts (CD4^{+}Cre$^{+/wt}$ *Tfam*$^{fl/fl}$).

3.4. T cell activation and differentiation

3.4.1. T cell activation (human)

For TCR stimulation, cells were left untreated or treated with T3b antibody (10 μg/ml) plus cross-linker (IgG, 5 μg/ml), with or without additional CD28 Ab (5 μg/ml) for co-stimulation. For antigenic stimulation, Raji cells were pulsed with 1 μg/ml SEE (20 min) and mixed with Jurkat cells or SEE-specific human T lymphoblasts (30 min); alternatively, Hom2 cells pulsed with 200 μg/ml HA peptide (3 h) were mixed with CH7C17 cells. Cells were lysed in 50 mM Tris-HCl, pH 7.5, containing 1% NP40, 0.2% Triton X-100, 150 mM NaCl, and phosphatase and protease inhibitors.

3.4.2. T cell activation and differentiation (mice)

Naive $CD4^+$ T lymphocytes were obtained from cell suspensions prepared from spleen and peripheral lymph nodes (LN) of *Tfam*$^{fl/fl}$ (wild type) and $CD4^+Cre^{+/wt}$ *Tfam*$^{fl/fl}$ (*Tfam*$^{-/-}$) mice. Pooled spleen and LN cells were incubated for 30 min at 4ºC with biotinylated antibodies to IgM, B220, CD19, CD8, Gr-1, CD44, CD25, MHC-II, F4/8, CD11c, CD11b and DX5 (BD Pharmingen) followed by extensive washing with PBS containing 1% BSA and 5mM EDTA. The cell suspension was incubated for 20 min at 4ºC with streptavidin microbeads (MACS; Miltenyi Biotec) and washed with PBS 1% BSA+5mM EDTA. Naive $CD4^+$ T cells were obtained by negative selection using the auto-MACS Pro Separator (Miltenyi Biotec). For *in vitro* activation, naive $CD4^+$ T cells were incubated in RPMI 1640 supplemented with 1% sodium pyruvate, penicillin, streptomycin, 50 mM 2-mercaptoethanol and uridine (0.25 mM) (all from Invitrogen) and 10% fetal calf serum (Sigma) in the presence of 5 μg ml^{-1} plastic-bound purified anti-CD3, 2 μg ml^{-1} soluble anti-CD28 (eBioscience) and 100 U ml^{-1} human IL-2 (Glaxo). For Th0 conditions, anti-IFN-γ (4 μg ml−1) and IL-4 (4 μg ml−1) were added. For Th1 conditions, culture was supplemented with IL-12 (10 ng ml−1) and anti-IL-4 (4 μg ml−1). For Th2 conditions, IL-4 (10 ng ml−1) and anti-IFN-γ (10 μg ml−1) were added. For Th17 conditions, anti-IL-2 (10 μg ml−1), anti-IL-4 (10 μg ml−1), anti-IFN-γ (10 μg ml−1), TGF-β (5 ng ml−1), IL-23 (20 ng ml−1) and IL-6 (20 ng ml−1) were included in cultures. For Treg cell differentiation, TGF-β (10 ng ml−1) was added. Cells were collected on day 6, or as indicated. To obtain differentiated T lymphoblasts, naive $CD4^+$ cells were cultured for 36-48h with 2 μg ml^{-1} concanavalin A (Sigma), and subsequently 50 U ml^{-1} human recombinant IL-2 (Glaxo) was added to the medium every 2 days during a 4-6 day incubation. For lymphoblast restimulation, cells were activated overnight either with 50 ng ml^{-1} phorbol myristate acetate (PMA) and 750 ng ml^{-1} ionomycin.

For proliferation assays, cells were fluorescently labeled with 1 μM Cell Trace Violet (Invitrogen) for 10 min at room temperature and activated with anti-CD3 and anti-CD28. For intracellular cytokine staining, cells were stimulated at 37°C for 4 h in the presence of GolgiStop (BD PharMingen), PMA (Sigma), and ionomycin (Sigma). After 4 h, cells were collected with 5 mM EDTA in PBS and fixed with 1% formaldehyde. Cells were then permeabilized with saponin (Sigma) solution (0.5% saponin in PBS) and stained with anti-IL-17, anti-FoxP3 or anti-IFN-γ (BD Biosciences). To gate on $CD4^+$ T cells only, T cells were stained with anti-CD4 antibody (BD Biosciences). Data were acquired on a FACSCanto flow cytometer (BD Bioscience) and analyzed using the FLOWJO software (Tree Star).

3.4.3 Flow cytometry analysis of lymphocyte populations

Viable cells were identified by Hoechst 42 exclusion. Singlet cells were discerned with a stringent multiparametric gating strategy based on FSC and SSC (pulse width and height). For surface labeling, cells were stained with antibodies diluted in PBS-0.5% BSA on ice. For intracellular and surface staining, cells fixed with 1% formaldehyde were stained with the indicated primary and secondary antibodies diluted in PBS-0.5% BSA and 0.5% Saponin. Cell suspensions from spleen and lymph nodes were blocked with Fc-block (CD16/CD32, BD), washed in PBS and 1% BSA and incubated with the following primary antibodies diluted in PBS and 1% BSA: CD11b, CD11c, B220, CD3, CD4, CD8 and CD45.1 (BD Biosciences). Fluorochrome-conjugated antibodies were purchased from BD Biosciences or eBioscience. Cell sample data were acquired on a FACSCanto flow cytometer and analysed using FACSDiva software (BD Biosciences) and FlowJo software.

3.4.4 Analysis of the extracellular levels of inflammatory cytokines by ELISA

Cell culture supernatants from equal amounts of activated $CD4^+$ T cells and restimulated with PMA and ionomycin were assayed for mouse IL-17, IL-10, IL-6, IFN-γ and IL-4 (from eBioscience) by enzyme-linked immunosorbent assay (ELISA) based on colorimetric quantification. The absorbance at $A_{405\ nm}$ was measured in a microplate reader (Bio-Rad Model 550) and results were expressed as means of duplicate wells.

3.4.5 Induction of a contact hypersensitivity (CHS) response

CHS was induced by painting shaved mouse abdomen skin with 200 μl 3% oxazolone (4-Ethoxymethylene-2-phenyl-2-oxazolin-5-one, Sigma) diluted in ethanol. After 4 days mice were challenged with 20 μl 1% oxazolone on each side of the right ear. The left ear was painted with

vehicle as a control. Ear thickness was measured every day for nine days. For analysis of the in vivo Th1 response, ear lymph nodes were removed from mice 5 days after challenge, single-cell suspensions were prepared, and intracellular staining of activated $CD4^+$ T cells for IFN-γ was performed as described above.

3.4.6 DSS-induced colitis model

Colitis was induced in wild-type and $Tfam^{-/-}$ mice by daily administration of 3% dextran sodium sulfate (DSS, Mw 30.000–40.000) for 7 days in drinking water. The clinical parameters used to score the disease were weight loss, loose stools/diarrhea and presence of occult/gross bleeding. The animals were weighed before starting the treatment (initial weight) and every day until the end of the treatment. Animals were also checked daily for stool consistency and for the presence of blood in the stools. At the end of treatment, colons were processed for histological analysis to check for the presence of infiltrates in the lamina propia, and mesenteric lymph nodes were processed to study cytokine production of immune cells by flow cytometry.

3.5. Mitochondrial function and metabolic assays

3.5.1 Assessment of mitochondrial membrane potential (Δψm)

The mitochondria-directed, fluorescent sensitive probe JC-1 was used to determine variations in mitochondrial membrane potential ($\Delta\psi_m$) (Solaini et al., 2007) The reversible formation of JC-1 aggregates upon membrane polarization was detected as a shift in emitted light from 520 nm (JC-1 monomeric form, FL1) to 590 nm (JC-1 aggregate, FL2). To assess $\Delta\psi_m$ in stimulated Jurkat T cells or T lymphoblasts, cells preloaded with JC-1 (2 μg/ml) were analyzed by flow cytometry (FACScalibur, Becton Dickinson) and FL1 and FL2 laser emissions were recorded (330 V and 320 V, respectively). The mitochondrial depolarizing agent fluoro-carbonyl cyanide phenylhydrazone (FCCP, 250 nM) was used as a positive control.

$\Delta\Psi_m$ of single mitochondria was assessed as described (Twig et al., 2008). Briefly, mitoYFP-transfected T cells were loaded with 50 nM TMRM, washed twice and allowed to settle on CD3 plus CD28 Ab coated coverslips. A single Z confocal plane was acquired, corresponding to the cell contact with the activating surface, with a TCS SP5 confocal microscope. For every time point, the TMRM and mitoYFP fluorescences were used to determine changes in $\Delta\psi_m$ using the accompanying confocal software (LCS, Leica).

3.5.2 ATP content

ATP content was analyzed in control and Drp1-silenced cells. Cells stimulated with CD3 plus CD28 Abs were treated with vehicle or oligomycin (4 μM). Cells were then stained with MgGr –AM ester (Invitrogen, 5 μM) for 30 min. Emission intensity of the probe increases as a function of free Mg^{+2}, but decreases with ATP content. Global ATP content in T cell lysates from wild-type and $Tfam^{-/-}$ T cells were measured with the ATP luciferase determination kit (Molecular Probes). Mitochondrial derived-ATP synthesis in T cell lysates was measured by a kinetic luminescence assay (Acin-Perez et al., 2014).

3.5.3 Mitochondrial content and ROS

Mitochondrial mass was measured from the fluorescence level after staining with 50 nM Mitotracker green (Life Technologies) for 30 min at 37°C. Mitochondria-associated ROS levels were measured by staining cells with 2.5μM MitoSOX (Life Technologies) for 30 min at 37 °C. Cytosolic ROS was measured with 2',7'-dichlorodihydrofluorescein diacetate (DCFDA; Life Technologies) for 30 min at 37°C. Cells were then washed with PBS and re-suspended in cold PBS containing 1% FBS for flow cytometry analysis. Dead cells were excluded by staining with Hoechst 42 (Sigma).

3.5.4 Blue-native gel electrophoresis and mitochondrial complexes activities

Cellular lysates from wild-type and *Tfam*$^{-/-}$ T lymphocytes were lysed in the presence of digitonin and proteins separated on 5–13% gradient blue-native gels (Lapuente-Brun et al., 2013). The activities of individual complexes were measured spectrophotometrically as previously described (Acin-Perez et al., 2014).

3.5.5 Extracellular flux analysis and metabolic assays

Oxygen consumption rates (OCR) and extracellular acidification rates (ECAR) were measured in a XF-96 Extracellular Flux Analyzers (Seahorse Bioscience) in cells suspended in XF medium (nonbuffered RPMI 1640 containing either 25 mM glucose or 1 mM palmitate, 2 mM L-glutamine, and 1 mM sodium pyruvate). Three measurements were obtained under basal conditions and upon addition of the mitochondrial inhibitors oligomycin (1 μM), to inhibit mitochondrial ATP synthase, FCCP (1.5 μM), to uncouple ATP synthesis from oxygen consumption by the electron-transport chain; and rotenone (100 nM) + antimycin A (1 μM), to inhibit the electron transport chain (all from Sigma). Basal oxygen consumption rate was

established by measurement the OCR in the absence of drugs. ATP was measured with the ATP determination kit (Invitrogen).

3.5.6 Lipidomic analyses

Ultra performance liquid chromatography coupled to mass spectrometry (UPLC-MS) was used for optimal profiling of glycerolipids, glycerophospholipids, sterol lipids and sphingolipids as described in (Barr et al., 2012). Briefly, cells were lysed and proteins precipitated by adding 4 volumes of methanol at room temperature. After brief vortex mixing, chloroform was added to the samples at room temperature. Samples were incubated at -20 °C for 30 min and after brief vortex cell extracts were mixed with water (pH=9). Following brief vortex mixing, the samples were incubated for 1 h at -20 °C and afterwards centrifuged at 16,000 x g for 15 min. The organic phase was collected and dried by speed-vacuum centrifugation. Dried extracts were then reconstituted in acetronitrile/isopropanol (1:1), centrifuged (16,000 x g for 5 min), and transferred to vials for UPLC-MS analysis. Data pre-processing generated a list of chromatographic peak areas for the metabolites detected in each sample injection. Data were normalized using the procedure described in (van der Kloet et al., 2009). Univariate statistical analyses were performed to calculate group percentage changes, and unpaired Student's *t*-test (or Welch's t test where unequal variances were found) was used to compare *Tfam*$^{-/-}$ and wild-type T lymphocytes.

3.5.7 Mitochondrial isolation and immunoblotting.

For mitochondrial fractionation, cells were lysed in ice-cold isotonic sucrose buffer (10 mM Tris pH 7.5, 0.25 M sucrose, 0.1 mM EDTA) containing protease and phosphatase inhibitors (Roche, Basel, Switzerland). Cells were then homogenized using a 23G needle. Lysates were spun at 1000 g (4ºC, 10 min) to remove debris and nuclei, and the supernatant was further centrifuged at 13000 g (4ºC, 30 min) to yield the mitochondrial fraction. Mitochondrial enriched fractions were washed and proteins resolved by SDS-PAGE and transferred to nitrocellulose membranes. After blocking, membranes were blotted with primary and peroxidase-labeled secondary antibodies and detected with western reagents (GE Healthcare, UK) and the LAS-3000 chemiluminiscent system (Fujifilm).

3.6. Immune synapse analysis

3.6.1 Cell conjugate formation

Raji B cells or Hom2 B cells were loaded with the CMAC tracker and incubated with SEE or HA-peptide. T cells ($1x10^5$ cells) were mixed with APC (1:1), centrifuged at low speed to favor conjugate formation, gently resuspended, and plated onto poly-L-lysine(PLL)-coated

slides (50 μg ml^{-1}). Cells were allowed to settle for 30 min at 37ºC, fixed with 4% paraformaldehyde in PBS, and permeabilized with 0.2% Triton X-100 in TBS for 5 min. Cells were processed for immunofluorescence, stained with the indicated primary antibodies (5 μg ml^{-1}) followed by alexa488- or Rhodamine Red X-labeled secondary antibodies (5 μg ml^{-1}), and mounted in Prolong antifade medium (Invitrogen).

For time-lapse confocal microscopy analysis, Raji APCs ($5x10^5$; SEE-pulsed or unpulsed) were allowed to adhere to PLL coated coverslips in Attofluor open chambers (Invitrogen) at 37ºC in a 5% CO_2 atmosphere. T cells were added (1:1 ratio) and a series of fluorescence and differential interference contrast frames were captured using a TCS SP5 confocal laser scanning unit attached to an inverted epifluorescence microscope (DMI6000) fitted with an HCX PL APO 63x/1.40-0.6 oil objective. Images were acquired and processed with the accompanying confocal software (LCS; Leica).

3.6.2 CD3, MTOC and mitochondria translocation

To measure the maximum diameter of CD3 clusters, J77 T cells were preincubated at 37ºC, 4h with 200nM FCCP (Fluka, Germany), 50μM mdivi-1, 4 μM oligomycin or DMSO (Sigma-Aldrich), and then incubated 30 min with SEE-pulsed or unpulsed CMAC-loaded Raji B cells. CD3 maximum diameter was quantified in 3 independent experiments using ImageJ software.

CD3 organization at the IS was analyzed in APC-conjugated control and Drp1-silenced T cells. 3D Z-stacks of the cell-cell contact area were reconstructed, and maximum diameter and the number of CD3 clusters were quantified in 15-20 conjugates in at least 3 independent experiments.

CD3, mitochondria, Drp1 and pMLC accumulation at the IS was quantified in J77 or CH7C17 T cells conjugated with antigen-pulsed or non-pulsed Raji or Hom2 cells loaded with CMAC. For quantification in individual ISs we used a home-made plugin for Image J software (http://rsbweb.nih.gov/ij/) called "*Synapse Measures*". By comparing fluorescence signals from multiple regions of the T cell, APC, IS, and background fluorescence, the program yields accurate measurements of localized immunofluorescence. A detailed description of *Synapse Measures*, including the algorithms used, is described (Calabia-Linares et al., 2011).

The proportion of conjugates showing redistribution of the T cell MTOC close to the APC contact area was determined as described (Ibiza et al., 2006).

Mitochondrial accumulation at the IS was calculated as the ratio of the FI of T cell mitochondria located in the third of the cell near the APC contact area to the FI of the mitochondria in the rest of the cell.

3.6.3 Time-lapse fluorescence confocal microscopy and total internal reflection fluorescence microscopy (TIRFM)

Activating planar lipid bilayers were formed in FCS2 flow chambers as previously described (Carrasco et al., 2004; Grakoui et al., 1999). Briefly, unlabeled GPI-linked ICAM-1 liposomes and biotinylated lipids were mixed with 1,2-dioleoyl-PC (DOPC) lipids (Avanti Polar Lipids, Inc.) to obtain the molecular density required. The chambers were then blocked with 2% FCS in PBS and loaded with streptavidin labeled AlexaFluor-647 and monobiotinylated T3b Ab as surrogate antigen. T cells were injected into the warmed chamber (37ºC) at time zero, and were imaged with a Zeiss Axiovert LSM 510-META inverted microscope fitted with a 40x oil objective and analyzed with LSM 510 software (Zeiss, Germany) and ImageJ software.

For TIRFM, J77 T cells transfected with mitoYFP were allowed to settle onto CD3 plus CD28 coated coverslips in Attofluor open chambers (Invitrogen), and mitochondria were visualized with a Leica AM TIRF MC M mounted on a Leica DMI 6000B microscope. Images were acquired and processed with the accompanying confocal software (LCS; Leica).

3.7. Calcium measurements

3.7.1 Calcium measurement in T cell-APCs conjugates.

J77 cells were loaded with Fluo-4 AM (2μM) in HBSS containing 20 mM HEPES for 30 min at 37ºC washed in 10% FCS RPMI medium and then in HBSS containing 20 mM HEPES and 1% FCS. Cells in 20 mM HEPES, 1% FCS HBSS were settled onto MatTek glass bottom dishes and CMAC-loaded Raji APCs were added at a 1:1 ratio. After 1 min of baseline recording, images were acquired every 15 s, using a TCS SP5 confocal laser scanning unit attached to an inverted epifluorescence microscope (DMI6000) fitted with an HCX PL APO 40x/1.40-0.6 oil objective. The 488 nm argon laser line was used to excite fluo4 fluorescence, which was measured using a band-pass filter from 505 to 550 nm and digitized to 12 bit resolution. Images were acquired and processed with the accompanying confocal software (LCS; Leica). The results are expressed as the fold increase in mean Fluo4 fluorescence intensity relative to the time before the T-APC stable contact. Ionomycin (0.5 μg/ml) was used as a positive control.

3.7.2 Intracellular calcium levels by Flow Cytometry

To track intracellular calcium levels, cells were incubated with Indo-1 (5 μg/ml) in pre-warmed HBSS containing 10 mM HEPES and 1%FCS. After 30 min at 37ºC cells were washed and resuspended in HBSS containing 1% FCS, and protected from light at room temperature for 15 min. Pre-warmed cells were activated with CD3 Ab (10 μg/ml). $Ca^{2+}{}_i$ flux was measured as

the ratio of emission at 395-415 nm to 500-520 nm over time using an FACSCanto system (BD Biosciences), and analyzed with Flow-Jo Software. Ionomycin (0.5 μg/ml) was used as a positive control.

3.7.3 Lysosomal calcium measurement by Flow Cytometry

Lysosomal calcium was measured with the membrane-permeable calcium indicator Indo-1 (Invitrogen). Cells were loaded as recommended by the manufacturer for 30-60 min at 20 °C, washed and calcium release assessed from the Indo-1 fluorescence intensity ratio at 340/380 nm, detected by flow cytometry on a FACSCanto flow cytometer equipped with a 355 laser. After basal recording, cells were treated with bafilomycin-A1 to promote lysosomal calcium release as described (Lloyd-Evans et al., 2008) for the indicated times. Results are expressed as the increase in the Indo-1 signal in bafilomycin A1- or ionomycin-treated cells relative to their basal levels.

3.8. Electron microscopy

Mitotracker Orange-loaded T cells, treated with vehicle (DMSO) or mdivi-1 inhibitor for 4 h, were conjugated with CMAC-loaded, SEE-pulsed Raji cells (APC) for 30 min on poly-L-Lys-coated coverslips (Bellco). Conjugates were fixed in 2.5% glutaraldehyde (Sigma-Aldrich) in PBS for 15 min, washed, and treated with 1% osmium tetroxide (Sigma-Aldrich) for 45 min. Samples were extensively washed with water and dehydrated through increasing concentrations of ethanol (25%, 50%, 75%, 95% and absolute). Samples were then embedded in DURCUPAN resin (Fluka) and stored overnight at room temperature. The resin column was polymerized by baking at 60ºC for 48 h, and ultrathin sections were cut and contrasted. Sections were examined with a JEOL JEM1010 electron microscope (100KV) equipped with a BioScan digital camera (Gatan). Images were monitored with DigitalMicrograph 3.1 (Gatan). T cell mitochondria perimeter, area and distance from the IS were analyzed with ImageJ software.

Wild-type and *Tfam*$^{-/-}$ lymphoblasts and Jurkat T cells stably transfected with shControl and shTfam were fixed in 2.5% glutaraldehyde (Sigma-Aldrich) in PBS for 15 min, washed, and treated with 1% osmium tetroxide (Sigma-Aldrich) for 45 min. Samples were extensively washed with water and dehydrated through increasing concentrations of ethanol (25%, 50%, 75%, 95% and absolute). Samples were then embedded in DURCUPAN resin (Fluka) and stored overnight at room temperature. The resin column was polymerized by baking at 60°C for 48 h, and ultrathin sections were cut and contrasted. Sections were examined with a JEOL JEM1010 electron microscope (100 KV) equipped with a BioScan digital camera (Gatan). Images were monitored with DigitalMicrograph 3.1 (Gatan).

3.9. Exosome analysis

3.9.1 Exosome purification and sucrose gradient purification

Cells were cultured in RPMI medium supplemented with 10% exosome-depleted FBS (depleted of bovine exosomes by overnight centrifugation at 100,000 *g*). Supernatant fractions were collected from 16-20 h cell culture supernatants from equal number of cells, and exosomes were obtained by serial centrifugation as described (Thery et al., 2006). Briefly, cells were pelleted (320 *g* for 10 min) and the supernatant was centrifuged at 2,000 *g* for 15 min to discard debris and dead cells. Supernatant was collected, ultracentrifuged at 10,000 *g* for 30 min at 4 ºC (Beckman Coulter Optima L-100 XP, Beckman Coulter) and exosomes were pelleted by ultracentrifugation at 100,000 *g* for 70 min at 4 °C. The exosome pellet was washed in PBS and collected by ultracentrifugation at 100,000 *g* for 70 min. For sucrose density gradient, isolated exosomes were layered on the top of a discontinuous sucrose gradient and centrifuged with a SW40 rotor at 192,000 *g* and 4 °C for 18-20 h. Sucrose gradient fractions were prepared in a SW40 centrifuge tube (14 x 95 mm; Beckman Coulter), ranging from 2.5 M at the bottom to 0.4 M at the top. Fractions of 1 mL were collected from the top of the gradient and vortexed. Exosomal proteins were extracted by precipitation with 1:1 ice-cold acetone for at least 2 h at -20 ºC. Samples were then centrifuged and resuspended in an equal volume of loading buffer for analysis by western blot.

3.9.2 Nanoparticle Tracking Analysis (NTA)

Exosome number and size-distribution were analyzed by measuring the rate of Brownian motion using the NanoSight LM10 system, which is equipped with fast video capture and particle-tracking software (NanoSight, Amesbury, U.K.). Samples were diluted before analysis to 2 x 10^8 to 20 x 10^8 particles ml^{-1} and the relative concentration was calculated according to the dilution factor. Briefly, 0.5 ml of diluted supernatant was loaded into the sample chamber of an LM10 unit (Nanosight, Malvern Instruments) and three 30 second videos were recorded of each sample. Data were analyzed with *NTA 2*.1 software (Nanosight). Samples were analyzed using manual shutter and gain adjustments, resulting in shutter speeds of 15 or 30 milliseconds and camera gains between 280 and 560. The detection threshold was kept above 2; blur was set to auto; and minimum expected particle size was set to 50 nm.

3.10. Cell and exosome western blot analysis

Cells or exosome preparations were lysed in 50 mM Tris pH 7.5, containing 0.3 M NaCl, 0.5% Triton X-100, 0.1% NP-40, and a cocktail of protease inhibitors (Roche). Cell lysates were cleared of nuclei by centrifugation at 15,000 *g* for 10 min. Protein extracts from cells or exosomes were separated by 4–12% SDS–PAGE and transferred to a nitrocellulose membrane (Biorad). Proteins were visualized with LAS-3000 after membrane incubation with specific antibodies (5 μg ml^{-1}) and secondary antibodies conjugated to peroxidase (5 μg ml^{-1}). Band intensities were quantified using ImageJ software (NIH) and results are expressed relative to controls.

3.11. Quantitative real-time-PCR and mtDNA content analysis

Total RNA was extracted from cells using the RNeasy kit (QIAGEN) and cDNA was synthesized with the High Capacity cDNA Reverse Transcription Kit (Applied Biosystems). Triplicate reactions were run on a 7500 Fast Real Time PCR System (Applied Biosystems) using SYBR Green PCR reagents (Applied Biosystems). The expression of mRNA for genes of interest was normalized to the expression of β-actin and beta-2-microglobulin. Data were analyzed using Biogazelle QBasePlus software (Biogazelle). For analysis of mtDNA levels, total DNA was extracted with the DNeasy kit (QIAGEN). mtDNA was amplified using primers specific for the genes for mitochondrial cytochrome c oxidase subunit 1 (mtCO1) and mitochondrially encoded NADH dehydrogenase 1 (mtND1) and normalized to genomic DNA by amplification of the succinate dehydrogenase (SDH) nuclear gene.

3.12 Confocal microscopy analysis of autophagy and mitophagy

For autophagosome-lysosome fusion assays, shControl and shTfam Oli-Neu cells were transfected using Lipofectamine (Invitrogen) with LC3-GFP-RFP, and left untreated or treated with Rapamycin (Sigma) during 3 hr and LC3- GFP-RFP fluorescence was examined with a Leica SP5 confocal microscope (Leica) fitted with a 63X objective. Cells were acquired with the same laser parameters using the same image magnification. Images were processed and assembled using Leica software. The number of GFP, RFP and GFP- RFP-positive autophagosomes were analyzed using Image J imaging software (NIH). For mitophagy assays, shControl and shTfam Oli-Neu cells transfected with Parkin-GFP were left untreated or treated with carbonyl cyanide m-chlorophenyl hydrazone (CCCP, Sigma) during 3 hr and Parkin-GFP fluorescence was examined with a Leica SP5 confocal microscope (Leica) fitted with a 63X objective. Images were processed and assembled using Leica software and the area of Parkin-GFP fluorescence was analyzed with Image J imaging software (NIH).

3.13. Statistical analyses

Data were tested for normality using the D'Agostino-Pearson omnibus normality test, or the Kolmogorov-Smirnov test when the sample was small due to experimental conditions. Differences between means were tested by Student's *t* test for normal data, whereas non-normal data were analyzed by the Mann-Whitney test. Data from multiple groups were analyzed by ANOVA followed by Newman-Keuls multiple comparison test.

All values were expressed as the mean ± s.e.m. Samples were analyzed using Student's *t*-test for two groups and ANOVA for multiple groups. For *in vitro* experiments, statistical analyses were calculated with a paired Student's *t*-test; for *in vivo* experiments, differences between groups were calculated using the Mann–Whitney U test for unpaired data (GraphPad Prism version 5.0). Differences were considered significant when * $p \leq 0.05$, ** $p \leq 0.01$, *** $p \leq 0.001$.

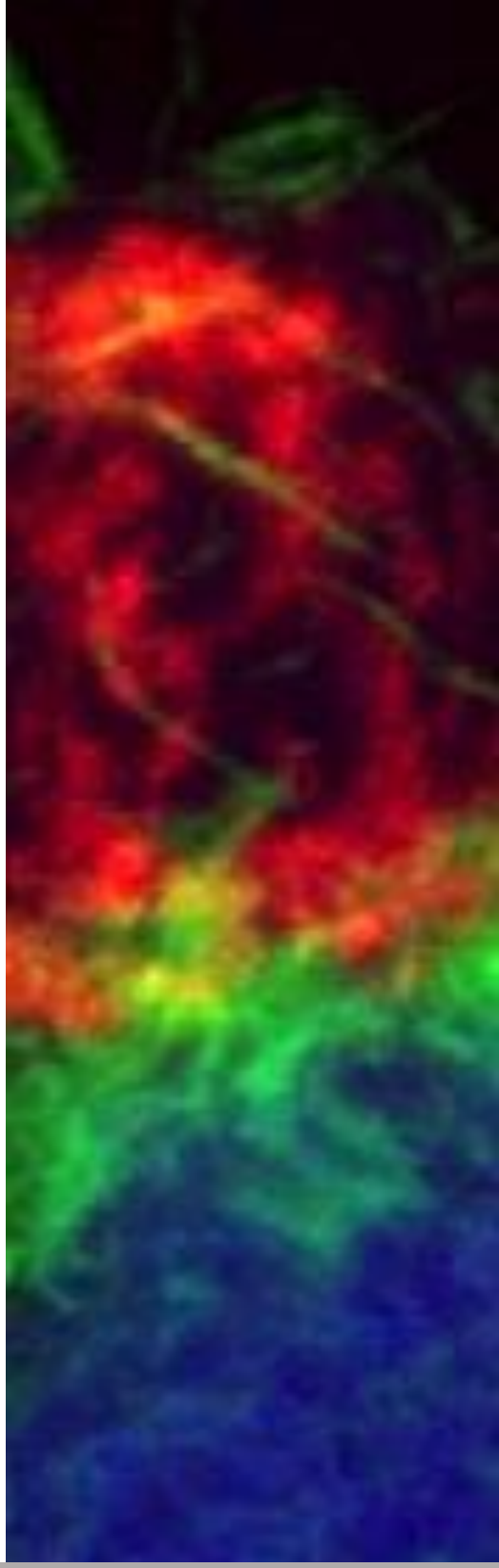

Results

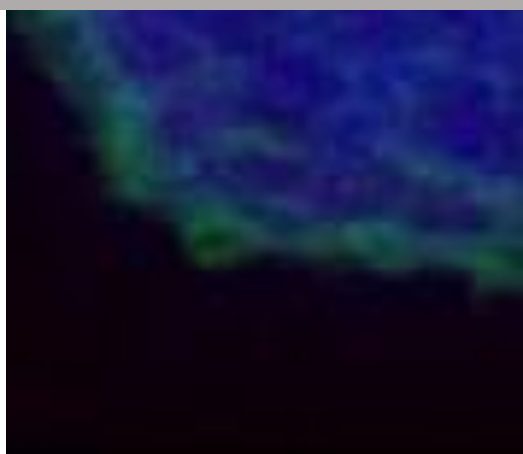

4. RESULTS

4.1 T cell activation promotes mitochondrial translocation toward the pSMAC

We first assessed the precise localization of mitochondria during IS formation by confocal microscopy of Jurkat T cells conjugated with superantigen-E (SEE)-pulsed Raji cells or hemagglutinin peptide (HA)-pulsed HOM2 B cells as antigen-presenting cells (APC). In both experimental systems of cell activation, most T cell mitochondria moved in an orchestrated manner toward the IS, where the microtubule-organizing center (MTOC) and the TCR/CD3 cluster were situated (Figure R1A-C). These synaptic mitochondria surrounded the central TCR/CD3 cluster and were located beneath the actin ring at the pSMAC (Figure R1D and R1E).

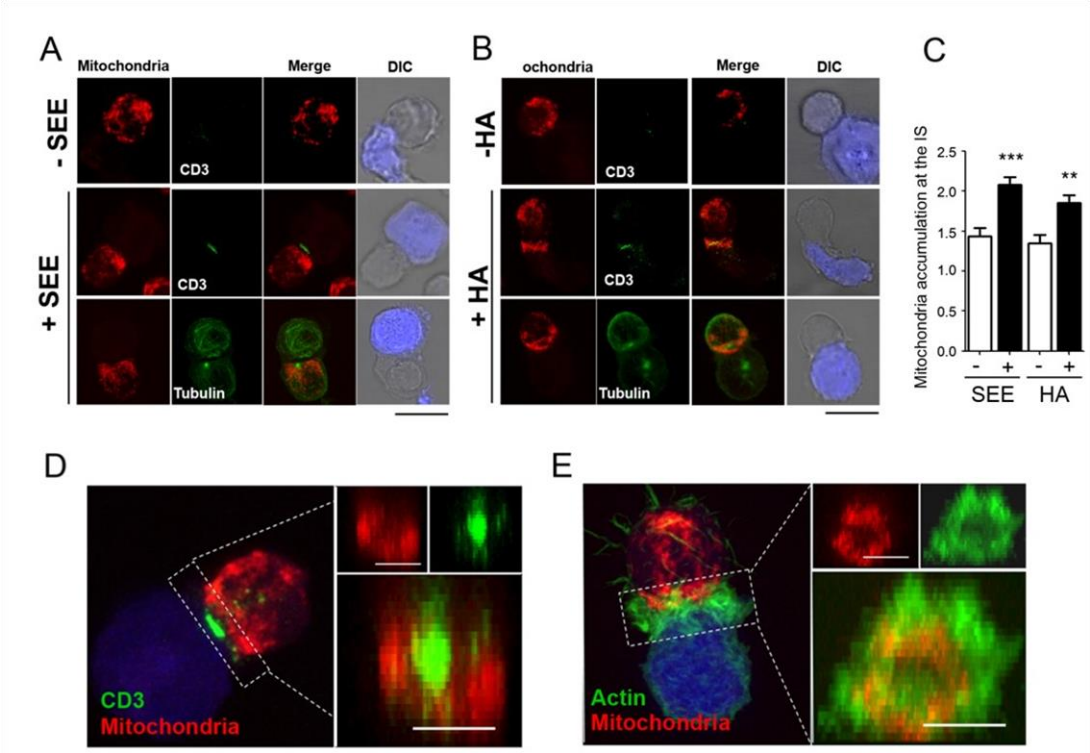

Figure R1. Mitochondria translocate toward the pSMAC upon T cell activation. (**A**) J77 T cells loaded with Mitotracker Orange (red) were conjugated with unpulsed or SEE-pulsed Raji B cells loaded with CMAC (blue). Cells were stained with anti-CD3 or tubulin-FITC (green) to reveal TCR clustering and MTOC orientation. (**B**) Analysis as in **A** of HA-specific CH7C17 T cells conjugated with unpulsed or HA-pulsed Hom2 APCs. Scale bars, 10 µm. (**C**) Mitochondrial accumulation at the IS of conjugates stimulated as in **A** and **B**. (**D**,**E**) Maximum projection of a confocal Z-stack of conjugates stimulated as in **A**. Cells were stained with CD3 Ab (**D**) or phalloidin (green) (**E**) to determine the areas of the cSMAC and pSMAC. Right panels show maximal projection of 3D-reconstructions from the IS. Scale bars, 5 µm.

The kinetics of mitochondria translocation during IS formation was studied in human primary T lymphoblasts plated onto planar lipid bilayers containing GPI-linked ICAM-1 and anti-human CD3 antibody. CD3 microclusters appeared early at the periphery of the IS structure, and then moved centripetally to form the cSMAC (Figure R2A). Simultaneously with the redistribution of CD3 to form a central cluster, mitochondria spread near the cell-bilayer interface during the first 3 min after plating and then relocated toward the pSMAC to form a ring around the TCR/CD3 central cluster (Figure R2A and R2B). This mitochondrial reorganization was also analyzed by total internal reflection fluorescence microscopy (TIRFM), revealing movement of mitochondria from the periphery of the contact area toward the center of the IS (Figure R2C). Although some mitochondria appeared to move in and out of the cSMAC, most were localized at the pSMAC. These results indicate that during the formation of the IS mitochondria relocate to form a ring-shaped structure at the pSMAC of the IS.

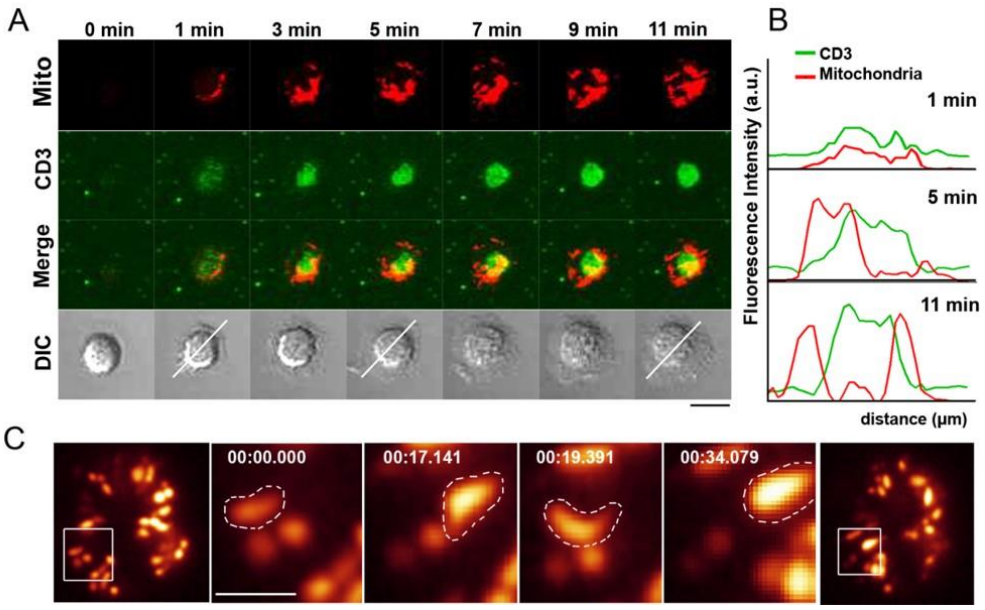

Figure R2. Mitochondria move centripetally toward the pSMAC. (**A**) Migration of mitochondria toward the IS in mitotracker-preloaded human T lymphoblasts adhered to GPI-linked ICAM-1 and anti-CD3-containing lipid bilayers. CD3 clusters (green) and mitochondria (red) were detected by confocal microscopy at the indicated times on a single confocal plane. Scale bar, 5 μm. (**B**) Fluorescence intensity profiles from A show the pSMAC localization of mitochondria at the indicated times. (**C**) TIRF microscopy of mitoYFP expressing T cells plated on a CD3 plus CD28 Ab surface. Magnified views show forward-backward movement of a mitochondrion at the edge of the contact with the activating surface. Scale bar, 1 μm.

4.2 Drp1 regulates mitochondrial positioning at the Immune Synapse (IS) and IS architecture

The mitochondrial fission factor Drp1 is a key component of the mitochondrial dynamics machinery (Chen et al., 2010). Previous studies showed that dissociation of Drp1 from mitochondria occurs concomitantly with mitochondrial mislocalization (Varadi et al., 2004), suggesting that Drp1 may play a role in mitochondrial redistribution and positioning in highly polarized cells. We therefore studied whether, in response to antigen-pulsed APC, Drp1 associates with mitochondria in T cells and enables their translocation and positioning at the IS. Double immunofluorescence microscopy analysis showed that Drp1 localized with mitochondria at the IS of T cells conjugated with SEE- or HA-pulsed APC (Figure R3A-C). Accordingly, cell fractionation analysis confirmed recruitment of Drp1 to mitochondria in antigen-specific T cell-APC conjugates (Figure R3D and R3E) but not in the absence of antigen (not shown).

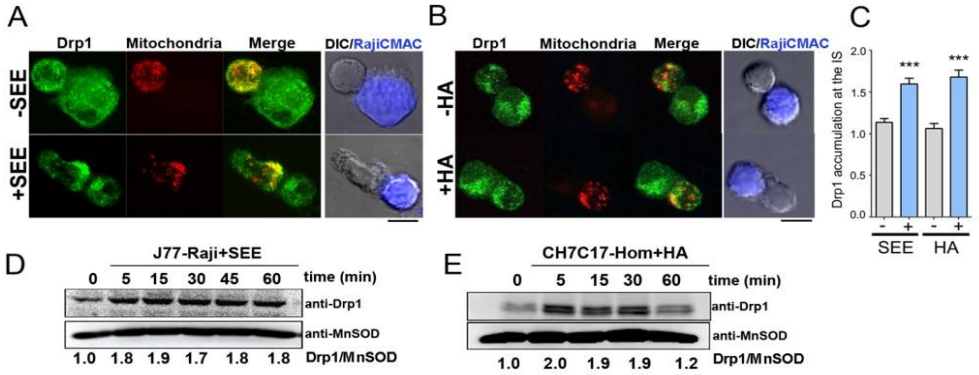

Figure R3. Drp1 is recruited to mitochondria upon T cell-APC conjugates. Immunofluorescence localization of Drp1 (green) in mitotracker-loaded T cells (red) conjugated with unpulsed or antigen-loaded APCs (CMAC-loaded, blue): (**A**) J77 T cells plus SEE-pulsed Raji B cells; (**B**) CH7C17 T cells plus HA-pulsed Hom2 cells. (**C**) Endogenous accumulation of Drp1 at the IS in T cell-APC conjugates. Maximum projections of a confocal Z stack were quantified. Data are means ± s.d. of 60 conjugates from two independent experiments. (**D,E**) Time course of Drp1 content in the mitochondrial fractions of APC-activated J77 and CH7C17 T cells. MnSOD was used as mitochondrial marker.

To determine whether Drp1 drives the redistribution of mitochondria toward the IS, we silenced Drp1 expression in J77 T cells using Drp1-specific siRNAs (Figure R4A) and studied the localization of their mitochondria in antigen-specific conjugates with APC. Mitochondrial translocation towards the IS was reduced in Drp1 knockdown J77 T cells stimulated with SEE-pulsed Raji B cells (Figure R4B and R4C). Interestingly, under these experimental conditions,

MTOC translocation was unaffected (Figure R4C). The expression of YFP-fused wild-type Drp1 (Drp1WT-YFP) in Drp1 knockdown J77 T cells restored SEE-dependent mitochondrial translocation (not shown), confirming that Drp1 silencing specifically interfered with this process.

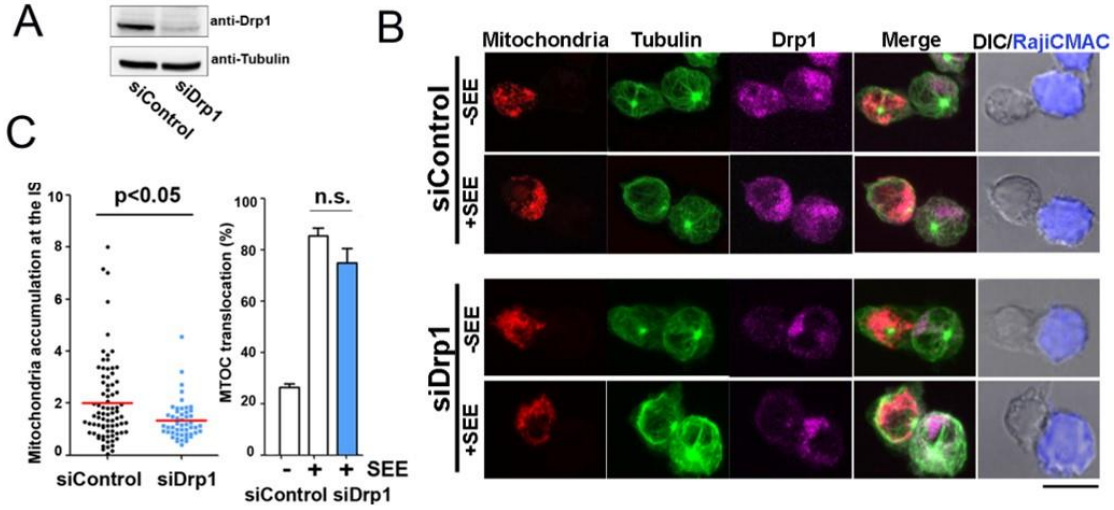

Figure R4. Drp1 regulates mitochondrial positioning at the IS. (**A**) Western blot analysis of siRNA Drp1 silencing in J77 T cells after 48 h. (**B**) Confocal localization of mitochondria (mitotracker, red), MTOC (tubulin, green) and endogenous Drp1 (purple) in J77 T cells conjugated with Raji B cells (CMAC-loaded, blue). Scale bar, 10 µm. (**C**) Mitochondrial accumulation and MTOC positioning at the IS. Data in **C** represent means ± s.d. of 60 conjugates from three experiments ($p<0.05$, Mann Whitney test).

The above results suggest that Drp1 regulates mitochondrial localization directly by acting on mitochondria dynamics. To assess this, we uncoupled Drp1 from mitochondria by two approaches: overexpression of a phosphomimetic S637D mutant of Drp1 (Drp1S637D-YFP) or treatment of cells with mitochondrial division inhibitor-1 (mdivi-1). These approaches prevent Drp1 docking at the mitochondrial outer membrane and consequently reduce mitochondrial fission (Cassidy-Stone et al., 2008; Cereghetti et al., 2008; Tanaka and Youle, 2008). Expression of Drp1S637D-YFP reduced SEE-induced mitochondrial redistribution compared with overexpression of Drp1WT-YFP or a non-phosphorylable Drp1 mutant (Drp1S637A-YFP) (not shown). Similar results were obtained when T cells were treated with mdivi-1 (Figure R5A and R5B). Transmission electron microscopy (TEM)-based morphometric studies of T cell-APC conjugates revealed that mitochondria in mdivi-1-treated cells were farther from the IS and were enlarged in area and perimeter compared with control cells (Figure R5C and R5D).

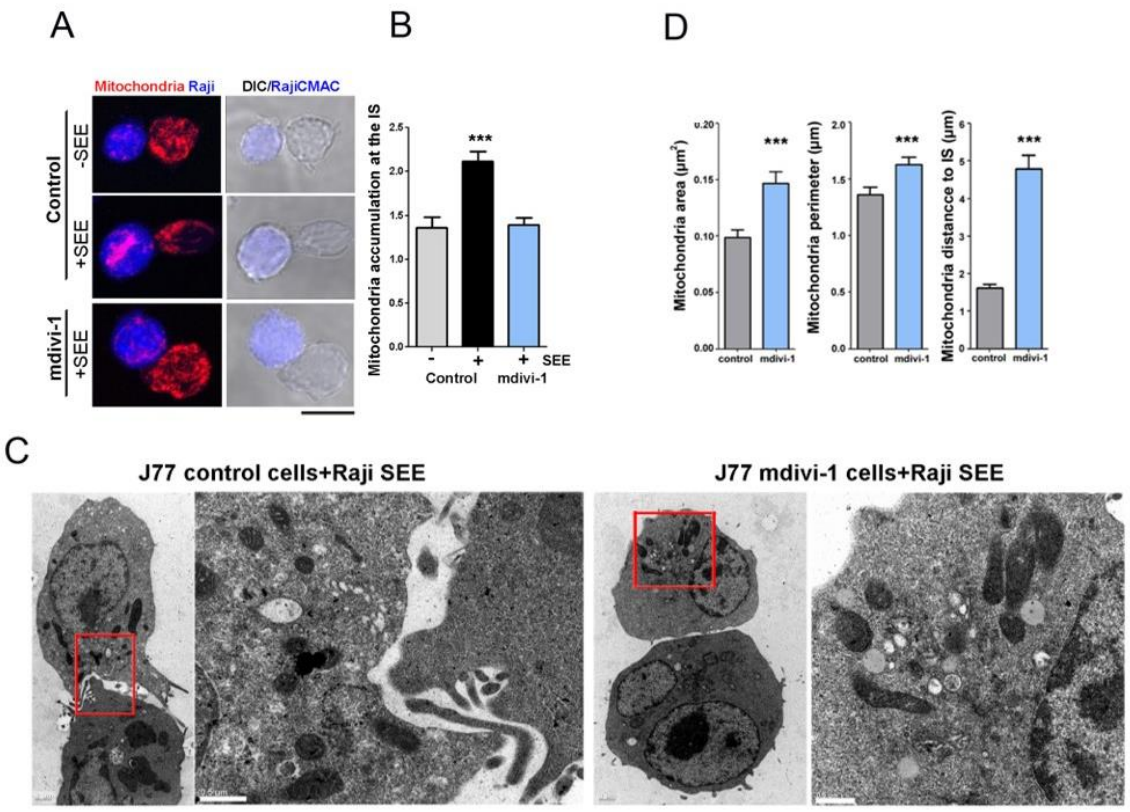

Figure R5. Drp1-mediated mitochondrial fission regulates translocation of mitochondria toward the IS. (**A**) Confocal localization of mitochondria (MnSOD, red) in J77 conjugated with Raji B cells (CMAC-loaded, blue) under the indicated treatments. Scale bar, 10 µm. (**B**) Mitochondria accumulation at the IS (248 control and 100 mdivi-1-treated conjugates, *** $p<0.001$. (**C**) Transmission electron microscopy images from J77-Raji B cell conjugates. Right, magnified views of mitochondria. (**D**) Mitochondria distance to the IS and morphometric analysis (109 mitochondria in ten control conjugates and 89 mitochondria from seven mdivi-1–treated conjugates, * $p<0.05$).

To determine whether Drp1-mediated mitochondrial redistribution and positioning at the pSMAC is important for IS organization, we studied the effect of Drp-1 silencing on CD3 assembly at the cSMAC. Although Drp1 knockdown did not alter the expression levels of CD3 or LFA-1 on the plasma membrane of J77 T cells (data not shown), the central clustering of TCR/CD3 at the IS was inhibited (Figure R6A and R6B). 3D-reconstruction of the IS formed by Drp1-silenced J77 cells and SEE-pulsed APCs revealed a scattered distribution of CD3, an enlarged cSMAC diameter and an increased number of CD3 clusters (Figure R6C-6F). Consistently, in planar lipid bilayer assays, Drp1-silenced cells did not form a cSMAC, and CD3 microclusters were unable to coalesce at the center of the IS. In these cells, in contrast with control cells, mitochondria did not relocate to the IS and did not form a ring-shaped structure around the

cSMAC (not shown). These results indicate that Drp1 plays an important role in the formation of the IS, linking mitochondrial positioning to the molecular organization of CD3 at the cSMAC.

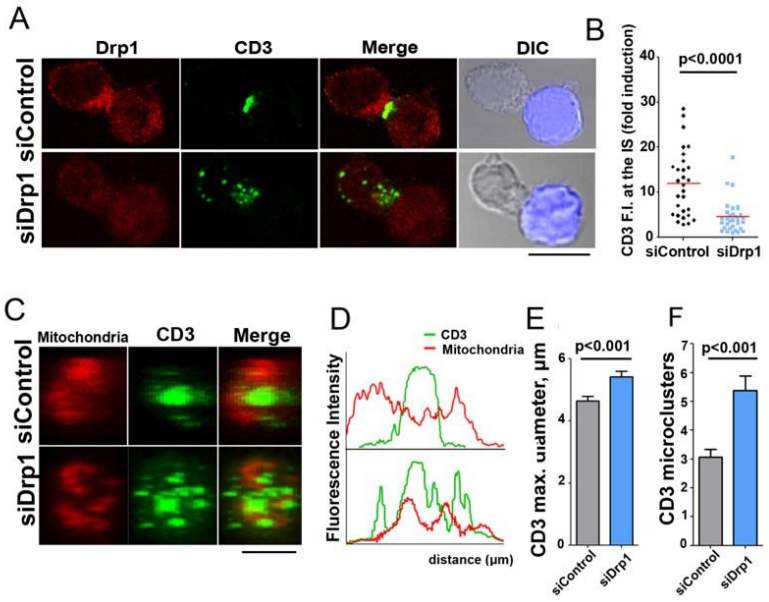

Figure R6. Drp1 controls IS organization. (**A**) Distribution of Drp1 (red) and CD3 (green) in J77 T cells conjugated with Raji B cells (CMAC-loaded, blue). Scale bar, 10 µm (**B**) CD3 accumulation at the IS calculated from maximal confocal Z projections ($p<0.0001$, Mann Whitney test) (**C**) 3D reconstructions of the cell-cell contact area in J77-APC conjugates. Scale bar, 5 µm. (**D**) Profile plot of CD3 (green) and mitochondria (red) in the structures depicted in **C**. (**E**,**F**) CD3 diameter and cluster number calculated from 3D reconstructions of T cell-APC contacts. Data are means ± s.d from three independent experiments, $p<0.001$, Student's *t* test.

4.3 Mitochondria depolarize at sites of TCR activation

To explore the mechanism by which Drp-1-mediated mitochondrial redistribution regulates cSMAC assembly, we assessed mitochondrial function and energy status in activated T cells. We first monitored mitochondrial membrane potential ($\Delta\psi_m$) by time-lapse confocal microscopy of J77 T cells expressing MitoYFP and labeled with the potentiometric dye TMRM. When these cells were plated onto CD3/CD28 Ab activating surfaces, the mitochondria closest to the bottom surface abruptly depolarized as indicated by the drop in TMRM fluorescence (Figure R7A), whereas plating onto poly-L-lysine plus control Ab had no effect (not shown). These results were confirmed by flow cytometry of whole cell populations labeled with the mitochondria-specific cation tracker JC-1. The JC-1 emission maximum at high $\Delta\psi_m$ is 590 nm (red, detected in FL2) and shifts to 520 nm (green, detected in FL-1) as $\Delta\psi_m$ decreases (Solaini et al., 2007).

Using this label, we found that CD3/CD28 engagement diminished $\Delta\psi_m$ in human primary T lymphoblasts whereas mitochondrial depolarization was significantly enhanced in Drp1-silenced cells, even in the absence of stimulation (Figure R7B and R7C).

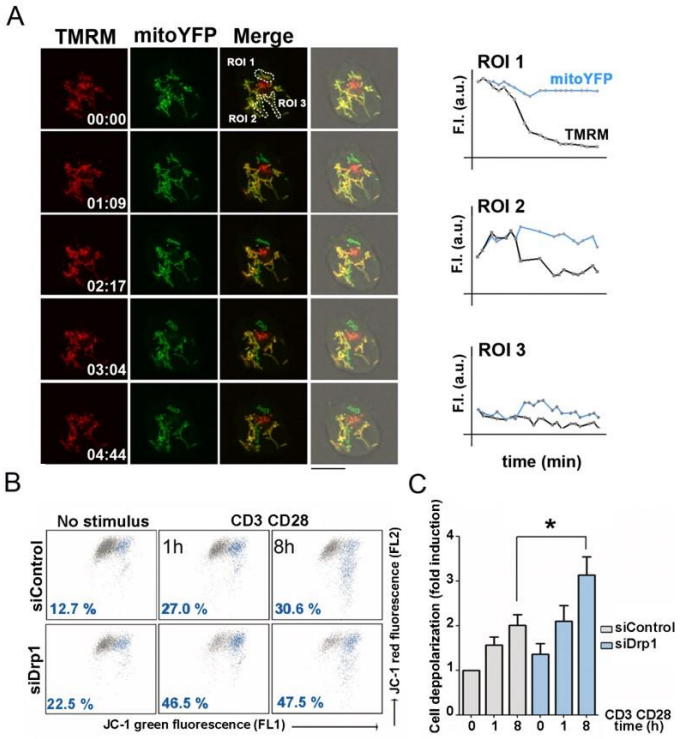

Figure R7. Mitochondria depolarize at sites of TCR activation. (**A**) Time-lapse confocal microscopy of mitoYFP-J77 T cells loaded with TMRM and plated on anti-CD3/CD28 coated coverslips. Profile plots show variations in fluorescence intensity in the indicated mitochondria (regions of interest, ROI). (**B**,**C**) JC-1 flow cytometry analysis of mitochondrial membrane potential (FL2 vs. FL1) in human T lymphoblasts. Percentage of cells with depolarized mitochondria (blue) is indicated. Data are means ± s.d. from four donors (* $p<0.05$).

4.4 Drp1 regulates myosin fueling at the IS

We next assessed the effect of CD3/CD28 engagement on T lymphoblast intracellular ATP levels. ATP content increased in activated T cells with respect to untreated cells, an effect reverted by the mitochondrial ATP-synthase inhibitor oligomycin (not shown). In contrast, CD3/CD28 stimulation did not significantly change ATP levels in Drp1-interfered cells (not shown). Mitochondrial membrane potential and ATP production are thus compromised in Drp1 silenced T cells during activation, suggesting a role for Drp1 in the regulation of IS organization through the control of mitochondrial function. To test this possibility, T cells were treated with the mitochondrial uncoupling agent FCCP (which abolishes ψ_m), the ATP synthase inhibitor oligomycin, or the mitochondrial fission inhibitor mdivi-1. Treatment of SEE-specific T cell-APC conjugates with any of these agents inhibited clustering of CD3 at the IS to a similar extent as Drp1 silencing (Figure R8A and R8B), thus linking Drp1-dependent mitochondrial function and depolarization to IS organization.

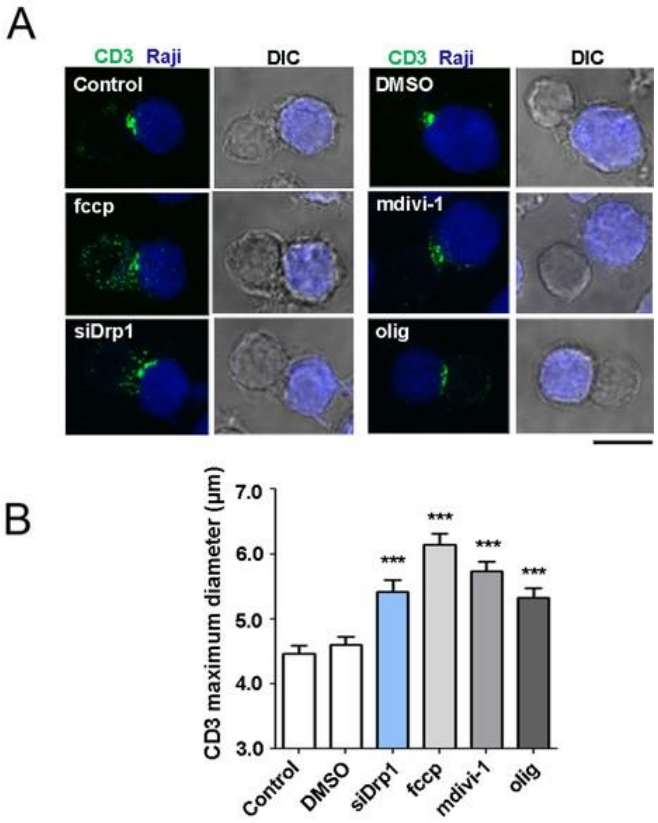

Figure R8. Mitochondrial depolarization impairs TCR clustering at the IS. (**A**) Confocal analysis of CD3 organization (green) in conjugates formed by control, Drp1-silenced, or J77 T cells treated with mdivi-1, FCCP, oligomycin or vehicle. SEE-pulsed Raji B cells, CMAC (blue). Scale bar, 10 µm. (**B**) CD3 maximum diameter in J77 T cells conjugated as in A: The numbers of conjugates analyzed 409 (control), 136 (siDrp1), 313 (midiv-1), 339 (FCCP) and 230 (oligomycin). Data are means ± s.d from three independent experiments (*** $p<0.001$).

Consistent with these results, myosin activation, an ATP-dependent process involved in IS formation (Ilani et al., 2009), was impaired in Drp1-silenced T lymphoblasts and J77 cells, which showed lower levels of myosin regulatory light chain (MLC) phosphorylation at Ser19 than control cells (Figure R9A and R9B). MLC phosphorylation in SEE-specific T cell-APC conjugates mostly took place at the IS of control T cells, and was strongly reduced by Drp1 silencing (Figure R9C and R9D). Given that phosphorylation of MLC at Ser19 increases the motor activity of myosin (Huttenlocher et al., 1995), and that myosin IIA localizes at the IS of T cells (Ilani et al., 2009), our results strongly suggest that ATP-dependent myosin contractile activity is diminished at the IS of Drp1-silenced T cells. Together these results support that Drp1 regulates mitochondrial-dependent myosin fueling at the IS by impeding persistent mitochondrial depolarization and thereby favoring ATP synthesis.

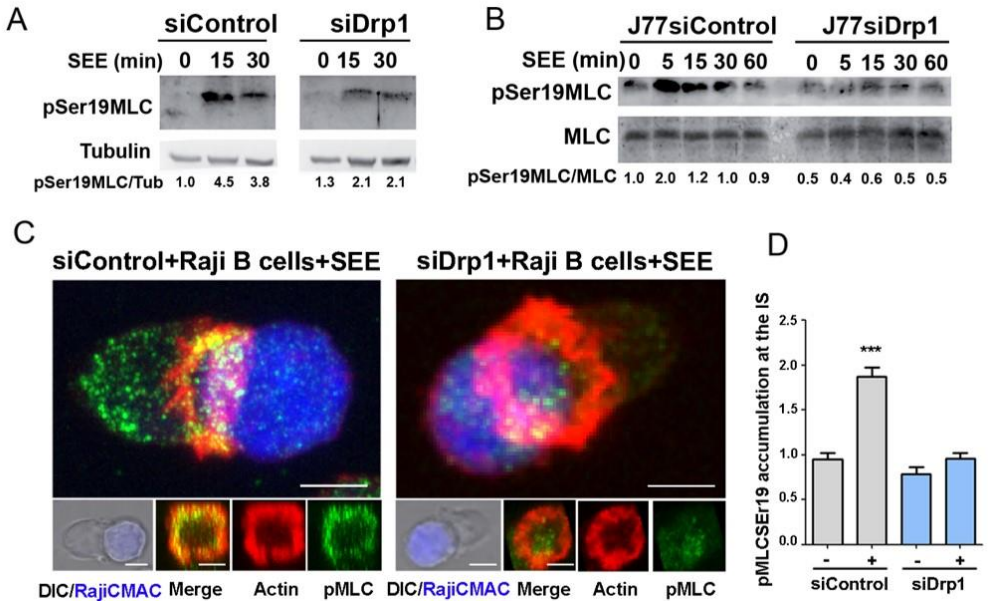

Figure R9. Drp1 regulates myosin fueling at the IS. Phosphorylation of MLC at Ser 19 in conjugates formed between human T lymphoblasts (**A**) or J77 T cells (**B**) and SEE-pulsed Raji B cells. MLC and tubulin are shown as loading controls. (**C**) Confocal analysis of pMLCSer19 (green) and actin (red) in J77 T cells conjugated with Raji B cells (CMAC, blue). 3D stack reconstructions show pMLCSer19 and the actin ring at the T cell-APC contact site. (**D**) pMLCSer19 accumulation at the IS in SEE-specific conjugates. Data are means ± s.d from two independent experiments (*** $p<0.001$).

4.5 Drp1 modulates TCR signal strength

We next assessed the role of Drp1 in TCR/CD3 signaling. Microclusters of tyrosine-phosphorylated proteins were peripherally distributed in the IS of Drp1-silenced T cell-APC conjugates, contrasting with their concentration at the cSMAC in control conjugates (Figure R10A). Drp1 silencing provoked dispersal of the phospho-ERK signal at the SEE-dependent IS (Figure R10B) and a longer-lasting phosphorylation of ERK1/2 and PLC-γ1 in SEE stimulated primary T lymphoblasts and J77 T cells (Figure R10C and R10D). Moreover, $Ca^{2+}{}_i$ flux was also maintained for longer in Drp1-silenced J77 T cells upon conjugation with SEE-pulsed Raji APCs (not shown). Finally, Drp1 silencing increased the secretion of IL-2 in SEE-dependent T cell-APC conjugates (not shown). These results suggest that Drp1 modulates TCR proximal signaling and IL-2 production through the control of mitochondria positioning and activity at the IS.

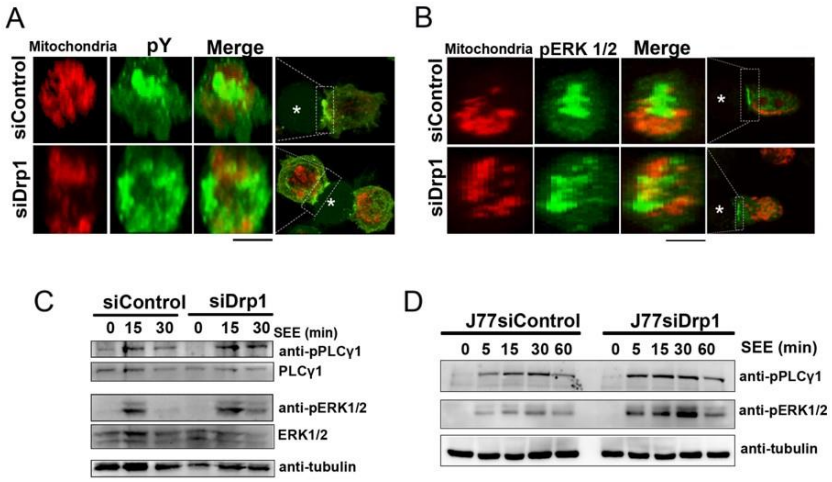

Figure R10. Drp1 regulates TCR signal strength. Confocal 3D stack reconstructions showing the distribution of phosphotyrosine (pY) (**A**) and phosphorylated ERK1/2 (**B**) at the contact site between mitotracker-loaded J77 T cells and SEE-pulsed Raji B cells (asterisks). Time course of the phosphorylation status of PLC-γ1 and ERK 1/2 in control and Drp1-silenced human primary lymphoblast T cells (**C**) or J77 T cells (**D**) activated with SEE-pulsed Raji B cells. Tubulin or total protein expression are shown as loading controls. Immunoblots are representative of three independent experiments

4.6 Tfam depletion induces a respiratory-chain deficiency in T cells

The requirement for mitochondrial function in fueling T cell activation prompted us to further investigate the mechanisms by which mitochondria regulate immune responses. We generated a mouse model specifically lacking Tfam in $CD4^+$ T cells by crossing mice with loxP-flanked Tfam alleles with $CD4^+$Cre mice. Consistent with gene deletion in the early stages of T cell development, Tfam deletion efficiently decreased the mRNA of Tfam in $CD4^+$ and in $CD8^+$ T naive lymphocytes (not shown). $CD4^+Cre^{+/wt}Tfam^{fl/fl}$ mice (herein $Tfam^{-/-}$ mice) developed normally and showed similar frequency of double negative and double positive thymocytes to their control littermates (Figure R11A), indicating that Tfam is not required during early T cell development. $Tfam^{-/-}$ mice presented slightly lower percentages of $CD4^+$ and $CD8^+$ T cells in the spleen and peripheral lymph nodes, but had similar numbers of total splenocytes, B cells and dendritic cells to littermate $CD4^+Cre^{wt/wt}Tfam^{fl/fl}$ controls (herein wild-type mice, wt) (Figure R11B and not shown).

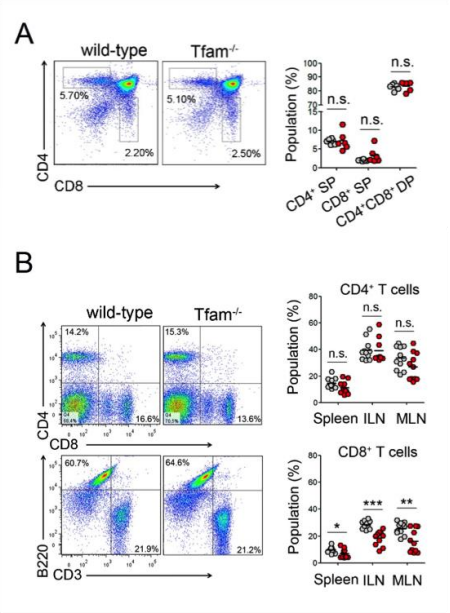

Figure R11. Tfam depletion does not impact T cell development. (A) Dot plots show CD4 and CD8 expression in thymocytes from wt and *Tfam*$^{-/-}$ mice. Right, percentage of CD4 and CD8 single positive (SP), and CD4/CD8 double positive (DP) cells. **(B)** Dot plots show CD4 and CD8 T cells, and CD3 and B220 cells from the spleens. Right, percentages of CD4 and CD8 cells in the spleen, inguinal (ILN) and mesenteric lymph nodes (MLN) (n=11).

Naive *Tfam*$^{-/-}$ CD4^{+} T cells expressed comparable levels of specific T cell surface markers to wild-type cells and responded normally to *in vitro* differentiation toward T lymphoblasts, adopting a polarized morphology (Figure R12A and R12B). The levels of Tfam were efficiently suppressed throughout lymphoblast differentiation, excluding the selection of Tfam-positive cells during *in vitro* expansion (Figure R12C).

Figure R12. Tfam depletion does not impact T cell blastogenesis. (A) Flow cytometry analysis of cell surface markers in T-lymphoblasts differentiated with concanavalin A (ConA, 48h) and IL-2 over 4 days. **(B)** Immunofluorescence images show the polarized organization of cytoskeletal components in wt and *Tfam*$^{-/-}$ CD4^{+} T lymphoblasts by actin, tubulin and ERM (ezrin-radixin-moesin) staining. **(C)** Tfam mRNA levels in naive CD4^{+} T cells (day 0) and during lymphoblast differentiation. Tfam mRNA (center) and protein levels (right) in wild-type and *Tfam*$^{-/-}$ CD4^{+} T lymphoblasts.

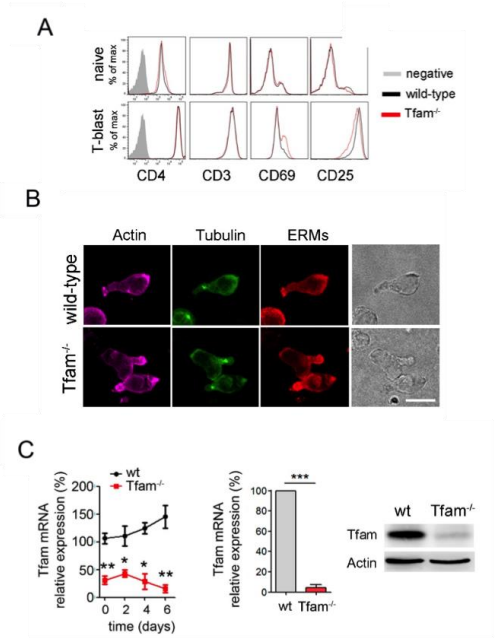

Consistent with the close relationship between levels of Tfam and mtDNA (Ekstrand et al., 2004; Larsson et al., 1998), lack of *Tfam* induced a severe decrease in mtDNA content, both in *Tfam*$^{-/-}$ CD4^{+} T lymphoblasts and in human Jurkat T cells stably transfected with Tfam short hairpin RNAs (shTfam) (Figure R13A). Tfam deficiency reduced the mRNA expression of mtDNA-encoded subunits of mitochondrial complexes I, III, IV and V, whereas nuclear-encoded subunits were not significantly affected (Figure R13B). Consistently, the protein levels of complexes I and IV, which include mtDNA-encoded subunits, were below normal, whereas the fully nuclear-encoded complex II was unaffected (Figure R13C).

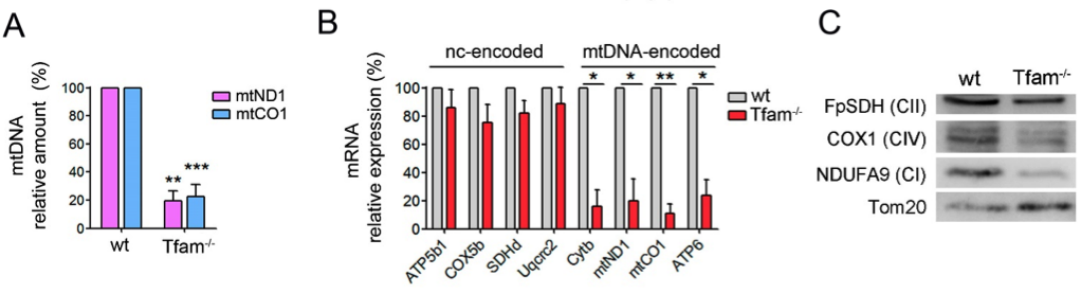

Figure R13. Tfam deletion decreases mtDNA. (**A**) mtDNA levels relative to genomic DNA in T lymphoblasts. (**B**) mRNA levels of mtDNA-encoded and genome-encoded mitochondrial subunits. Results (A, B, C) are expressed relative to wt. (**C**) Immunoblot of T lymphoblast mitochondrial proteins. Protein levels of Complex I (CI) were immunodetected with anti-NDUFA9, CII with anti-FpSDH, and CIV with anti-CO1. The mitochondrial outer membrane protein Tom20 was used as loading control. Data (A, B, C) are means ± SEM (n > 3); *p<0.05, **p<0.01 and ***p<0.0001 (Student's *t*-test).

In response to these respiratory-chain alterations, *Tfam*-deficient cells increased mitochondrial content (Figure R14). However, electron microscopy analysis revealed severely aberrant mitochondrial morphology in *Tfam*$^{-/-}$ CD4^{+} T cells, accompanied by impaired cristae organization and loss of mitochondrial electron density (Figure R15), consistent with a mitochondrial dysfunction caused by depletion of *Tfam* in T cells.

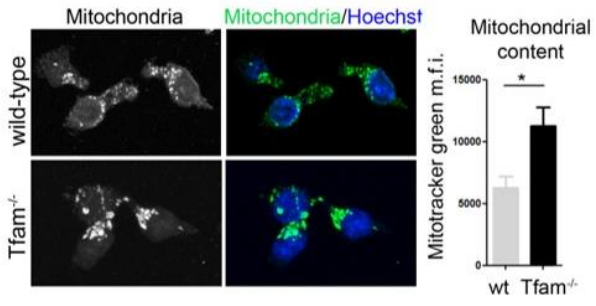

Figure R14. Abnormal mitochondrial morphology in Tfam-deficient cells. Confocal images of mitochondria (anti-MnSOD, green) in T lymphoblasts. Right, flow cytometry analysis of mitochondrial mass by Mitotracker green mean fluorescence intensity ± SEM of three independent experiments; *p<0.05 (Student's *t*-test).

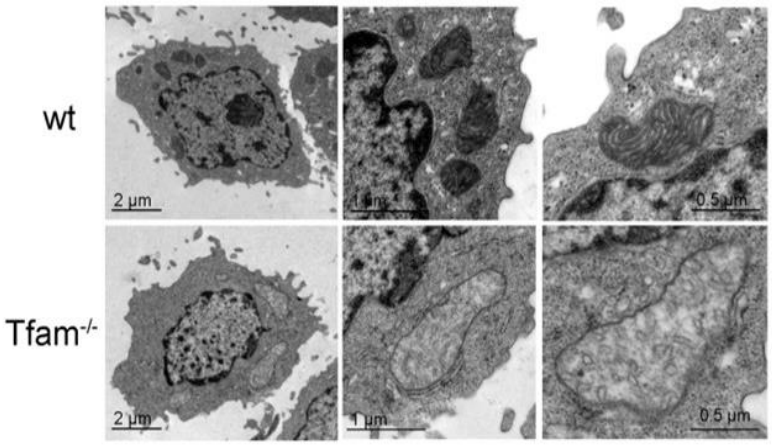

Figure R15. Abnormal mitochondrial cristae in Tfam-deficient cells. Electron microscopy images showing enlarged mitochondria and altered cristae organization in *Tfam*$^{-/-}$ CD4^{+} T lymphoblasts.

We next studied the effect of *Tfam* silencing on the assembly of mitochondrial complexes (Lapuente-Brun et al., 2013). Blue native gel electrophoresis (BNGE) of extracts from *Tfam*-silenced cells revealed severe loss of complexes I and III but not II, and associated alterations in mitochondrial supercomplex assembly (Figure R16A). Accordingly, *Tfam*-depleted cells showed stronger impairment of electron transport from NADH (complexes I+III) than from FADH2 (complexes II+III) (Figure R16B), demonstrating an imbalance in the NAD^{+}/NADH ratio in respiratory-chain deficient cells, as described for cells with mutations in mitochondrial complex I subunits (Santidrian et al., 2013). Connected with the reduced electron transport chain function, *Tfam*-deficient T cells also had below-normal content of mitochondrial reactive oxygen species (ROS) assessed by MitoSOX (Figure R16C), and reduced mitochondrial ATP generation (Figure R16D). Despite the effect on mitochondrial ATP production, total cellular ATP content in primary CD4^{+} *Tfam*$^{-/-}$ T cells and Jurkat shTfam T cells was comparable with controls (Figure R16E and not shown). In addition, the phosphorylation level of the metabolic sensor AMP-activated protein kinase (AMPK) (Hardie et al., 2012) did not differ between *Tfam*-deficient and control cells (Figure R16F), indicating that global energy status is not compromised in *Tfam*-depleted cells.

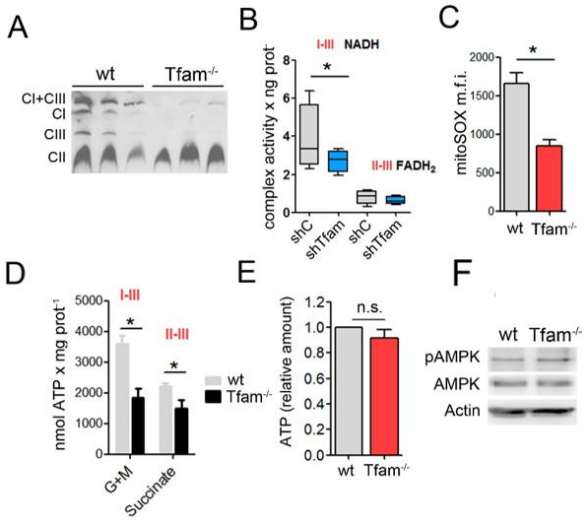

Figure R16. Tfam deletion decreases mitochondrial function in T cells. (**A**) Blue-native gel electrophoresis analysis of electron-transport-chain complexes (detection of NDUFA9, FpSDH and Core1 for complexes I, II and III, respectively). **(B)** Combined mitochondrial complex activities. **(C)** Flow cytometry analysis of mROS (MitoSOX). **(D)** Glutamate- and pyruvate-driven ATP-dependent production. **(E)** Cellular ATP content. **(F)** Immunoblot analysis of AMPK phosphorylation at Thr172 in T lymphoblasts. Actin was used as a loading control.

We then analyzed the metabolic consequences of *Tfam* deletion on CD4$^+$ T cells by flux analysis. In activated CD4$^+$ T cells, we measured the extracellular acidification rate (ECAR), as an index of lactate production and glycolysis, and the oxygen consumption rate (OCR) as an indicator of mitochondrial oxidative phosphorylation (OXPHOS). Upon activation with anti-CD3 and anti-CD28, wild-type T cells used glycolysis and OXPHOS for glucose consumption, as described (Michalek et al., 2011a; van der Windt and Pearce, 2012; Wang et al., 2011). In contrast, *Tfam*$^{-/-}$ T cells presented a low OCR and an ECAR above wild-type levels, demonstrating anaerobic glucose utilization (Figure R17). Additionally, we examined mitochondrial fatty acid ß-oxidation (FAO) in respiration-deficient cells. Naive wild-type and *Tfam*$^{-/-}$ CD4$^+$ T cells were activated over 48h and then incubated with fatty acids prior to flux analysis. In these conditions, activated wild-type CD4$^+$ T cells showed increased OXPHOS and reduced glycolysis (Figure R17), thus relying on fatty acid ß-oxidation and mitochondrial OXPHOS for energy production. In contrast, *Tfam*$^{-/-}$ T cells showed severely reduced OCR, supporting the conclusion that FAO is impaired in respiratory-chain deficient cells (Figure R17).

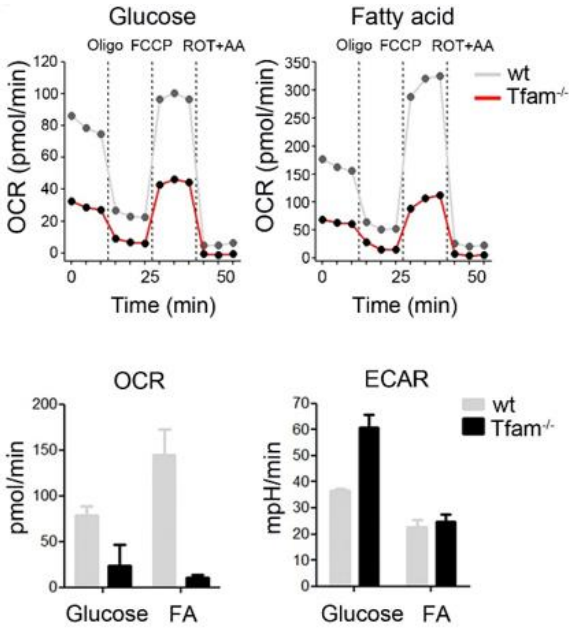

Figure R17. Tfam deletion imposes a metabolic switch. Spleens and lymph nodes were harvested from wild-type and *Tfam*$^{-/-}$ mice and naive CD4$^+$ T cells were isolated by negative selection using magnetic separation and activated for 48h with anti-CD3 and anti-CD28. Cells were fed either with glucose or the fatty acid palmitate for 2 hours and the oxygen consumption rate (OCR) and extracellular acidification rate (ECAR) were measured in real time (upper panels). Lower panels show the basal OCR and ECAR from a representative

Tfam deletion thus promotes loss of mtDNA, mitochondrial oxidative phosphorylation (OXPHOS) deficiency, and compromised mitochondrial function, but has no significant impact on cellular energy status or survival. Additionally, mitochondrial respiration deficiency induces a metabolic reprogramming characterized by increased anaerobic glucose consumption and impaired fatty acid oxidation.

4.7 Tfam deficiency exacerbates inflammatory responses

We next assessed how these mitochondrial alterations caused by Tfam deficiency affect T cell effector function. Upon T cell activation, *Tfam* expression increased concomitantly with an increase in mtDNA levels (Figure R18A), suggesting that mitochondrial adaptation to T cell activation requires an increase in mtDNA levels. We then determined the functional consequences of *Tfam* deletion during T cell activation and acquisition of effector functions.

T cells from wild-type and *Tfam*$^{-/-}$ mice were labeled with the proliferation indicator Cell Violet, stimulated with anti-CD3 and anti-CD28 antibodies, and evaluated by flow cytometry. *Tfam*$^{-/-}$ T cells showed reduced proliferation (Figure R18B). Moreover, upon *in vitro* cell activation, there was no evidence of higher apoptosis in *Tfam*$^{-/-}$ T cells, as assessed by flow cytometry analysis of annexin V and H58 staining (not shown). CD4^{+} *Tfam*$^{-/-}$ cells showed similar levels of the activation markers CD69 (very early activation antigen) and CD25 (IL-2Ralpha) (Figure R18C). Stimulated *Tfam*$^{-/-}$ CD4^{+} T lymphocytes showed increased numbers of IFN-γ- and T-bet-producing cells compared to wild-type cells (Figure R18D). RT-PCR analysis indicated strikingly elevated mRNA expression of the pro-inflammatory cytokines IFN-γ, IL-6, IL-1α and IL-1β and increased IFN-γ and IL-6 secretion were detected in the supernatant of *Tfam* $^{-/-}$ T cells (Figure R18E). In contrast, mRNA levels and cytokine secretion of IL-4 and IL-10 were below-normal in *Tfam*-deficient cells (Figure R18F). These *in vitro* data highlight the requirement on mitochondrial function for the fine regulation of T cell responses.

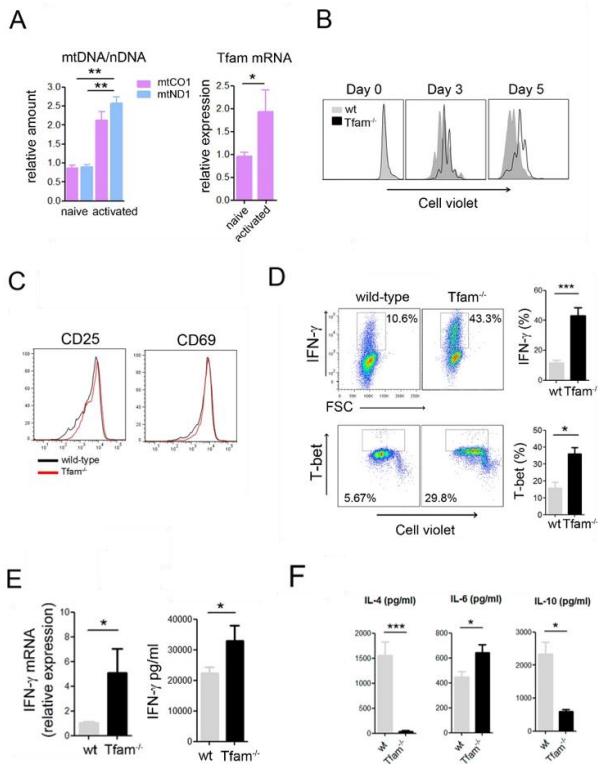

Figure R18. Inhibition of OXPHOS exacerbates inflammatory responses. (A) mtDNA content and Tfam mRNA levels in naive and anti-CD3/CD28 activated T cells (48h). Results expressed relative to unstimulated naive T cells. **(B)** Cell proliferation in T cells stained with Cell Violet. **(C)** Flow cytometry analysis of CD69 and CD25 in activated T cells. **(D)** Intracellular IFN-γ and T-bet levels. **(E)** Left, IFN-γ levels in the supernatant measured by ELISA. Right, IFN-γ mRNA levels. **(F)** IL-4, IL-6 and IL-10 levels in the supernatant measured by ELISA. Data are means ± SEM of at least 3 independent experiments; *p<0.05, **p<0.01, ***p<0.0001 (Student's *t*-test).

To assess the role of mitochondria in the regulation of the inflammatory function of T cells *in vivo*, we first examined a model of contact hypersensitivity (CHS), which is mainly mediated by IFN-γ. The specificity of the CHS response is generally defined as the difference between ear swelling responses to a hapten such as oxazolone in naive and sensitized animals. Upon sensitization to oxazolone, *Tfam*$^{-/-}$ mice showed larger increases in ear thickness, lymph node cellularity, and IFN-γ-producing CD4^{+} T lymphocytes (Figure R19A). In addition, we performed a model of DSS-induced colitis, which is driven by Th1 and Th17 cells and suppressed by Treg cells. Wild-type mice and *Tfam*$^{-/-}$ mice were fed with DSS to induce gut damage and trigger disease. *Tfam*$^{-/-}$ mice showed increased disease severity, as reflected by higher weight loss over time, increased disease score and shorter colon length than wild-type mice (Figure R19B-E). Remarkably, *Tfam*-deficiency increased the frequency of IFN-γ- and T-bet-expressing CD4^{+} T cells in the mesenteric lymph nodes upon DSS-treatment (Figure R19F and not shown). These results indicate that respiration-impaired T cells develop a stronger inflammatory response *in vitro* and *in vivo* and support a critical role for mitochondria in the regulation of T cell effector functions during immune responses.

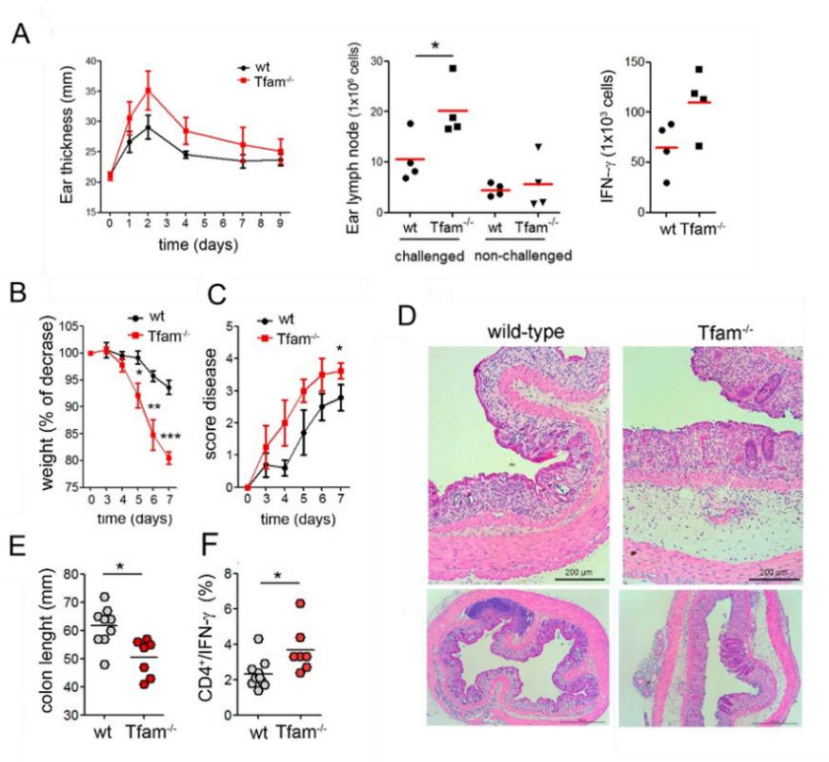

Figure R19. Tfam depletion exacerbates inflammatory responses *in vivo*. (A) Left, ear thickness upon oxazolone re-challenge. Center, cell number in the lymph nodes. Right, IFN-γ-producing CD4^{+} T cells in the challenged ear lymph nodes. **(B)** Weight and **(C)** disease score in mice fed with 3% dextran sulfate sodium (DSS) in the drinking water. **(D)** Representative H&E staining of colon sections and colon length **(E)** on day 7 after DSS treatment. **(F)** IFN-γ-producing CD4^{+} T cells in the mesenteric lymph nodes. Data (B-F) are means ± SEM (n ≥ 7 mice in two independent experiments); *p<0.05, **p<0.01 and ***p<0.0001 (Student's *t*-test).

4.8 Mitochondrial dysfunction deviates T cell differentiation toward pro-inflammatory Th1 subsets

To provide further insights into how mitochondrial function controls T cell differentiation, we assessed the ability of *Tfam*-deficient T cells to differentiate into effector T cell subsets. The balance among different functional effector T cell subsets determines the outcome of the immune response and is essential to prevent undesired inflammation and autoimmune diseases. Naive $CD4^+$ T cells were labeled with Cell Violet, differentiated *in vitro* with different cytokines and neutralizing antibodies to Th1, Th2 and Th17 T cell subsets, and assessed for proliferation and expression of specific transcription factors and cytokines. *Tfam* deficiency greatly impaired proliferation in all the skewing conditions (Figure R20A and R20C), thus indicating a reliance on mitochondrial function in all the polarizations tested. *Tfam*-depleted cells showed higher expression of the Th1-specific transcription T-bet, higher numbers of IFN-γ-producing cells and higher levels of IFN-γ secretion (Figure R20A and R21). In all polarization conditions, $Tfam^{-/-}$ $CD4^+$ T cells secreted less IL-4 than wild-type cells (Figure R21), demonstrating a Th1/Th2 imbalance toward the Th1 response in the absence of *Tfam*.

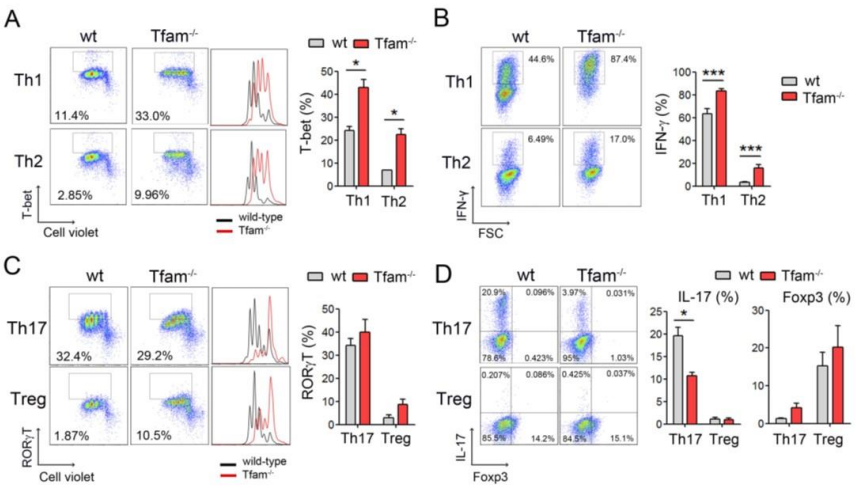

Figure R20. Mitochondrial dysfunction subverts T cell differentiation toward Th1 cell subsets. (A) Cell Violet dilution and T-bet expression in CD4 T cells cultured under Th1 and Th2 conditions over 3 days. Chart, percentage of T-bet expressing cells (n=3). **(B)** Flow cytometry analysis of IFN-γ-producing cells under Th1 and Th2 conditions over 6 days. Graph, quantification of IFN-γ-producing cells (n=6). **(C)** Naive CD4 T cells were cultured under Th17 and Treg conditions over 3 days. Dot plots show RORγT-expressing cells and histograms show cell proliferation assessed by Cell Violet dilution. Chart, percentage of RORγT-expressing cells (n=3). **(D)** Flow cytometry analysis of CD4 T cells producing IL-17 and Foxp3. Chart shows percentage of IL-17 and Foxp3-producing cells (n=6). Data are means ± SEM ($n \geq 3$); *p<0.05 and ***p<0.001 (Student's *t*-test).

When polarized toward Th17 T cell subset, no substantial differences were found in the number of RORγt-expressing cells between *Tfam*$^{-/-}$ and wild-type cells (Figure R20C). However, impaired mitochondrial function in *Tfam*$^{-/-}$ CD4^{+} T cells significantly reduced the levels of IL-17-producing cells and impaired IL-17 and IL-10 secretion, while increasing the frequency of IFN-γ-producing cells and IFN-γ secretion (Figure R20D and R21). Thus, *Tfam*-deficiency favoured the appearance Th17 cells which coexpress RORγt and T-bet, and produce high levels of IFN-γ but reduced amounts of IL-10, and which have been proposed to be pathogenic Th17 cells involved in autoimmune diseases in mice (Huber et al., 2011; Peters et al., 2011). Collectively, these results reveal a role for mitochondrial function in the regulation of T cell differentiation and indicate that mitochondrial dysfunction is associated with a deregulation of T cell differentiation toward pro-inflammatory Th1 cell subsets.

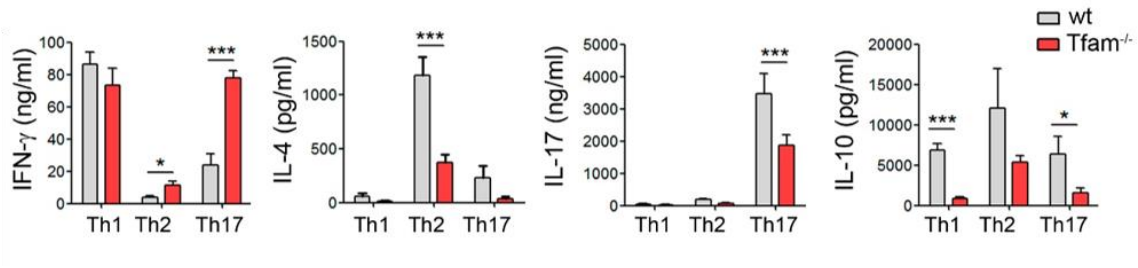

Figure R21. **Tfam depletion induces Th1 cytokine profile.** Polarized CD4^{+} T cells at day 6 were cultured in equal numbers in fresh medium followed by activation with PMA/ionomycin for 16h. Cytokines were measured by ELISA in the supernatants. Graphs show quantification of IFN-γ, IL-4, IL-17 and IL-10 in at least 4 independent experiments. *p<0.05, ***p<0.0001 (Student's t-test).

4.9 Mitochondrial oxidative phosphorylation is required for exosome secretion through reactive oxygen species signaling

In addition to the profound morphological and functional mitochondrial alterations, electron microscopy studies revealed striking intracellular vesiculation in *Tfam*-deficient cells (Figure R22A). These abnormalities prompted us to explore the role of mitochondria in the regulation of the endolysosomal system. We investigated the abundance and organization of the endosomal compartment in *Tfam*-deficient cells. The early endosome marker EEA1 showed no substantial differences, but expression of the late endosomal markers HRS and the lysobisphosphatidic acid (LBPA) was elevated in respiratory-chain deficient cells (Figure R22B). LBPA, an unconventional phospholipid specifically found in late endosomes and MVBs, regulates intraluminal vesicle (ILV) formation during exosome biogenesis (Matsuo et al., 2004). Immunofluorescence analysis with an antibody against LBPA revealed enlargement of late

endosome/multivesicular bodies (MVBs) in *Tfam*-deficient cells (Figures R22C) and in shTfam Jurkat T cells (Figures R22D). Strikingly, electron microscopy analysis of *Tfam*-deficient T cells revealed enlarged late endosomes with decrease numbers of ILVs (Figure R22E), suggesting impaired MVB maturation.

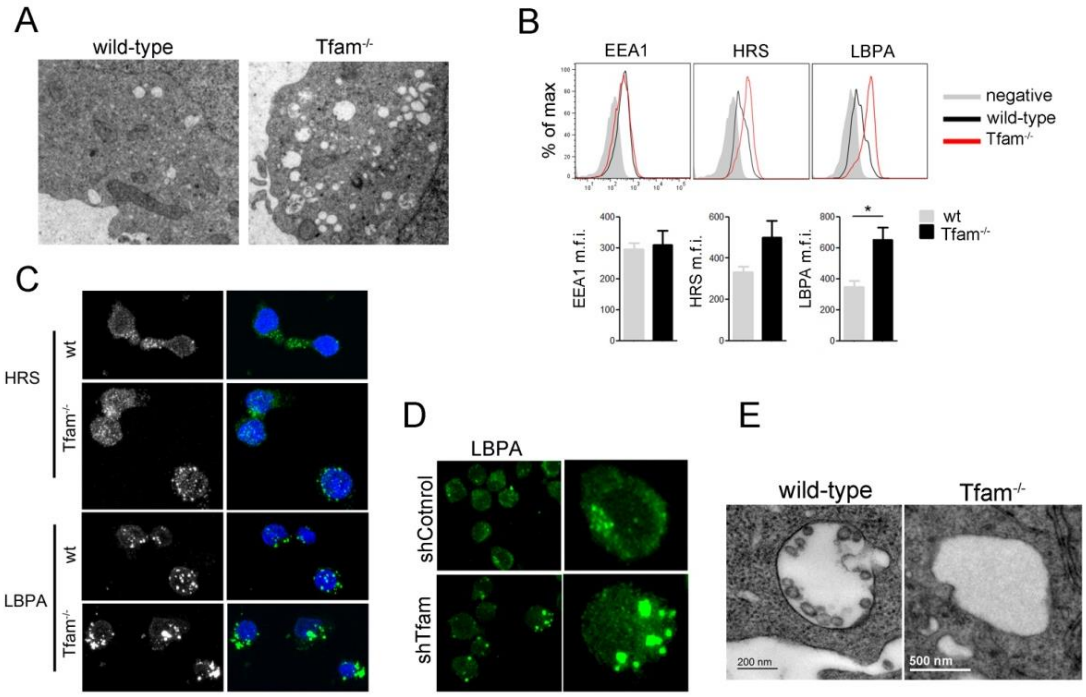

Figure R22. Tfam regulates multivesicular body maturation. (A) Electron microscopy images show the abnormal intracellular accumulation of vesicles in *Tfam*$^{-/-}$ T cells. **(B)** Flow cytometry analysis of EEA1, HRS and LBPA content in CD4^{+} T lymphoblasts. Results show mean fluorescence intensity (m.f.i.) from three independent experiments. *p<0.05 (Student's *t*-test). **(C)** Confocal detection of HRS and LBPA in T lymphoblasts. Nuclei were stained with HOECHST (blue). **(D)** Immunofluorescence analysis of LBPA in Jurkat T cells. **(E)** Electron microscopy images from wild-type and *Tfam*$^{-/-}$ T lymphoblasts.

To determine the impact of *Tfam* depletion on the regulation and maturation of the late endosomal compartment, we analyzed exosome secretion. Exosomes were purified by serial ultracentrifugation from equal numbers of control and *Tfam*-deficient cells. Tfam-silenced cells secreted 30-40% fewer nanoparticles than control cells, quantified by nanoparticle tracking analysis (NTA) (Figure R23A). Exosomes obtained from shTfam-silenced Jurkat T cells had a significantly below-normal protein content of the exosomal markers CD63, CD81, CD9, and ERMs (Figure R23B), a reduction also confirmed in primary *Tfam*$^{-/-}$ T lymphoblasts (Figure R23B). In addition, Tfam-silenced cells showed decrease exosome secretion in response to PMA

and ionomycin (not shown), indicating that constitutive and activation-induced exosome release is compromised in respiration-impaired cells. Sucrose gradient characterization of exosomes derived from Tfam-silenced cells showed low levels of the exosomal markers CD63, CD81 and ERMs in the fractions corresponding to the density of exosomes (Figure R23C). Lack of *Tfam* thus induces a respiration deficiency associated with enlarged LBPA-positive MVBs and decreased biogenesis and secretion of exosomes. These data reveal an unanticipated link between mitochondrial function and regulation of exosome secretion.

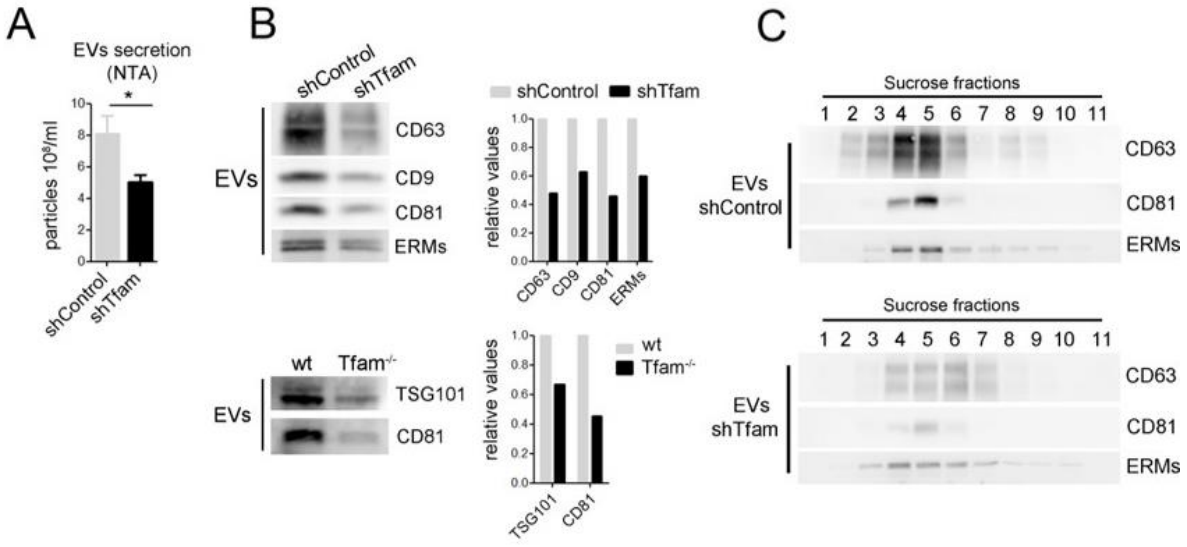

Figure R23. Tfam regulates exosome secretion. (A) Number of released extracellular vesicles obtained from equal numbers of Jurkat T cells and quantified by nanoparticle tracking analysis (NTA). Data are means ± SEM of three independent experiments. *p<0.05 (Student's *t*-test). **(B)** *Upper panel*, protein immunoblot of the exosomal proteins ERMs, CD63, CD81 and CD9, detected in the exosome fraction of Jurkat T cells. *Lower panel*, purified exosomes secreted by primary $CD4^+$ T lymphoblasts and immunoblotted for the exosome markers CD81 and TSG101. **(C)** Western blot showing enrichment of the exosome markers CD81, CD63 and ERMs in sucrose fractions. Exosomes were laid on top of discontinuous sucrose gradient and floated by overnight centrifugation. Gradient fractions were collected and analyzed by immunoblot to show the distribution of exosomal proteins in the sucrose fractions from lower (left) to higher sucrose densities (right).

To investigate the impact of cell metabolism in the regulation of exosome secretion, we treated wild-type T cells with dichloroacetate (DCA), which shifts metabolism from glycolysis toward OXPHOS by inhibiting pyruvate dehydrogenase kinase (PDK). PDK inhibition activates pyruvate dehydrogenase (PDH), promotes pyruvate mitochondrial oxidation and reduces lactate secretion.

Treatment of wild-type T lymphoblasts with DCA increased exosome secretion (Figures R24A). To confirm the involvement of OXPHOS in exosome secretion, we promoted mitochondrial oxidative phosphorylation through fatty acid ß-oxidation by supplying fatty acids to wild-type and *Tfam*$^{-/-}$ T cells. In these conditions, activated wild-type CD4^{+} T cells increased oxidative respiration and reduced glycolysis, thus relying on fatty acid ß-oxidation and mitochondrial oxidative phosphorylation for energy production. In contrast, *Tfam*$^{-/-}$ T cells fed with fatty acids showed severely reduced OCR supporting impaired fatty acid ß-oxidation (Figure R17). Treatment of cells with fatty acids, increased exosome secretion in wild-type cells but not in *Tfam*$^{-/-}$ T cells (Figures R24B), which indicated that fatty acid ß-oxidation enhance exosome secretion in OXPHOS-competent cells but not in respiration-impaired *Tfam*$^{-/-}$ T cells. Altogether, these data suggest that mitochondrial OXPHOS is essential for exosome secretion.

The main source of cellular reactive oxygen species (ROS) is mitochondria. We then explored whether mitochondrial ROS (mROS) regulate exosome secretion. T cells treated with N-acetylcysteine (NAC), a ROS scavenger, showed reduced exosome secretion (Figure R24C), whereas induction of mROS by the complex I inhibitor rotenone resulted in robust mROS production and increased exosome secretion (Figure R24C). These results suggest that mitochondrial respiration regulates exosome secretion in a ROS-dependent manner.

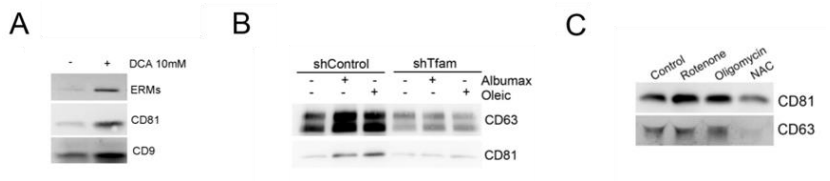

Figure R24. Mitochondrial OXPHOS regulates exosome secretion through ROS signaling. (A) Western blot analysis of exosome derived from control or DCA-treated T cells. (B) Protein immunoblot of the exosomal proteins CD63 and CD81, in the exosome fraction of shControl and shTfam cells supplemented with Albumax or Oleic acid for 16h. (C) Protein immunoblot of CD63 and CD81, detected in the exosome fraction obtained from J77 T cells treated with rotenone (1µM) or NAC (5 mM) for 16h.

4.10 Mitochondrial dysfunction promotes lysosomal disorder and sphingolipidosis

Besides the defects in late endosomal maturation and exosome secretion, lysosomes, identified by staining for LAMP1 and Lysotracker, appeared to be more abundant in Tfam-deficient cells than in wild-types (Figure R25A-C), indicating expansion of the late endosome-lysosome compartment in cells that lack Tfam. Lysosomal biogenesis is regulated by TFEB, a master

regulator of the CLEAR (coordinated lysosomal expression and regulation) gene network (Sardiello et al., 2009). During lysosomal stress or starvation, cytosolic TFEB relocates to the nucleus and activates a transcriptional program aimed at increasing autophagy, lysosomal biogenesis and function (Settembre and Ballabio, 2011; Settembre et al., 2013a). TFEB is also responsible for the transcriptional activation of PGC1α, which adjusts the content of mitochondrial and peroxisomal enzymes and the expression of components that increase lipid catabolic reactions (Settembre et al., 2013b). Immunofluorescence analysis revealed that TFEB is mostly translocated to the nucleus in Tfam-depleted cells (Figure R25D). Nuclear localization of TFEB was confirmed by cell fractionation assays (Figure R25E), and correlated with upregulated expression of the TFEB target genes LAMP1, FABP3, CD36, Acacb, Cyp4a10 and PGC1α (Figure R25F), which are involved in lipid uptake, lipid catabolism and mitochondrial function. These results suggest that the enlarged lysosomal compartment observed in respiration-impaired *Tfam*$^{-/-}$ cells is associated with TFEB activation.

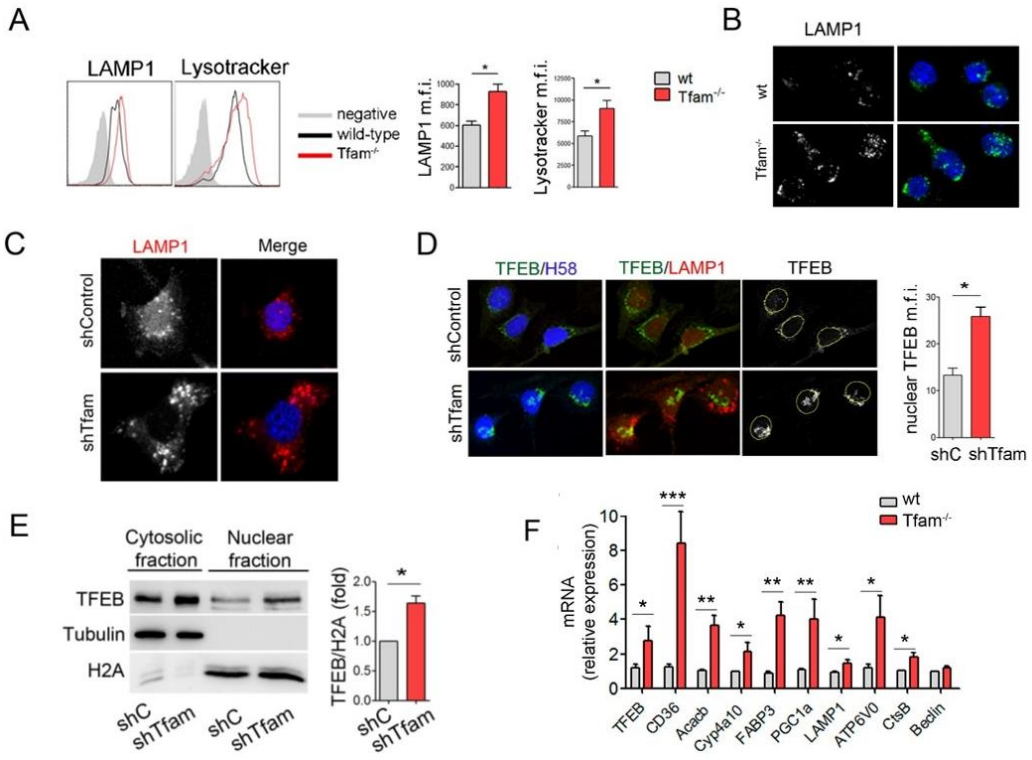

Figure R25. Tfam controls lysosomal biogenesis through TFEB. (A) Lysosomes content in T lymphocytes. **(B)** IF analysis of LAMP1 in T lymphocytes and **(C)** the oligodendroglia cell line (Oli-Neu). **(D)** Confocal subcellular localization of TFEB (green) and LAMP1 (red) in Oli-Neu cells. Graph, quantification of nuclear TFEB m.f.i. **(E)** Western blot analysis of TFEB in subcellular fractions in J77 T cells. Graph, ratio of nuclear TFEB to histone 2A. Cytosol and nuclear fractions were blotted for TFEB, tubulin (cytoplasmic marker), and histone 2A (nuclear marker). **(F)** mRNA levels of TFEB and selected target genes. Data are means ± SEM; *p<0.05, **p<0.01 and ***p<0.0001 (Student's *t*-test).

To further examine the impact of Tfam deficiency on lysosome function, we measured the levels of calcium in lysosomes after inducing its release with bafilomycin-A1 (Lloyd-Evans et al., 2008), a selective inhibitor of the vacuolar-type H+ ATPase. Lysosomal calcium mobilization was weaker in *Tfam*-deficient cells (Figure R26A), whereas the subsequent addition of ionomycin, which releases calcium from remaining stores, triggered comparable release in wild-type and *Tfam*$^{-/-}$ T cells. Measurement with a specific lysosomal pH-sensitive probe indicated reduced pH in lysosomes from respiration-deficient *Tfam*$^{-/-}$ cells (not shown). The activity of the lysosomal endopeptidase cathepsin B and was significantly reduced in *Tfam*$^{-/-}$ T cells (Figure R26B), whereas acid phosphatase activity showed no difference (not shown).

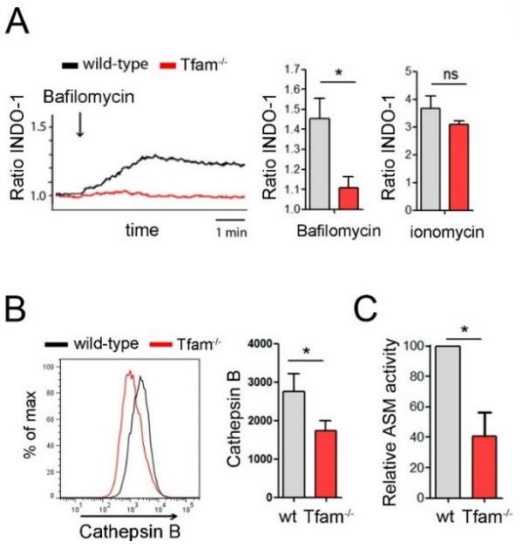

Figure R26. Tfam controls lysosomal function. (A) Lysosomal calcium in T lymphoblasts loaded with the Indo-1, treated with bafilomycin-A1 and detected by flow cytometry. Left, Indo-1 340/380 nm ratio upon bafilomycin-A1 treatment and right, quantification of Indo-1 increase in bafilomycin-A1- or ionomycin-treated cells relative to the basal level. **(B)** Cathepsin B activity measured by flow cytometry (MagicRed). Histogram and bar chart shows the quantification of mfi. **(C) ASM** activity in T lymphocytes. Data (B,C) are means ± SEM of at least four independent experiments;

Sphingomyelins and other lipids such as cholesterol, glycosphingolipids and sphingosine accumulate abnormally as a result of the impaired lysosomal degradation in metabolic diseases known as lysosomal storage disorders (LSDs) (Schulze and Sandhoff, 2011). Lipidomic analysis showed that CD4^{+} *Tfam*$^{-/-}$ T cells have an altered lipid profile compared with wild-type cells, affecting 90 out of 218 lipids analyzed and characterized by elevated levels of several lipid species. Consistent with the reduced lysosomal degradation capacity, respiration-impaired *Tfam*$^{-/-}$ cells showed a significant accumulation of sphingomyelins and triacylglycerides (TAGs) (Figure R27). Supporting lysosomal dysfunction and sphingomyelin accumulation in respiration-impaired cells, *Tfam*$^{-/-}$ T cells showed significantly reduced acid sphingomyelinase (ASM) activity (Figure R26C).

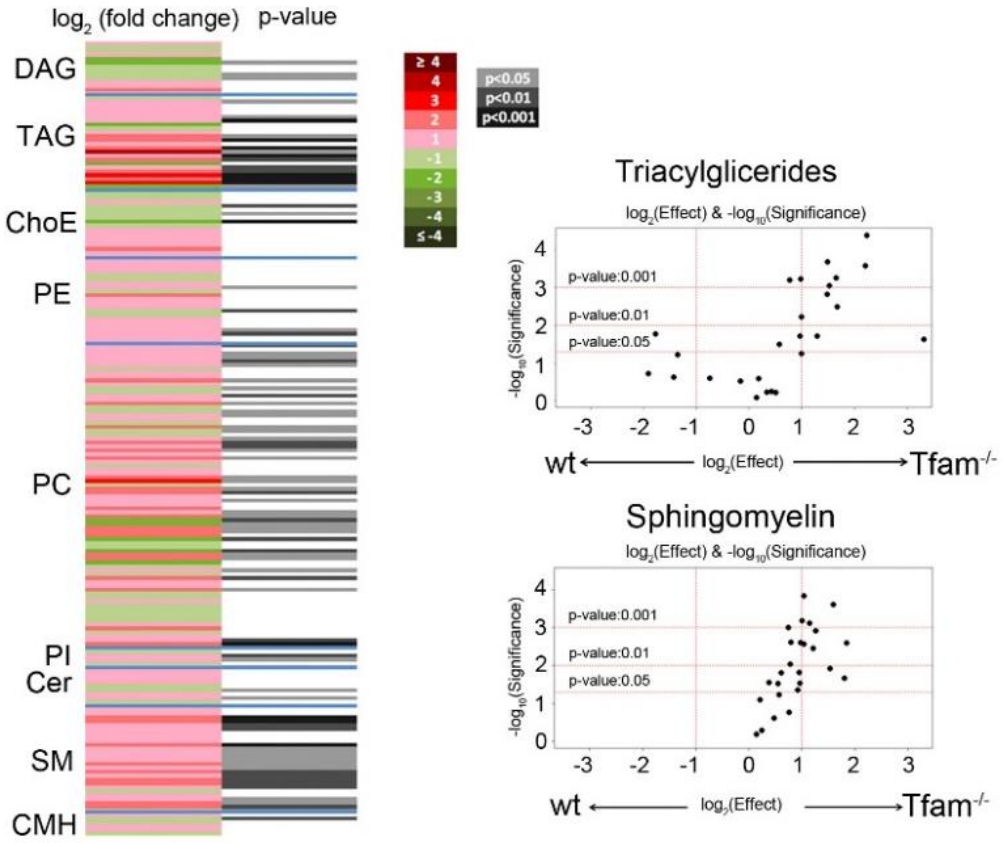

Figure R27. Abnormal sphingolipid accumulation in respiration-deficient cells. The heatmap represents cell lipidomic signatures of wt and *Tfam*$^{-/-}$cells obtained from three mice per genotype, and shows the log2(fold change) and p-values for the detected metabolites. Log-transformed ion abundance ratios are depicted as shown in the scale. More intense colors indicate larger drops (green) or elevations (red) of the metabolite levels in *Tfam*$^{-/-}$ samples. Gray lines indicate significant fold changes of individual metabolites, with color intensity used to indicate statistical significance ($p<0.05$, $p<0.01$ or $p<0.001$) in Student's t-test analysis. The metabolites present in the heatmap are ordered according to their carbon number and the degree of unsaturation of their acyl chains. Right panels show volcano plots [log10(p-value) vs. log2(fold change)] for the comparison of *Tfam*$^{-/-}$and wild-type T cells for the indicated metabolites. DAG, diacylglycerides; TAG, triacylglycerides; ChoE, cholesteryl esters; PE, phosphatidylethanolamines; PC, phosphatidylcholines; PI; phosphatidylinositols; Cer, ceramides; SM, sphingomyelins; CMH, monohexosylceramides.

Defects in lipid trafficking and autophagosome-lysosome fusion are commonly observed in sphingolipidoses. The reduced lysosomal calcium and abnormal sphingomyelin accumulation detected in respiration-impaired cells prompted us to investigate the ability of lysosomes to fuse with autophagosomes. In cells transfected with the autophagosome marker LC3GFP-RFP, GFP fluorescence is decreased when autophagosomes fuse with lysosomes because it is more sensitive to pH than the RFP signal, which is maintained in acidic compartments. In these experimental settings, control cells showed increased RFP puncta upon induction of autophagy by rapamycin treatment (Figure R29). In contrast, *Tfam*-deficient cells showed a significant reduction in the number of RFP-positive puncta, indicating impaired autophagosome-lysosome fusion in the absence of *Tfam*.

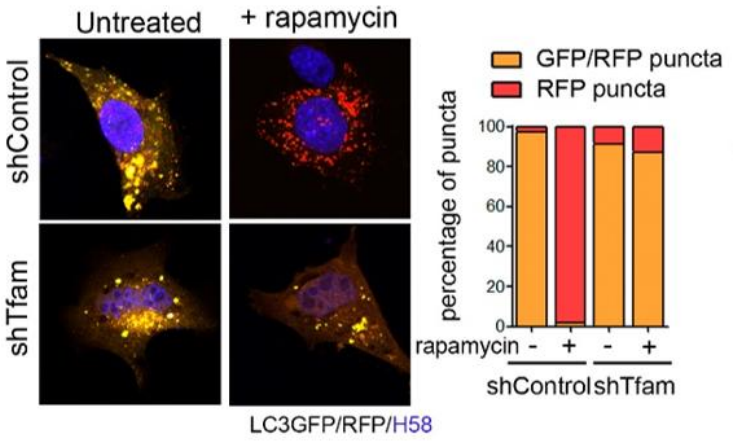

Figure 28. Autophagosome-lysosome fusion defects in Tfam deficient cells. Oli-Neu were transfected with GFP-RFP-LC3 and treated or not with rapamycin. Representative confocal images are shown in the left panel. The graph shows percentage of the GFP/RFP puncta (yellow vesicles) and the percentage of RFP puncta (red vesicles) from at least 100 vesicles in two independent experiments. Nuclei were stained with HOESCHT58 (blue).

Assessment of mitochondrial degradation by mitophagy upon acute membrane depolarization with CCCP revealed larger parkin-GFP aggregates in *Tfam*-deficient cells than in control cells (Figure R30A), indicating impaired parkin clearance and mitochondrial degradation. In accordance with impaired autophagic flux, Tfam–depleted cells showed increased levels of the lipidated form of LC3 (LC3-II) (Figure R30B). Additionally, flow cytometry, western blot and confocal analysis showed a significant accumulation of the autophagic substrate p62 in *Tfam*-deficient cells (Figure R31). Blocking protein synthesis with cycloheximide revealed slower p62 turnover in respiration-impaired cells than in wild-types, confirming that the accumulation of p62 was caused by impaired lysosomal degradation and not by increased mRNA transcription (Figure R31).

Cells that lack Tfam exhibit lysosomal defects similar to those seen in LSDs: abnormal lipid trafficking, altered calcium mobilization and defective autophagosome-lysosome fusion. Overall, these results reveal a novel link between a primary mitochondrial dysfunction and the acquisition of a lysosomal storage disorder.

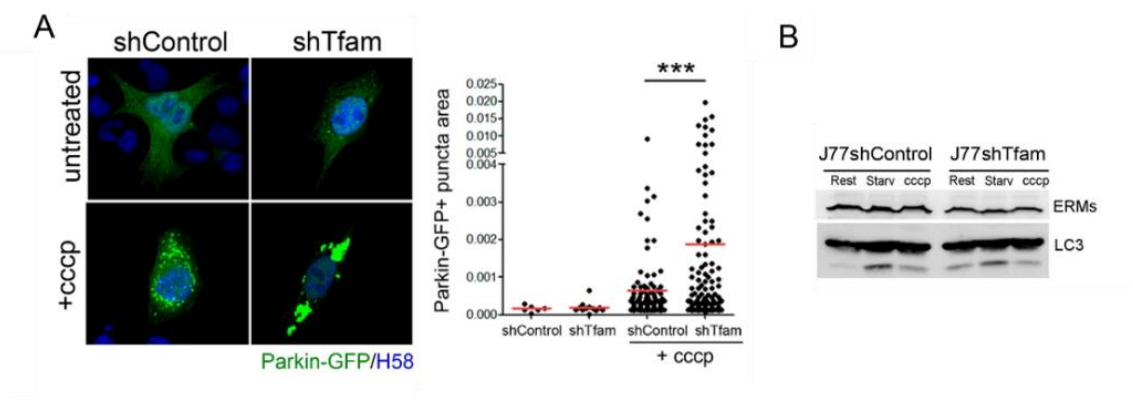

Figure 29. Impaired mitophagy in Tfam-deficient cells. **(A)** Immunofluorescence microscopy in OliNeu cells transfected with Parkin-GFP and left untreated or cccp-treated during 4h. Representative confocal images are shown on left panel. Graph, quantification from the area of at least 100 vesicles in two independent experiments. Images show the subcellular localization of Parkin-GFP (green). Nuclei were stained with HOESCHT58 (blue). **(B)** Western blot analysis of LC3 in the indicated conditions.

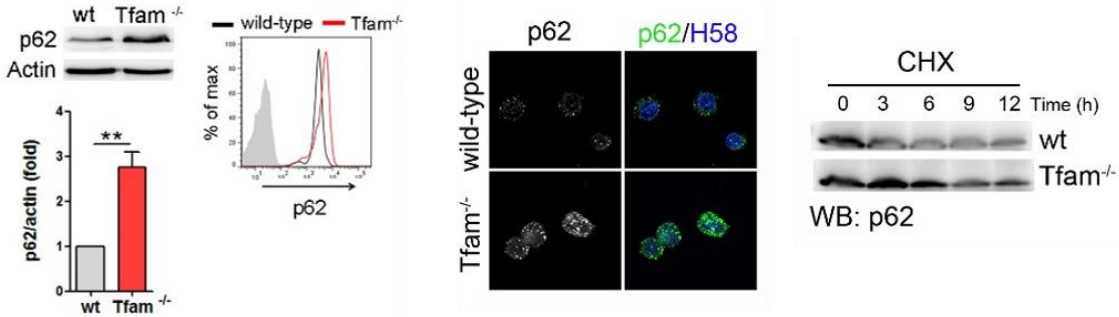

Figure 30. Impaired autophagic degradation in Tfam-deficient cells. Analysis of p62 by western blot, flow cytometry and confocal immunofluorescence in T lymphoblasts. Bar chart, densitometry analysis of p62 by western blot (n = 4). **p<0.01 (Student's t-test). Western blot analysis of p62 protein turnover in cells treated with cycloheximide for the indicated times.

To dissect how mitochondria regulate lysosomal function, we investigated whether cells containing point mutations in mtDNA genes for specific mitochondrial respiratory complexes undergo the same lysosomal calcium defects. Mouse fibroblasts that carry a high load (98%) of a

null mutation in the mt-ND6 gene (complex I subunit) showed impaired lysosomal calcium mobilization, upregulation of TFEB target genes, and reduced ASM activity (Figure R32A). Notably, impaired lysosomal calcium mobilization was also detected in fibroblasts from two human patients, one carrying a high load (88%) of a point mutation in the mt-tRNA^{Asn} gene (m.5658T>C), and another carrying a 50% load of a point mutation in the complex I subunit mt-ND5 gene (m.13513G>A) (Figure R32B). These results indicate that lysosomal calcium levels are decreased not only by the severe OXPHOS-deficiency associated with *Tfam*-depletion, but also by point mutations in mtDNA associated with complex I dysfunction, both in mice and in human patient samples.

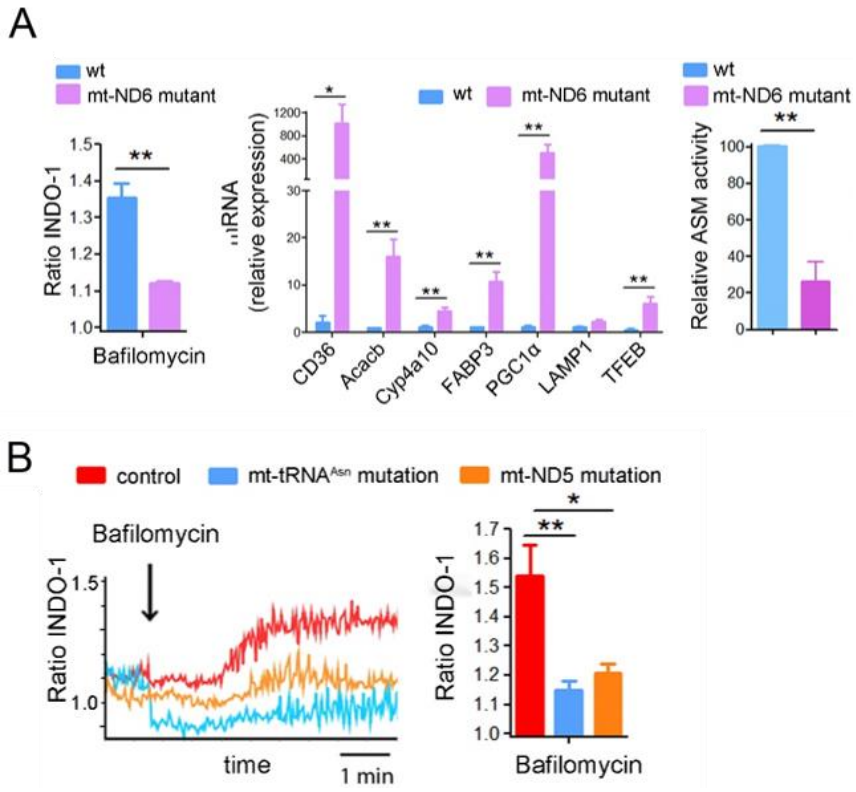

Figure R31. Punctual mutations in mtDNA impair lysosomal function in human and mice. (A) *Left*, ratio of Indo-1 signal upon bafilomycin-A1 treatment relative to the basal level. Center, mRNA levels of TFEB and selected target genes. Right, acid sphingomyelinase (ASM) activity. **(B)** Lysosomal calcium in human fibroblasts. Right, Indo-1 340/380 nm ratio in cells upon bafilomycin-A1 treatment. Data are means ± SEM of three independent experiments; *p<0.05 and **p<0.01 (Student's t-test).

4.11 Increasing intracellular NAD^+ content boosts lysosomal function and dampens Th1 responses in respiratory-deficient cells

We then investigate whether lysosomal dysfunction caused by mitochondrial respiration deficiency is involved in the increased inflammatory responses observed in Tfam-deficient cells. Naive wild-type $CD4^+$ T cells activated in the presence of the lysosomal inhibitor leupeptin or sphingomyelin (SM) showed increased levels of IFN-γ mRNA (Figure R33), suggesting that the lysosomal dysfunction caused by mitochondrial respiration-deficiency might contribute to the increased pro-inflammatory profile of *Tfam*$^{-/-}$ $CD4^+$ T cells.

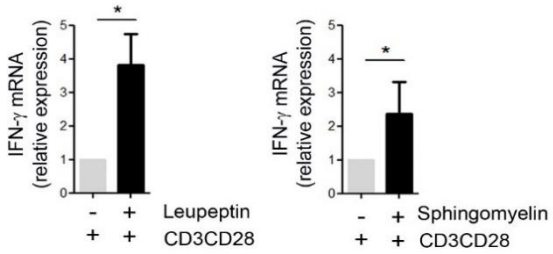

Figure R32. Lysosomal dysfunction increases inflammatory responses. mRNA levels of IFN-γ in $CD4^+$ T cells activated for 6 days with anti-CD3/CD28 in the presence of leupeptin (1 µM) or sphingomyelin (25 µM). Results are expressed relative to untreated cells, and data are means ± SEM of three independent experiments.

To ascertain the involvement of lysosome function in the regulation of T cell responses, we studied T cell activation and differentiation in mice lacking the acid sphingomyelinase, which mimics the LSD Niemann Pick disease Type A (NPA) and, similarly to *Tfam*$^{-/-}$, shows SM accumulation, lysosomal disorder and autophagy impairment (Gabande-Rodriguez et al., 2014). Naive $CD4^+$ T cells from $ASM^{-/-}$ mice activated in non-skewing conditions with anti-CD3 and anti-CD28 antibodies showed a higher frequency of IFN-γ-producing cells than wild-type $CD4^+$ T cells (Figure R34A). In addition, naive $CD4^+$T cells from wild-type and $ASM^{-/-}$ mice were differentiated *in vitro* toward Th1 subsets. Similarly to respiratory-deficient *Tfam*$^{-/-}$ cells, $ASM^{-/-}$ cells showed higher frequency of IFN-γ-producing cells, and higher levels of IFN-γ secretion (Figure R34A and R34B). Collectively, these results showed that lysosome dysfunction caused by ASM deficiency deregulates efficient T cell differentiation toward pro-inflammatory Th1 T cell subset.

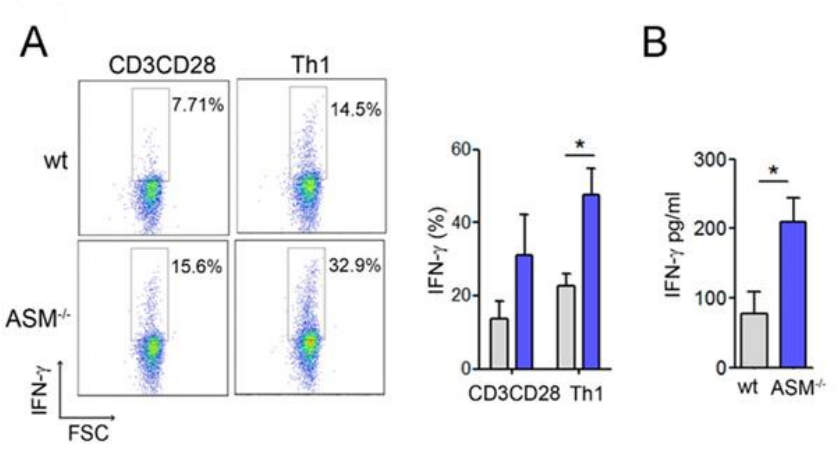

Figure R33. Lysosomal dysfunction increases inflammatory responses. (A) $CD4^+$ T lymphocytes from acid sphingomyelinase-deficient ($ASM^{-/-}$) and wt mice, activated with anti-CD3/CD28 or under Th1 differentiation. Flow cytometry analysis and quantification of the frequency of $CD4^+$ T cells producing IFN-γ. **(B)** IFN-γ levels in the supernatant were measured by ELISA (left panel). Data are means ± SEM (n=3); *p<0.05 (Student's *t*-test).

Increasing intracellular levels of NAD^+ has been proposed to be a therapeutical strategy to restore mitochondrial function in respiratory-chain deficiencies (Cerutti et al., 2014; Gomes et al., 2013; Karamanlidis et al., 2013; Mouchiroud et al., 2013). To assess whether modulation of the cellular NAD^+/NADH ratio may be involved in the regulation of lysosomal function, we treated *Tfam*-deficient T cells with the nicotinamide precursor NAM to reestablish NAD^+/NADH balance, and assessed parameters of lysosome function. Addition of NAM increased ASM activity, reduced p62 accumulation, and downregulates TFEB target genes in *Tfam*-deficient cells (Figure R35A-C), suggesting that modulation of mitochondrial NAD^+/NADH levels impacts lysosome function. Finally, to determine whether restoring lysosomal function would limit the increased pro-inflammatory profile in respiration-impaired $Tfam^{-/-}$ T cells, naive $CD4^+$ T cells were activated in the presence of NAM for 72h and their cytokine profile assessed. NAM treatment reduced the frequency of IFN-γ-producing $Tfam^{-/-}$ T cells (not shown). Additionally, under Th1 polarization conditions, naive $Tfam^{-/-}$ $CD4^+$ T cells cultured in the presence of NAM showed a reduced percentage of IFN-γ-producing cells (Figure R35D), indicating that improved lysosomal function reduces the exacerbated inflammatory response of mitochondrial respiration-deficient cells.

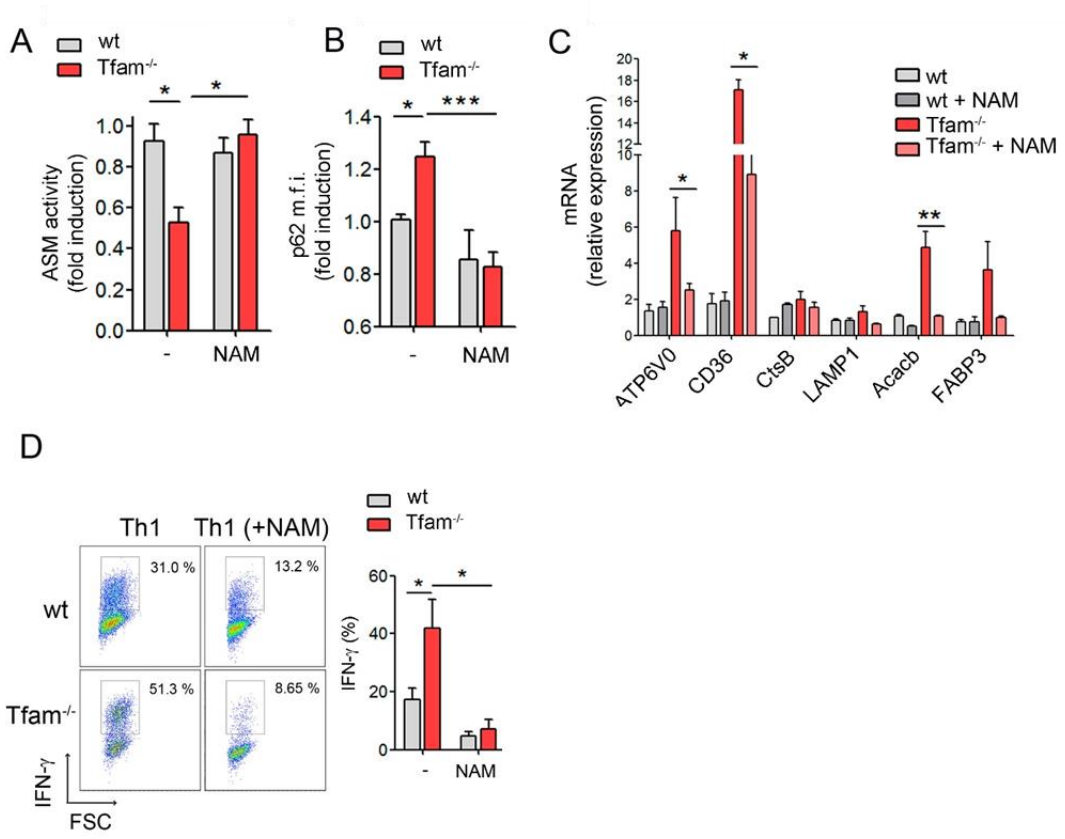

Figure R34. Increasing NAD$^+$ levels improves lysosome function and reduces inflammatory responses in *Tfam*-deficient cells. (A) ASM activity, **(B)** p62 levels and **(C)** mRNA levels of TFEB target genes in T-lymphoblasts treated with the nicotinamide precursor NAM (10mM) for 2 days. **(D)** Flow cytometry analysis and quantification of IFN-γ-producing cells in CD4$^+$ T cells cultured towards Th1 conditions in the presence of absence of NAM. Data are means ± SEM; *p<0.05 and **p<0.01 (Student's *t*-test).

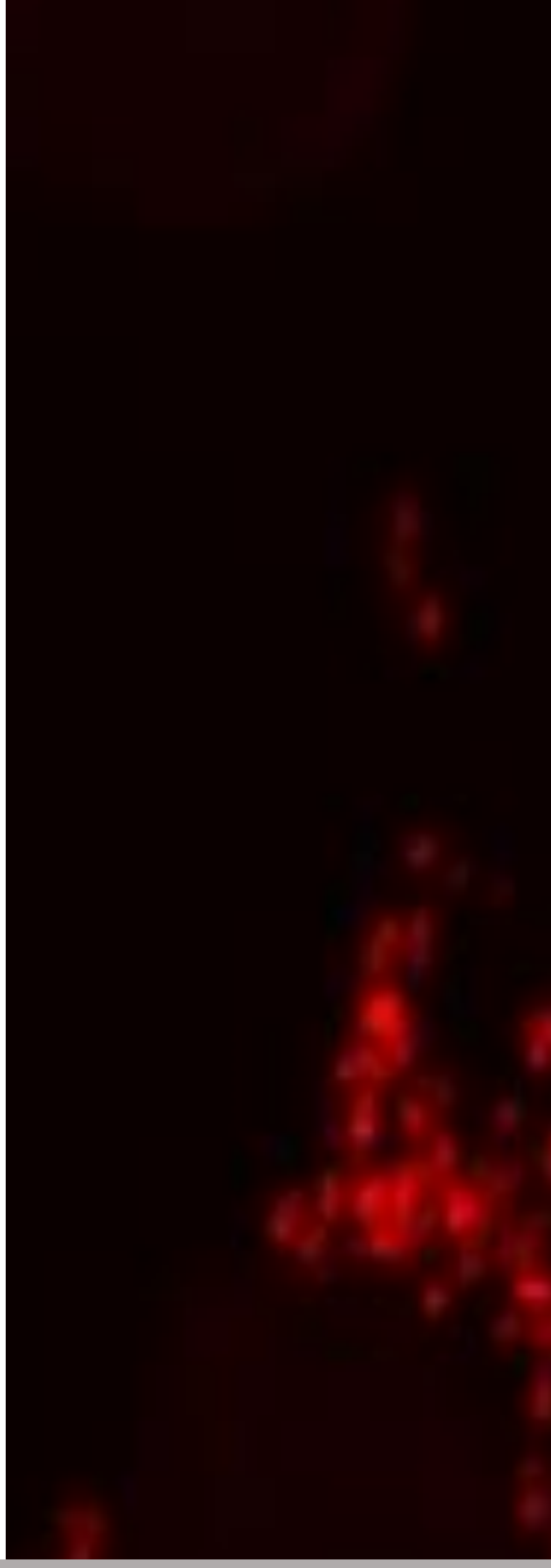

Discussion

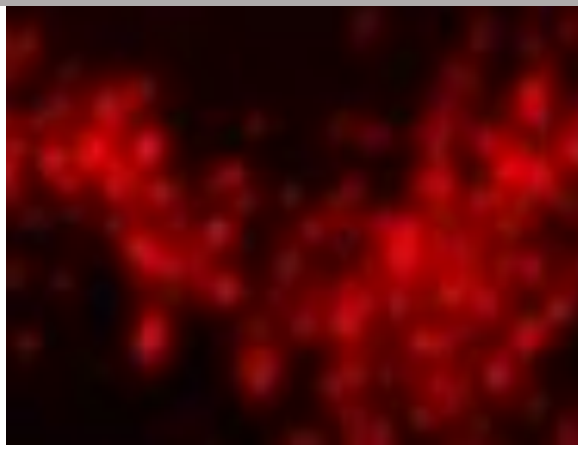

5. Discussion

Here we present evidence suggesting a critical role for mitochondria in the regulation of adaptive immune responses. Our results underscore a fundamental role of mitochondria in almost every step of T cell function, starting with the control of IS organization and early TCR signaling to T cell differentiation, cytokine production and regulation of the outcome of immune responses. By regulating IS organization and the balance between OXPHOS and glycolysis, mitochondria provide a metabolic context appropriate for efficient regulation of inflammatory responses. In addition, our results on the functional regulation between mitochondria and the endolysosomal compartment link for the first time these organelles and provide a novel role for mitochondria in the regulation of MVB maturation, exosome biogenesis and secretion. Finally, we present evidence indicating a major role of mitochondria in the regulation of lysosome biogenesis and function, which associate mitochondrial deficiencies and lysosomal storage disorders.

The mitochondrial network: how to fuel the IS.

Mitochondria are actively relocalized to cellular places with high demand of ATP or where the buffering of intracellular Ca^{2+} flux is needed. The best example of the importance of mitochondrial positioning occurs in highly polarized cells such as neuronal cells, in which mitochondria preferentially relocate into synaptic structures to fuel neurotransmitter release and regulation of calcium signaling (MacAskill and Kittler, 2010). In the immune system, lymphocytes are not inherently polarized, do not show strong front-rear polarity in the absence of stimulation and organelles are usually evenly distributed within the cytosol. However, following migration in response to soluble stimuli such as chemokines and stimulation through cell-cell contact with antigen-presenting cells (APC), T cells adopt front-rear polarity. Contact with the APC and subsequent TCR-induced signaling triggers rapid cytoplasmic and membrane remodeling within the T cell that recruits organelles such as mitochondria, the secretory apparatus, and signaling machinery to the contact site to efficiently orchestrate the events of the immune response (Martin-Cofreces et al., 2014).

The findings presented here describe how mitochondria preferentially localize into the vicinity of the IS upon TCR activation where these organelles exert an important role in T cell activation by regulating calcium signaling and the orchestration of IS formation and stability (Baixauli et al., 2011). The movement and localization of mitochondria towards the IS depends on the fusion and fission dynamics of mitochondria, although other factors have been described, such as integrin adhesion, cell polarization or transport along cytoskeleton by kinesin and dynein

motor proteins (Baixauli et al., 2011; Contento et al., 2010; Morlino et al., 2014; Quintana et al., 2007).

Increased ATP levels and mitochondrial ROS produced at the IS are needed for energy-consuming signaling at the IS (Ilani et al., 2009). Our results indicate that mitochondria play a particularly important role at the IS by supporting sustained calcium influx that is required to support synaptic signaling and T cell effector functions (Kummerow et al., 2009). In addition, we demonstrate that energy supply is also needed for the ATP-dependent acto-myosin centripetal flux of TCR to the cSMAC (Baixauli et al., 2011), which is important for the termination of TCR signals by internalization and degradation of the CD3/TCR complexes. The findings presented here provide evidence that the mitochondrial fission protein Drp1 modulates T cell activation at the IS. Mitochondrial fission factor Drp1 regulates mitochondria localization towards nascent IS and there regulates energy supply and impacts IS architecture and TCR signal strength. Mitochondrial recruitment to the IS in T cells is impaired by blockade of Drp1 action, whether by siRNA silencing, treatment with the Drp1 inhibitor mdivi-1 or overexpression of a phosphomimetic S637D Drp1 mutant unable to bind to the OMM (Baixauli et al., 2011). Impairing Drp1 decreases centripetal flux of TCR to the cSMAC and increases persistent TCR activity within microclusters, proximal TCR signaling and IL-2 production. Thus, Drp1-dependent mitochondria redistribution is required for both the proper organization of the IS and the regulation of the intracellular signaling pathways generated through the TCR. Collectively, our results support a role for mitochondria not only in the regulation of the strength of T cell activation but also in the termination of IS signaling.

The finding that mitochondrial fission factors are involved in IS formation and T cell function further emphasizes the commonalities between the immune and neural systems. Proper distribution of mitochondria at dendritic spines and synapses is essential for neural function (Li et al., 2004) and neural specific deletion of Drp-1 decreases the number of neurites and promotes defective synapse formation (Ishihara et al., 2009). The actin-rich area of the pSMAC is highly homologous with the actin-rich areas at neuronal postsynaptic termini. These actin-rich, membrane receptor-driven structures serve as scaffolds for selective and profuse secretion, and our finding that mitochondria dock at the actin-rich pSMAC area of the IS suggests that similar mechanisms operate in T cells. Whereas actin is involved in mitochondrial docking at neuronal synapses (Hollenbeck, 2005; Macaskill et al., 2009), mitochondrial trafficking is dependent on microtubules and members of the microtubule-associated kinesin and dynein motor-protein families. Mutations in dynein heavy chain or p150GLUED block axonal mitochondrial trafficking, affecting both anterograde and retrograde transport (Pilling et al., 2006). Dynein/dynactin motor complexes are important for T cell activation, mediating MTOC

translocation and the formation of the CD3/TCR central cluster at the IS (Martin-Cofreces et al., 2008). In this regard, we also observed a defect in mitochondria re-localization at the IS when dynein/dynactin motor activity is inhibited. How Drp1-mediated mitochondrial fission facilitates transport remains unclear. It is feasible that binding to mitochondria exposes the dynein-binding site on Drp1 or that dynein more efficiently traffics fragmented mitochondria than an extensively fused mitochondrial meshwork. This would imply that dynein-dependent trafficking coordinates MTOC movement with mitochondrial activity for the local delivery of biological mediators at the IS, similar to the relationship observed between the MTOC and the T cell secretory machinery (Huse et al., 2006; Kupfer et al., 1986). MTOC translocation is unaffected by Drp1 silencing, providing further evidence that dynein/dynactin transports not only the MTOC but also mitochondria towards the IS through coordinated action with Drp1.

Mitochondrial trafficking and positioning have been demonstrated to be important during the contact between viruses and lymphocytes in the virological synapse (VS). The VS shares many similarities with the IS, including synaptic enrichment of adhesion proteins, formation of a receptor-bearing complex at the contact zone, cytoskeletal rearrangements, and polarized budding of virus that is reminiscent of polarized secretion from T cells at the IS. Electron microscopy tomographic reconstructions of the HIV-1 T cell VS have revealed the cytoplasmic polarization and clustering of organelles such as mitochondria and the MTOC proximal to the plasma membrane at the contact zone spatially associated with HIV-1 budding (Groppelli et al., 2015; Jolly et al., 2011). Mitochondria are actively recruited to the VS and inhibiting mitochondrial trafficking and positioning by treating cells with the mitochondrial fission inhibitor mdivi-1 reduces T cell motility and cell-cell spread of the viruses (Groppelli et al., 2015).

Mitochondrial positioning and immune synapse architecture

Here, we demonstrate a critical role of mitochondrial positioning and mitochondrial shaping proteins in the efficient formation and function of the IS between T lymphocytes and APCs. TCR activation is initiated in the early-assembled peripheral microclusters of TCR/CD3 complexes, and downmodulated in the central supramolecular activation complex (cSMAC), where activated TCR/CD3 signaling complexes are switched off after ubiquitination, internalization and degradation by CD2AP and members of the Cbl ubiquitin ligase and ESCRT families (Malissen, 2003; Vardhana et al., 2010; Varma et al., 2006). Therefore, trafficking and internalization of TCR/CD3 complexes and stimulatory molecules at the IS is critical for efficient fine-tuning of TCR signaling, as it is for the switching-off of the signal.

The cSMAC is thus considered a focal point where endocytosis reduces TCR/CD3 complexes and the number of CD28 co-stimulatory molecules engaged by CD80 or CD86

receptors at the APC (Qureshi et al., 2011), and exocytosis allows the unidirectional transfer of cytokines and microRNA-loaded exosomes from T cells to APCs (Mittelbrunn et al., 2011). In addition, a phagocytosis-dependent process has been depicted at a similar area of the IS, which would be clathrin-independent and import pMHC complexes bound to the TCR/CD3 signalosomes (Martinez-Martin et al., 2011). Our finding showing that reduced cSMAC assembly of CD3 in Drp1 silenced T cells is associated with increased activation of TCR proximal elements suggests that, by controlling cSMAC organization, Drp1 modulates T cell activation and function.

Our data underscore the importance of mitochondrial positioning for fueling molecular motors involved in IS formation, such as myosins. Myosin IIA is concentrated at the IS, from where it is suggested to control actin flux at the actomyosin contractile ring formed beneath the pSMAC (Ilani et al., 2009). The contractility of this ring is regulated by phosphorylation of myosin regulatory light chain (MLC) and is important for directing TCR/CD3 microclusters to the cSMAC. Silencing of myosin IIA prevents the formation of the cSMAC and the amplification of TCR signals (Ilani et al., 2009). Accordingly, our data show that Drp1 silencing reduces MLC phosphorylation at Ser19, elevates the number of CD3 microclusters, and disrupts TCR/CD3 complex organization at the cSMAC. A similar effect on MLC phosphorylation has been described for Drp1 mutants during the mobilization of pool vesicles at *Drosophila* neuromuscular junctions (Verstreken et al., 2005). Our findings provide a plausible explanation of how mitochondrial de-localization from the IS might disturb cSMAC formation and subsequent signaling. By reducing actomyosin fueling at the IS, mitochondrial de-localization in Drp1-interfered T cells slows centripetal flux of TCR/CD3 microclusters, thus enhancing signaling by maintaining TCR/CD3 complexes away from cSMAC-localized degradation pathways. Interestingly, other studies propose a similar role for Drp1 in the regulation of neuronal synapses by controlling mitochondrial positioning and function. In this respect, the pro-apoptotic Bcl-2 family member Bcl-xL regulates Drp1 to alter mitochondrial function in a manner that stimulates synapse formation (Li et al., 2008). Alternatively to altering mitochondrial function, Bcl-xL is able to directly regulate endocytic vesicle retrieval in hippocampal neurons mediating protein–protein interaction of Drp1 with components of the clathrin complex (Li et al., 2013). Thus, these data point that Drp1 could regulate TCR signaling and IS architecture directly regulating TCR/CD3 endocytic events at the IS through its binding to clathrin.

Mitochondrial function and TCR signaling

Our results showing that Drp1 silencing increases mitochondrial depolarization in stimulated and non-stimulated T cells argue for a direct role of Drp1 in controlling mitochondrial function during T cell activation. Enhanced mitochondrial depolarization prevents both the

clustering of the TCR/CD3 at the cSMAC and the cessation of TCR-dependent signaling, resulting in persistent T cell activation, intracellular Ca^{2+} flux and diminished ATP synthesis. Mitochondria located at sites of T cell stimulation control local Ca^{2+} influx (Schwindling et al., 2010), and our results therefore support a role for Drp1 in the regulation of mitochondrial positioning required for efficient Ca^{2+} signaling at the IS. The IS is the main entry point for Ca^{2+} upon TCR stimulation (Schwindling et al., 2010), which suggests that Drp1 impedes intra-mitochondrial diffusion of Ca^{2+} during TCR signaling by maintaining the compartmentalization of the mitochondrial network at the IS through fission events. In this regard, our results support the notion that T cells fine tune TCR responses through Drp1-mediated regulation of mitochondrial positioning and activity and underlie the importance of mitochondrial shape for the ability of the cell to respond to different cues. Furthermore, mitochondria positioning at the IS is essential for the management of intracellular Ca^{2+} levels, and Drp1-dependent fragmentation of the mitochondrial network may serve to protect T cells from amplified calcium signaling triggered by activation.

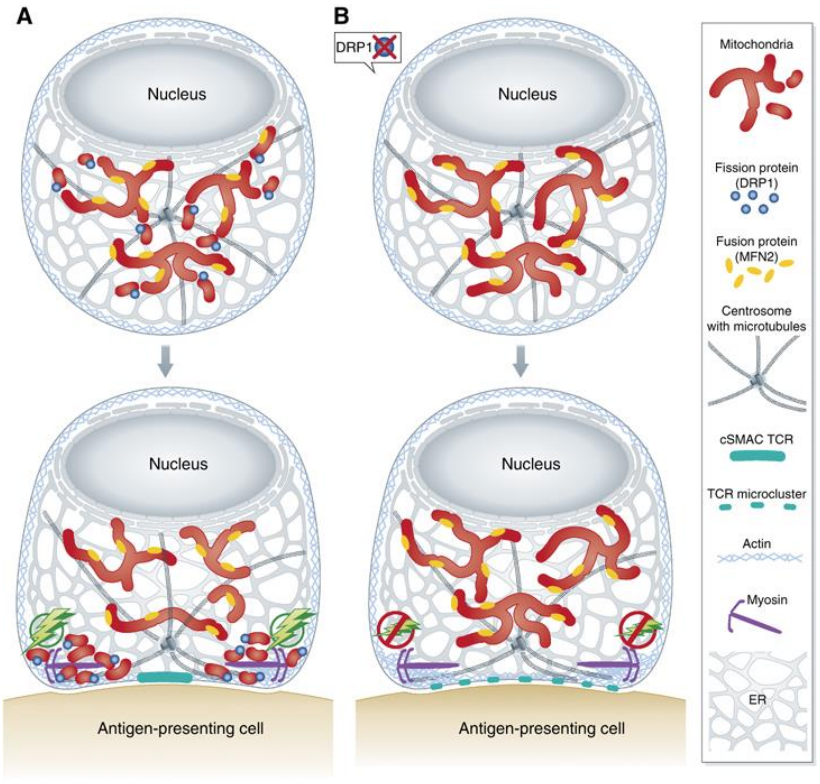

Proposed model for DRP1, mitochondrial localization and IS formation. (**A**) After IS formation with an antigen-presenting cell, mitochondria are transported towards the IS, where they provide proper energy supply for synaptic signalling including centripetal flux of TCR microclusters towards the cSMAC by myosin motors. (**B**) Inhibition of DRP1 induces unopposed fusion of mitochondria and they cannot be transported as well to the pSMAC. Baixauli et al, 2011 highlighted in (Junker and Hoth, 2011).

Further work is needed to address the relation between mitochondrial dynamics and transport machineries, to determine how mitochondria are anchored to the IS, and to identify the signals that relocate mitochondria to sites of high energy demand and Ca^{2+} buffering, such as extracellular glucose uptake, which has been demonstrated to control mitochondrial motility by regulating the activity of Miro-Milto complex (Pekkurnaz et al., 2014). Remarkably, exploring whether mitochondrial shaping proteins control the unequal partitioning of mitochondria during cell division depending on the different metabolic requirements of the specific T cell subsets, will also be of great interest.

Tfam-deficient mice as a model to study mitochondrial function

Although the different metabolic profiles of T cell subsets are well documented, it remains unclear why these cells must adopt these very different metabolic phenotypes for their differentiation and whether these metabolic changes are instructive versus responsive. Notably, it is being increasingly appreciated that metabolic pathways provide more than just ATP and biosynthetic intermediates, and importantly provide signaling intermediates that are essential for cellular function and also influence T cell fate.

Besides energy supply, mitochondria perform many other cellular functions that can participate during the orchestration of an adaptive immune response. The use of specific mitochondrial inhibitors and the few available genetic models of mitochondrial deficiency in T cells have underscored important and unanticipated functions of mitochondrial metabolism in the regulation of T cell activation, differentiation and fate (Weinberg et al., 2015). To understand how mitochondria influence T cell differentiation and ultimately affect immune disease progression, we have generated a mouse model of mitochondrial dysfunction by deleting Tfam in the T cell compartment using the CD4Cre LoxP system. Consistent with its role in the maintenance of mtDNA transcription and replication, deletion of Tfam in T lymphocytes promotes a reduction in the levels of mtDNA and the transcripts encoding the mitochondrial subunits of the ETC. Consequently, Tfam deletion reduces mitochondrial supercomplex assembly, electron transport between respiratory complexes and decreases mitochondrial ATP production. Besides these profound mitochondrial alterations, Tfam-deficiency triggers a general mitochondrial dysfunction without altering the general energetic status of the cell, as evidenced by the similar levels of total ATP and the absence of AMPK activation. In addition, metabolic flux experiments demonstrate that *Tfam*$^{-/-}$ cells maintain their energy status by promoting a "metabolic switch" characterized by increased anaerobic glycolysis and reduced OXPHOS. Importantly, deletion of Tfam in lymphocytes does not affect T cell development since similar numbers and proportions of CD4 T cells are found in the thymus and secondary lymph nodes from wild-type and Tfam$^{-/-}$ mice.

Altogether, these data support the use of *Tfam*$^{-/-}$ as a suitable genetic mice model to study mitochondrial function in T cell responses either *in vitro* or *in vivo*, and investigate novel functions of mitochondria during adaptive immune responses (Baixauli et al., 2015). Using this model, we reveal a critical role of mitochondria coordinating cellular metabolism and the biogenesis and function of the endolysosomal compartment during T cell activation and differentiation.

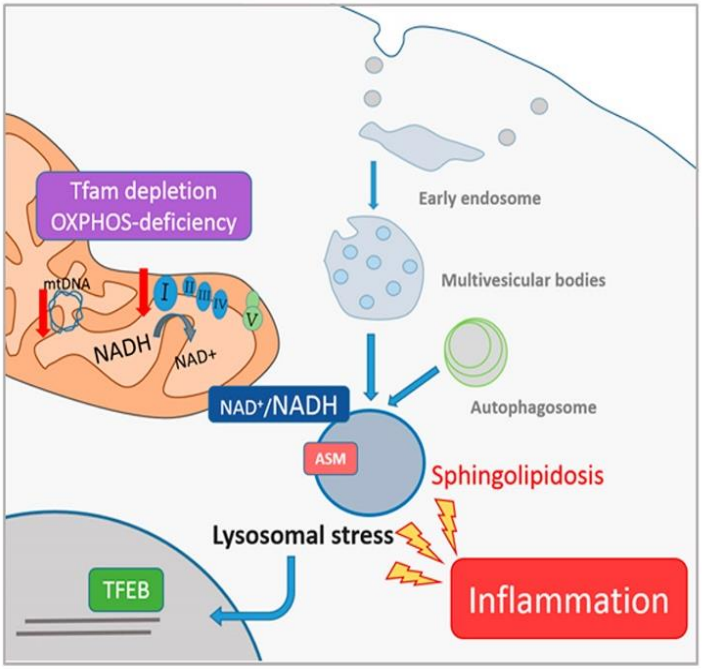

Proposed model for mitochondria in the regulation of adaptive immune responses. Critical role for mitochondria in the regulation of T cell inflammatory responses by controlling lysosome function. Abnormal endolysosomal function and sphingomyelin accumulation in respiration-impaired cells link mitochondrial dysfunction to lysosomal storage disorders and exacerbated inflammatory responses (Baixauli et al., 2015).

Mitochondrial OXPHOS regulates T cell activation, proliferation and differentiation

Activation of T cells is intimately linked to the engagement of specific metabolic pathways. This metabolic reprogramming is associated with a global change in the transcriptome linked to c-Myc and Hif-1α activation. Hif-1α maintains T cell glycolytic activities after entry into the cell cycle (Wang et al., 2011), whereas Myc drives the transcriptional program that coordinates glucose metabolic enzymes, glutamine catabolism (Gao et al., 2009), and mitochondrial biogenesis (Li et al., 2005). Glutamine provides a major source of energy and nitrogen for biosynthesis and a carbon substrate for anabolic processes in proliferating cells. Glutamine catabolism is tightly coupled to several biosynthetic pathways, but also generates the anaplerotic substrate α-ketoglutarate (α-KG), that is metabolized through the TCA cycle to generate citrate or pyruvate. Therefore, metabolism in proliferating cells, especially of glutamine, relies on continued mitochondrial function. In this regard, Myc also acts as a strong promoter of

mitochondrial biogenesis and induces the expression of many nuclear-encoded mitochondrial genes, among them, Tfam (Gomes et al., 2013). Our results show the concomitant increases in Tfam mRNA expression and mtDNA content during T cell activation, and suggest that metabolic reprogramming of T cells critically depends on mitochondrial function achieved in part through increased Tfam expression, most likely through upregulation of Myc transcriptional activity.

Our data support the role of mitochondria as central hubs integrating cellular metabolism, and emphasize the requirement of a tightly regulated mitochondrial function to fine tune the process of T cell activation. Mitochondrial respiration-deficient cells do not show altered T cell activation, but showed decreased proliferation and elevated IFN-γ secretion, concomitantly with an increased anaerobic glycolysis and reduced OXPHOS function. A recent study has demonstrated the mechanistic link between metabolic pathways and acquisition of T cell effector functions (Chang et al., 2013). The glycolysis enzyme GAPDH can repress IFN-γ mRNA expression by binding to its 3'-UTR. Upon T cell activation, engagement of aerobic glycolysis releases GAPDH from the 3'-UTR and allows IFN-γ mRNA expression (Chang et al., 2013). Based on these findings, we suggest that the metabolic reprogramming towards glycolysis in $Tfam^{-/-}$ T cells might contribute to their increased IFN-γ production.

Distinct metabolic pathways support the differentiation of CD4 T helper (Th) cells into their separate lineages. Our results reveal a role for mitochondrial respiration in the regulation of T cell differentiation, and indicate that mitochondrial dysfunction is associated with a deregulation of T cell differentiation toward pro-inflammatory Th1 cell subsets. Mitochondrial respiration-deficiency, which promotes a metabolic switch toward increased glycolysis and impaired fatty acid β-oxidation, favors the differentiation of pro-inflammatory Th1 subsets and dampens Th2 and Th17 differentiation. Interestingly, in other cells of the immune system, impaired mitochondrial respiration has been also associated with increased inflammatory responses. In macrophages, glycolysis is essential for pro-inflammatory M1 macrophage activation, whereas IL-4 induces lysosomal lipolysis and fatty acid oxidation essential for M2 activation (Huang et al., 2014). Interestingly, succinate accumulation promoted by impaired mitochondrial function, decreases prolyl hydroxylase activity, stabilizes Hif-1α and enhances IL-1β production (Tannahill et al., 2013), a mechanism likely contributing to the increased pro-inflammatory profile of Tfam-deficient T cells.

Glycolysis is important in driving Th17 differentiation through Hif-1α (Pearce et al., 2013). Hif-1α stabilization mediates Foxp3 proteosomal degradation and induction of Th17 cells (Dang et al., 2011; Shi et al., 2011). Additionally, a recent report describes the greater reliance on glutamine metabolism of Th17 cells (Gerriets et al., 2015). *$Tfam^{-/-}$* T cells show impaired Th17 differentiation and reduced number of IL-17-producing cells and IL-17 secretion. Besides the

prominent Hif-1α stabilization and increased glycolytic activity in respiration-deficient cells, defective glutaminolysis, which requires an intact ETC for its function, could explain the impaired Th17 differentiation observed in mitochondrial respiration-deficient cells. Nevertheless, our results show that mitochondrial respiration-deficiency favors the appearance of Th17 cells which co-express RORγt and T-bet, and produce high levels of IFN-γ but reduced amounts of IL-17 and IL-10, and which have been proposed to be pathogenic Th17 cells involved in autoimmune diseases in mice (Peters et al., 2011). With respect to Treg cells, we found similar numbers of Foxp3-expressing cells in wild-type and *Tfam*$^{-/-}$ cells but reduced amounts of the anti-inflammatory cytokine IL-10 in respiration-deficient cells. These results, together with the exacerbated *in vivo* inflammatory responses of *Tfam*$^{-/-}$ mice, support the critical role of mitochondrial function in Th17/Treg differentiation and function. Overall, our results suggest that cues derived from mitochondria besides regulation of cellular bioenergetics, can modulate the appearance of pathogenic Th17 cells and regulate inflammatory responses.

Mitochondria regulate the endolysosomal compartment during inflammatory responses

Our findings reveal a critical role for mitochondria in the regulation of endolysosomal function and the differentiation of pro-inflammatory T cell subsets, and identify mechanisms by which mitochondrial dysfunction might contribute to human disease by affecting the endolysosomal compartment. We show that lack of Tfam switches metabolism from aerobic FAO to anaerobic glucose consumption. This altered mitochondrial metabolism is associated with abnormal accumulation of lipids, especially sphingomyelins (SM), impaired endolysosomal function, and increased differentiation of pro-inflammatory T cell subsets, which promotes T cell differentiation toward the pro-inflammatory Th1 subset and dampens Th2 and Th17 differentiation. Our results support that loss of lysosomal homeostasis by a primary mitochondrial dysfunction triggers pro-inflammatory T cell responses. The lysosomal dysfunction and increased SM levels in respiration-deficient T cells appear to be associated with the acquisition of a pro-inflammatory profile. We show that lysosomal dysfunction triggered by pharmacological inhibition or the use of acid sphingomyelinase deficient T cells (ASM$^{-/-}$), a mice model of Niemann-Pick type A disease, show a similar pro-inflammatory cytokine profile than Tfam-deficient T cells, indicating that lysosomal dysfunction is sufficient to exacerbate pro-inflammatory responses in cells without altered mitochondrial respiration. Accordingly, immune deviation toward Th1 response and reduction of Th2 differentiation has been observed in a mouse model of Gaucher disease (Pandey et al., 2012) and the contribution of lysosomal homeostasis to the regulation of T cell function during adaptive immune responses has been recently demonstrated (Valdor et al., 2014).

It is well known how lysosomes regulate innate immune responses. Lysosomal destabilization regulates the release of highly pro-inflammatory cytokines interleukin-1β (IL-1β) and IL-18 by triggering inflammasome activation (Hornung et al., 2008). In addition, lysosomal degradation of TLR4 and TLR9 regulates pro-inflammatory cytokine production in macrophages (Wang et al., 2007; Yao et al., 2009). Furthermore, lysosomal biogenesis through TFEB plays a critical role in innate immunity and antiviral defense (Hasan et al., 2013). A recent publication shows how lysosomal function could regulate immune response by modulating cellular metabolism; by degrading key glycolytic enzymes, lysosome function regulates glycolysis and the production of effector cytokines, including IFN-γ and IL-1β (Lu et al., 2014). Concomitantly with the metabolic reprogramming, abnormal lipid accumulation, lysosome destabilization and impaired degradation capacity in Tfam-deficient T cells, might contribute to the exacerbated pro-inflammatory response of mitochondrial respiration-deficient cells.

Linking mitochondrial deficiencies to lysosome storage diseases

Lipid metabolism and the maintenance of membrane homeostasis require an extensive exchange of lipids and metabolic intermediates between cellular organelles. Our study identifies Tfam as a key player in the regulation of lipid metabolism that impacts endolysosomal-autophagy pathway and the membrane reorganizations required for MVB maturation and exosome secretion.

Sphingomyelins and other lipids such as cholesterol, glycosphingolipids and sphingosine, abnormally accumulate in a group of inherited diseases referred to as lysosomal storage disorders (LSDs) (Schulze and Sandhoff, 2011). For instance, sphingosine accumulation is an initiating factor in Niemann-Pick disease type C1 (NPC1), pathogenesis that causes altered lysosomal function, leading to the secondary storage of sphingolipids and cholesterol (Lloyd-Evans et al., 2008). Cholesterol accumulation directly affects the fusion of lysosomes with endosomes and with autophagic vacuoles by affecting the assembly and recycling of SNAP and SNARE proteins (Fraldi et al., 2010). Niemman Pick type A (NPA) is a sphingolipidosis caused by loss of function mutations in the gene SMPD1 encoding for the acid sphingomyelinase (ASM), enzyme that catalyzes sphingomyelin conversion into ceramide in lysosomes. Cells from NPA patients accumulate sphingomyelin in their lysosomes and present impaired protein degradation and macroautophagy (Gabande-Rodriguez et al., 2014). The accumulation of sphingomyelins in respiratory-deficient cells supports the hypothesis that lipid metabolism imbalance resulting from mitochondrial dysfunction is associated with lysosomal storage disease.

Previous studies have examined the role of Tfam in neurodegenerative diseases. Specific deletion of Tfam in neurons induces progressive parkinsonism in mice (Ekstrand et al., 2007),

and Tfam deletion in Schwann cells induces a neuropathy associated with axon degeneration and demyelination caused by the accumulation of acylcarnitines (Viader et al., 2013). Our findings on the role of mitochondrial respiration as a regulator of endolysosomal function may provide novel insights into the mechanisms by which mitochondria are involved in neurodegenerative diseases by regulating lysosomal degradative capacities. The connection between lysosomes and mitochondrial function is illustrated by Gaucher disease, in which a primary lysosomal defect causes accumulation of dysfunctional mitochondria and links lysosomal function to the preservation of mitochondrial integrity (Osellame et al., 2013). On the contrary, we provide herein the first evidence for a primary mitochondrial dysfunction leading to altered lysosomal function and sphingolipidosis. We also identify OXPHOS as a key regulator of lipid metabolism that influences membrane reorganization essential for endolysosomal and autophagy pathways. Our data indicate that either lowering the levels of mtDNA by Tfam deletion or punctual mtDNA mutations found in patients with OXPHOS deficiency impair lysosomal function.

Autophagy and lysosomes regulate lipid metabolism through a regulatory network linked to the activation and nuclear translocation of the transcriptional factor TFEB (Settembre et al., 2013a). A predominant nuclear localization of TFEB, however, has been detected in cells from LSD mouse models, suggesting that the TFEB pathway is activated after intralysosomal storage of non-degraded molecules as a cellular response to lysosomal stress (Sardiello et al., 2009). Tfam-deficient cells showed increased autophagy markers, enlarged lysosomal compartments but decreased lysosomal function and degradation capacity. The activation of TFEB in Tfam-deficient cells, as a physiological cell response to compensate the lysosomal dysfunction, supports the role of mitochondria in controlling the lysosomal compartment.

Lysosomal calcium level is impaired not only by Tfam deletion, which triggers a general lowering of the levels of mtDNA, but also in cells from patients with point mutations in mitochondrial respiratory complex I. Mitochondrial complex I is essential for maintenance of the NAD^+/NADH ratio through NADH dehydrogenase activity, and an imbalanced NAD^+/NADH ratio in cancer cells with mutations in mitochondrial complex I subunits is associated with impaired autophagy and p62 degradation (Santidrian et al., 2013). Inhibition of complex I activity with rotenone in a mouse model of Parkinson's disease impairs autophagic flux and promotes p62 and alpha-synuclein accumulation (Wu et al., 2015). Our data demonstrate that NAD precursors restore ASM activity and prevent p62 accumulation in Tfam-deficient cells, thus supporting a role of mitochondrial respiratory complex I and NAD^+/NADH ratio in the regulation of lysosomal function. In accordance, addition of NAM downregulates TFEB target genes in Tfam-deficient cells. These data support the notion that lysosomes adapt their biogenesis and function to the metabolic state of the cell by sensing intracellular NAD^+/NADH levels. Further research is

necessary to understand how NAD precursors reestablish ASM activity and lysosomal function, and whether it relies on transcriptional regulation by NAD-dependent deacetylases.

Mitochondrial metabolism in MVB biogenesis and exosome secretion.

Mitochondria are intimately connected to other organelles. Mitochondria establish physical contacts with the ER that are essential for the transport of calcium and phospholipids from the ER to the inner mitochondrial membrane (Osman et al., 2011), and are tethered by mitofusin 2 (Mfn2) (de Brito and Scorrano, 2008). Mfn2 also regulates the contact between mitochondria and melanosomes, the lysosome-related organelles of pigment cells, and these contacts are involved in melanosome biogenesis and maturation (Daniele et al., 2014). A contact site has also recently been identified between mitochondria and the lysosome-like yeast vacuole, and reported to act as an alternative route for phospholipid import into mitochondria when ER-mitochondria contacts are impaired (Elbaz-Alon et al., 2014; Honscher et al., 2014). These observations suggest the intriguing possibility that the impact of mitochondrial dysfunction on the endolysosomal system might be mediated through physical contacts between these organelles. Further investigations will be necessary to elucidate whether mitochondria physically connect with components of the endolysosomal compartment and to decipher the molecular mediators that participate in these contacts.

Recently, it has been described that mitochondria form mitochondrial derived vesicles (MDVs) as an early response to oxidative stress (Braschi et al., 2010; Neuspiel et al., 2008). These MDVs shuttle oxidized mitochondrial proteins to the lysosomes in order to preserve the integrity of the organelle in a quality control mechanisms that connects mitochondria with lysosomes via the formation of these vesicles. In response to mitochondrial oxidative stress, parkin induces, in a PINK1-dependent manner, the formation of mitochondrial vesicles, which are enriched for specific mitochondrial proteins. Thus, lysosomal targeting of MDVs constitutes an additional, mitophagy-independent quality control mechanism (Sugiura et al., 2014). It will be interesting to address whether MDVs support lysosome function or mediate the specific trafficking of lipids between mitochondria and lysosomes. In addition, it will be interesting to address the connection between MDVs and exosomes, and whether secretion of mitochondrial-derived content in exosomes can represent an additional quality control mechanism in circumstances in which cell degradation capacity is compromised.

Our results highlight the critical role of mitochondrial metabolism in MVBs and exosomes biogenesis. Exosomes are secreted by almost all cells, and provide a vehicle for intercellular communication (Mittelbrunn and Sanchez-Madrid, 2012). Cells of the adaptive and innate

immune system release exosomes that influence the immune response in a non-cell autonomous manner (Mittelbrunn et al., 2011; Okoye et al., 2014; Robbins and Morelli, 2014). The molecular mechanisms that regulate exosome biogenesis depend on the endosomal sorting complex required for transport (ESCRT), lipids and tetraspanins (Villarroya-Beltri et al., 2014). For the first time, we demonstrate that mitochondria are critical organelles in MVB maturation and exosome secretion. Our data therefore suggest novel strategies to manipulate exosome production by modulating mitochondrial metabolism, and identify Tfam as a regulator of exosome biogenesis The regulation of lipid metabolism by mitochondria is critical in membrane organization during MVB maturation and exosome biogenesis since respiratory deficient Tfam-depleted cells showed empty MVBs and decreased exosome secretion. The sphingolipid ceramide segregates exosome-associated microdomains to ILVs in a process dependent on neutral sphingomyelinases (Trajkovic et al., 2008). The phospholipid lysobisphosphatidic acid (LBPA) facilitates the inward transformation of the membrane during exosome biogenesis and the cholesterol levels (Chevallier et al., 2008; Matsuo et al., 2004). Lipidomic analysis showed normal levels of ceramide but abnormal sphingomyelin and LBPA accumulation in Tfam-deficient cells. These results indicated that accumulation of sphingomyelin precursors during ceramide synthesis is critical during ILV biogenesis and MVB maturation, regardless of the levels of LBPA or ceramides. Therefore, our results are consistent with the role of the neutral sphingomyelinase in exosome biogenesis, since inhibition of their activity, which reduces ceramide levels but promotes sphingomyelin accumulation, decreases ILV formation and exosome secretion (Trajkovic et al., 2008).

Overall, we have identified a novel mechanism by which mitochondria exert a key regulatory role coupling lipid metabolism and endolysosomal system to preserve acquisition of T cell differentiation and effector functions.

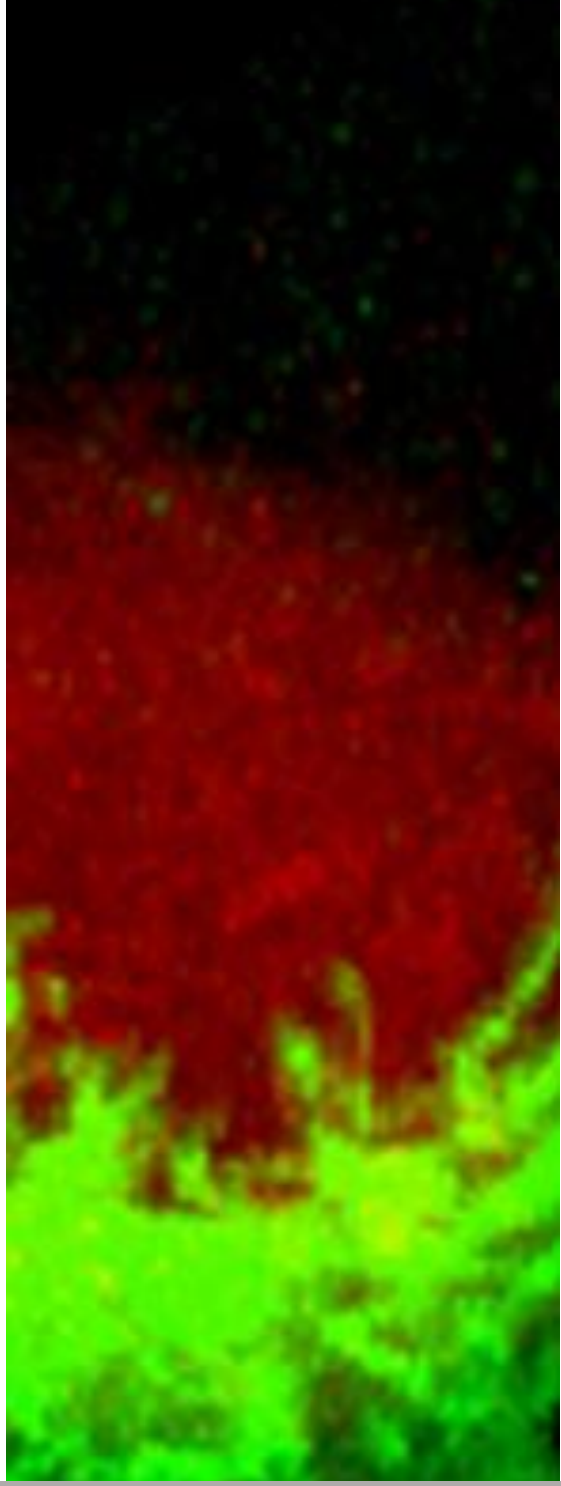

Conclusions

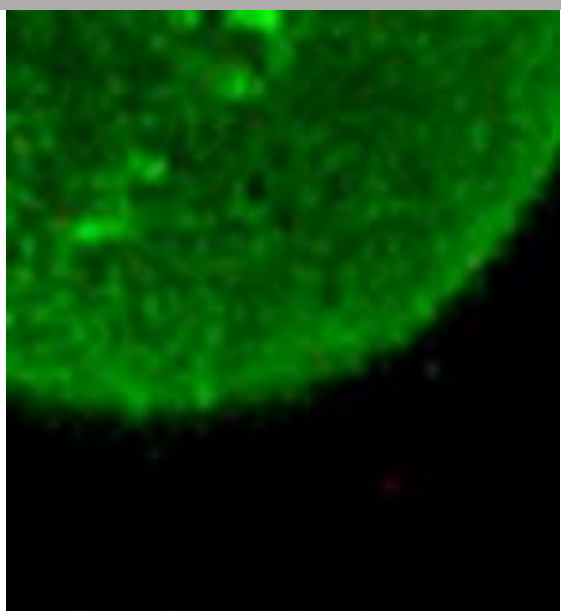

6. Conclusions

The findings presented herein support the following conclusions;

1. **The mitochondrial fission protein DRP1 regulates mitochondria localization towards nascent IS in coordination with the cytoskeleton transport machinery.**

2. **Synaptic mitochondria control energy supply, IS architecture and TCR signaling, thus regulating the strength of T cell activation but also the termination of IS signaling.**

3. **Mitochondrial OXPHOS regulates T cell activation, proliferation and differentiation.**

4. **Mitochondrial dysfunction deviates T cell differentiation toward pro-inflammatory Th1 cell subsets *in vitro* and exacerbates inflammatory responses in *in vivo* models of inflammation.**

5. **Mitochondrial respiration regulates endolysosomal function. Lysosome dysfunction in respiration-deficient cells link mitochondrial deficiencies with Lysosomal Storage Diseases (LSDs).**

6. **Mitochondrial respiration regulates the endolysosomal compartment during inflammatory responses. Raising NAD^+ levels improves lysosomal function and ameliorates inflammatory defects in respiration-deficient cells.**

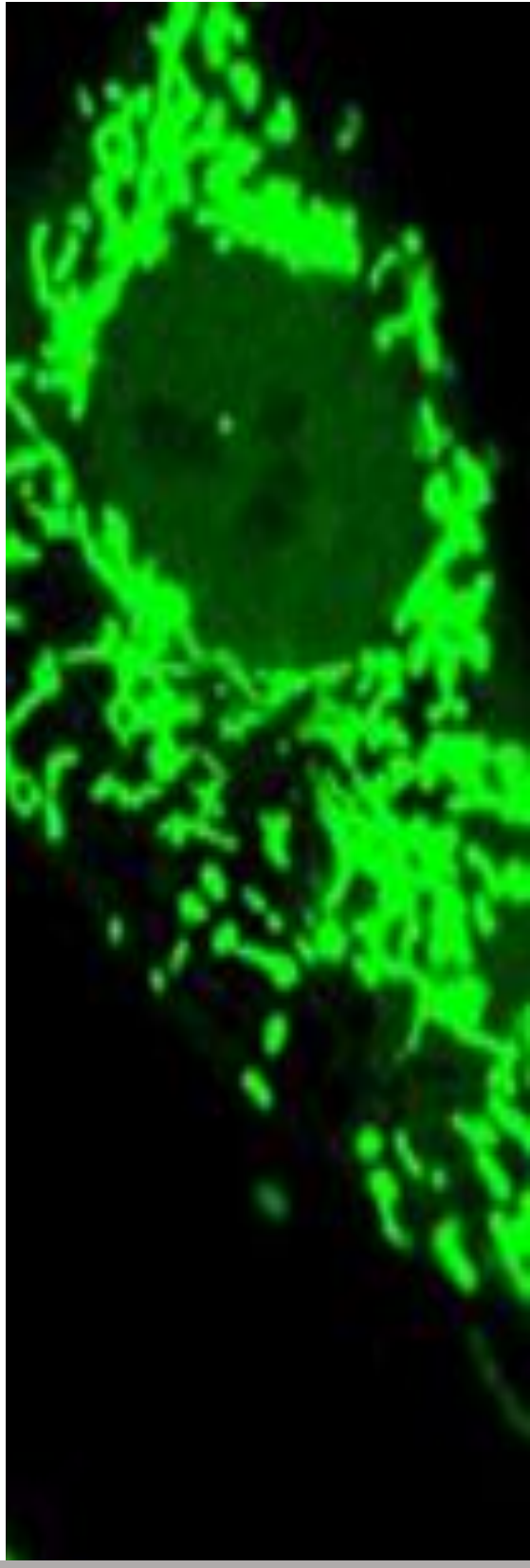

References

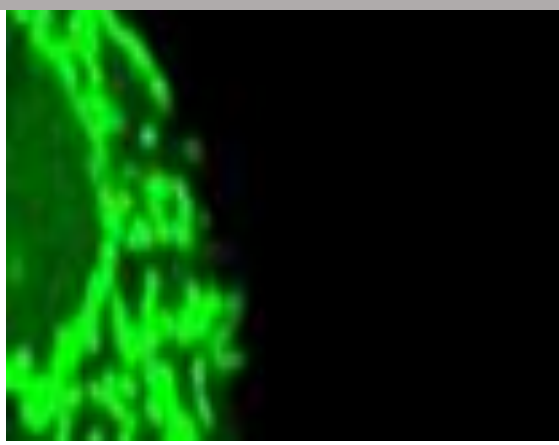

7. References

Abarca-Rojano, E., Muniz-Hernandez, S., Moreno-Altamirano, M.M., Mondragon-Flores, R., Enriquez-Rincon, F., and Sanchez-Garcia, F.J. (2009). Re-organization of mitochondria at the NK cell immune synapse. Immunol Lett *122*, 18-25.

Acin-Perez, R., Carrascoso, I., Baixauli, F., Roche-Molina, M., Latorre-Pellicer, A., Fernandez-Silva, P., Mittelbrunn, M., Sanchez-Madrid, F., Perez-Martos, A., Lowell, C.A., et al. (2014). ROS-Triggered Phosphorylation of Complex II by Fgr Kinase Regulates Cellular Adaptation to Fuel Use. Cell Metab *19*, 1020–1033.

Alonso, R., Mazzeo, C., Rodriguez, M.C., Marsh, M., Fraile-Ramos, A., Calvo, V., Avila-Flores, A., Merida, I., and Izquierdo, M. (2011). Diacylglycerol kinase alpha regulates the formation and polarisation of mature multivesicular bodies involved in the secretion of Fas ligand-containing exosomes in T lymphocytes. Cell Death Differ *18*, 1161-1173.

Area-Gomez, E., Del Carmen Lara Castillo, M., Tambini, M.D., Guardia-Laguarta, C., de Groof, A.J., Madra, M., Ikenouchi, J., Umeda, M., Bird, T.D., Sturley, S.L., et al. (2012). Upregulated function of mitochondria-associated ER membranes in Alzheimer disease. EMBO J *31*, 4106-4123.

Arruda, A.P., Pers, B.M., Parlakgul, G., Guney, E., Inouye, K., and Hotamisligil, G.S. (2014). Chronic enrichment of hepatic endoplasmic reticulum-mitochondria contact leads to mitochondrial dysfunction in obesity. Nat Med *20*, 1427-1435.

Baixauli, F., Acin-Perez, R., Villarroya-Beltri, C., Mazzeo, C., Nunez-Andrade, N., Gabande-Rodriguez, E., Ledesma, M.D., Blazquez, A., Martin, M.A., Falcon-Perez, J.M., et al. (2015). Mitochondrial Respiration Controls Lysosomal Function during Inflammatory T Cell Responses. Cell Metab *22*, 485-498.

Baixauli, F., Lopez-Otin, C., and Mittelbrunn, M. (2014). Exosomes and autophagy: coordinated mechanisms for the maintenance of cellular fitness. Front Immunol *5*, 403.

Baixauli, F., Martin-Cofreces, N.B., Morlino, G., Carrasco, Y.R., Calabia-Linares, C., Veiga, E., Serrador, J.M., and Sanchez-Madrid, F. (2011). The mitochondrial fission factor dynamin-related protein 1 modulates T-cell receptor signalling at the immune synapse. EMBO J *30*, 1238-1250.

Barr, J., Caballeria, J., Martinez-Arranz, I., Dominguez-Diez, A., Alonso, C., Muntane, J., Perez-Cormenzana, M., Garcia-Monzon, C., Mayo, R., Martin-Duce, A., et al. (2012). Obesity-dependent metabolic signatures associated with nonalcoholic fatty liver disease progression. J Proteome Res *11*, 2521-2532.

Bedoya, S.K., Lam, B., Lau, K., and Larkin, J., 3rd (2013). Th17 cells in immunity and autoimmunity. Clin Dev Immunol *2013*, 986789.

Bellingham, S.A., Guo, B.B., Coleman, B.M., and Hill, A.F. (2012). Exosomes: vehicles for the transfer of toxic proteins associated with neurodegenerative diseases? Front Physiol *3*, 124.

Boland, M.L., Chourasia, A.H., and Macleod, K.F. (2013). Mitochondrial dysfunction in cancer. Frontiers in oncology *3*, 292.

Boustany, R.M. (2013). Lysosomal storage diseases--the horizon expands. Nat Rev Neurol *9*, 583-598.

Braschi, E., Goyon, V., Zunino, R., Mohanty, A., Xu, L., and McBride, H.M. (2010). Vps35 mediates vesicle transport between the mitochondria and peroxisomes. Curr Biol *20*, 1310-1315.

Buck, M.D., O'Sullivan, D., and Pearce, E.L. (2015). T cell metabolism drives immunity. J Exp Med *212*, 1345-1360.

Calabia-Linares, C., Robles-Valero, J., de la Fuente, H., Perez-Martinez, M., Martin-Cofreces, N., Alfonso-Perez, M., Gutierrez-Vazquez, C., Mittelbrunn, M., Ibiza, S., Urbano-Olmos, F.R., et al. (2011). Endosomal clathrin drives actin accumulation at the immunological synapse. J Cell Sci *124*, 820-830.

Campello, S., Lacalle, R.A., Bettella, M., Manes, S., Scorrano, L., and Viola, A. (2006). Orchestration of lymphocyte chemotaxis by mitochondrial dynamics. J Exp Med *203*, 2879-2886.

Carrasco, Y.R., Fleire, S.J., Cameron, T., Dustin, M.L., and Batista, F.D. (2004). LFA-1/ICAM-1 interaction lowers the threshold of B cell activation by facilitating B cell adhesion and synapse formation. Immunity *20*, 589-599.

Cassidy-Stone, A., Chipuk, J.E., Ingerman, E., Song, C., Yoo, C., Kuwana, T., Kurth, M.J., Shaw, J.T., Hinshaw, J.E., Green, D.R., et al. (2008). Chemical inhibition of the mitochondrial division dynamin reveals its role in Bax/Bak-dependent mitochondrial outer membrane permeabilization. Dev Cell *14*, 193-204.

Cereghetti, G.M., Stangherlin, A., Martins de Brito, O., Chang, C.R., Blackstone, C., Bernardi, P., and Scorrano, L. (2008). Dephosphorylation by calcineurin regulates translocation of Drp1 to mitochondria. Proc Natl Acad Sci U S A *105*, 15803-15808.

Cerutti, R., Pirinen, E., Lamperti, C., Marchet, S., Sauve, A.A., Li, W., Leoni, V., Schon, E.A., Dantzer, F., Auwerx, J., et al. (2014). NAD(+)-dependent activation of Sirt1 corrects the phenotype in a mouse model of mitochondrial disease. Cell Metab *19*, 1042-1049.

Cogliati, S., Frezza, C., Soriano, M.E., Varanita, T., Quintana-Cabrera, R., Corrado, M., Cipolat, S., Costa, V., Casarin, A., Gomes, L.C., et al. (2013). Mitochondrial cristae shape determines respiratory chain supercomplexes assembly and respiratory efficiency. Cell *155*, 160-171.

Contento, R.L., Campello, S., Trovato, A.E., Magrini, E., Anselmi, F., and Viola, A. (2010). Adhesion shapes T cells for prompt and sustained T-cell receptor signalling. EMBO J *29*, 4035-4047.

Cuervo, A.M. (2013). Preventing lysosomal fat indigestion. Nat Cell Biol *15*, 565-567.

Chan, D.C. (2006). Mitochondrial fusion and fission in mammals. Annu Rev Cell Dev Biol *22*, 79-99.

Chandel, N.S., Maltepe, E., Goldwasser, E., Mathieu, C.E., Simon, M.C., and Schumacker, P.T. (1998). Mitochondrial reactive oxygen species trigger hypoxia-induced transcription. Proc Natl Acad Sci U S A *95*, 11715-11720.

Chang, C.H., Curtis, J.D., Maggi, L.B., Jr., Faubert, B., Villarino, A.V., O'Sullivan, D., Huang, S.C., van der Windt, G.J., Blagih, J., Qiu, J., et al. (2013). Posttranscriptional control of T cell effector function by aerobic glycolysis. Cell *153*, 1239-1251.

Chen, H., and Chan, D.C. (2005). Emerging functions of mammalian mitochondrial fusion and fission. Hum Mol Genet *14 Spec No. 2*, R283-289.

Chen, H., Chomyn, A., and Chan, D.C. (2005). Disruption of fusion results in mitochondrial heterogeneity and dysfunction. J Biol Chem *280*, 26185-26192.

Chen, H., Detmer, S.A., Ewald, A.J., Griffin, E.E., Fraser, S.E., and Chan, D.C. (2003). Mitofusins Mfn1 and Mfn2 coordinately regulate mitochondrial fusion and are essential for embryonic development. J Cell Biol *160*, 189-200.

Chen, H., McCaffery, J.M., and Chan, D.C. (2007). Mitochondrial fusion protects against neurodegeneration in the cerebellum. Cell *130*, 548-562.

Chen, H., Vermulst, M., Wang, Y.E., Chomyn, A., Prolla, T.A., McCaffery, J.M., and Chan, D.C. (2010). Mitochondrial fusion is required for mtDNA stability in skeletal muscle and tolerance of mtDNA mutations. Cell *141*, 280-289.

Chevallier, J., Chamoun, Z., Jiang, G., Prestwich, G., Sakai, N., Matile, S., Parton, R.G., and Gruenberg, J. (2008). Lysobisphosphatidic acid controls endosomal cholesterol levels. J Biol Chem *283*, 27871-27880.

Chi, H. (2012). Regulation and function of mTOR signalling in T cell fate decisions. Nat Rev Immunol *12*, 325-338.

Dang, E.V., Barbi, J., Yang, H.Y., Jinasena, D., Yu, H., Zheng, Y., Bordman, Z., Fu, J., Kim, Y., Yen, H.R., et al. (2011). Control of T(H)17/T(reg) balance by hypoxia-inducible factor 1. Cell *146*, 772-784.

Daniele, T., Hurbain, I., Vago, R., Casari, G., Raposo, G., Tacchetti, C., and Schiaffino, M.V. (2014). Mitochondria and melanosomes establish physical contacts modulated by Mfn2 and involved in organelle biogenesis. Curr Biol *24*, 393-403.

de Brito, O.M., and Scorrano, L. (2008). Mitofusin 2 tethers endoplasmic reticulum to mitochondria. Nature *456*, 605-610.

Delgoffe, G.M., Pollizzi, K.N., Waickman, A.T., Heikamp, E., Meyers, D.J., Horton, M.R., Xiao, B., Worley, P.F., and Powell, J.D. (2011). The kinase mTOR regulates the differentiation of helper T cells through the selective activation of signaling by mTORC1 and mTORC2. Nat Immunol *12*, 295-303.

Detmer, S.A., and Chan, D.C. (2007). Functions and dysfunctions of mitochondrial dynamics. Nat Rev Mol Cell Biol *8*, 870-879.

Dustin, M.L., Olszowy, M.W., Holdorf, A.D., Li, J., Bromley, S., Desai, N., Widder, P., Rosenberger, F., van der Merwe, P.A., Allen, P.M., et al. (1998). A novel adaptor protein orchestrates receptor patterning and cytoskeletal polarity in T-cell contacts. Cell *94*, 667-677.

Ekstrand, M.I., Falkenberg, M., Rantanen, A., Park, C.B., Gaspari, M., Hultenby, K., Rustin, P., Gustafsson, C.M., and Larsson, N.G. (2004). Mitochondrial transcription factor A regulates mtDNA copy number in mammals. Hum Mol Genet *13*, 935-944.

Ekstrand, M.I., Terzioglu, M., Galter, D., Zhu, S., Hofstetter, C., Lindqvist, E., Thams, S., Bergstrand, A., Hansson, F.S., Trifunovic, A., et al. (2007). Progressive parkinsonism in mice with respiratory-chain-deficient dopamine neurons. Proc Natl Acad Sci U S A *104*, 1325-1330.

Elbaz-Alon, Y., Rosenfeld-Gur, E., Shinder, V., Futerman, A.H., Geiger, T., and Schuldiner, M. (2014). A Dynamic Interface between Vacuoles and Mitochondria in Yeast. Dev Cell *30*, 95-102.

Feng, J., Bussiere, F., and Hekimi, S. (2001). Mitochondrial electron transport is a key determinant of life span in Caenorhabditis elegans. Dev Cell *1*, 633-644.

Fraldi, A., Annunziata, F., Lombardi, A., Kaiser, H.J., Medina, D.L., Spampanato, C., Fedele, A.O., Polishchuk, R., Sorrentino, N.C., Simons, K., et al. (2010). Lysosomal fusion and SNARE function are impaired by cholesterol accumulation in lysosomal storage disorders. EMBO J *29*, 3607-3620.

Frezza, C., Cipolat, S., Martins de Brito, O., Micaroni, M., Beznoussenko, G.V., Rudka, T., Bartoli, D., Polishuck, R.S., Danial, N.N., De Strooper, B., et al. (2006). OPA1 controls apoptotic cristae remodeling independently from mitochondrial fusion. Cell *126*, 177-189.

Friedman, J.R., Lackner, L.L., West, M., DiBenedetto, J.R., Nunnari, J., and Voeltz, G.K. (2011). ER tubules mark sites of mitochondrial division. Science *334*, 358-362.

Friedman, J.R., and Nunnari, J. (2014). Mitochondrial form and function. Nature *505*, 335-343.

Futerman, A.H., and van Meer, G. (2004). The cell biology of lysosomal storage disorders. Nat Rev Mol Cell Biol *5*, 554-565.

Gabande-Rodriguez, E., Boya, P., Labrador, V., Dotti, C.G., and Ledesma, M.D. (2014). High sphingomyelin levels induce lysosomal damage and autophagy dysfunction in Niemann Pick disease type A. Cell Death Differ *21*, 864-875.

Galluzzi, L., Kepp, O., Trojel-Hansen, C., and Kroemer, G. (2012). Mitochondrial control of cellular life, stress, and death. Circ Res *111*, 1198-1207.

Gao, P., Tchernyshyov, I., Chang, T.C., Lee, Y.S., Kita, K., Ochi, T., Zeller, K.I., De Marzo, A.M., Van Eyk, J.E., Mendell, J.T., et al. (2009). c-Myc suppression of miR-23a/b enhances mitochondrial glutaminase expression and glutamine metabolism. Nature *458*, 762-765.

Gerriets, V.A., Kishton, R.J., Nichols, A.G., Macintyre, A.N., Inoue, M., Ilkayeva, O., Winter, P.S., Liu, X., Priyadharshini, B., Slawinska, M.E., et al. (2015). Metabolic programming and PDHK1 control CD4+ T cell subsets and inflammation. J Clin Invest *125*, 194-207.

Gill, T., and Levine, A.D. (2013). Mitochondria-derived hydrogen peroxide selectively enhances T cell receptor-initiated signal transduction. J Biol Chem *288*, 26246-26255.

Gomes, A.P., Price, N.L., Ling, A.J., Moslehi, J.J., Montgomery, M.K., Rajman, L., White, J.P., Teodoro, J.S., Wrann, C.D., Hubbard, B.P., et al. (2013). Declining NAD(+) induces a pseudohypoxic state disrupting nuclear-mitochondrial communication during aging. Cell *155*, 1624-1638.

Gordan, J.D., Thompson, C.B., and Simon, M.C. (2007). HIF and c-Myc: sibling rivals for control of cancer cell metabolism and proliferation. Cancer Cell *12*, 108-113.

Grakoui, A., Bromley, S.K., Sumen, C., Davis, M.M., Shaw, A.S., Allen, P.M., and Dustin, M.L. (1999). The immunological synapse: a molecular machine controlling T cell activation. Science *285*, 221-227.

Groppelli, E., Starling, S., and Jolly, C. (2015). Contact-induced mitochondrial polarization supports HIV-1 virological synapse formation. J Virol *89*, 14-24.

Guo, C., Hildick, K.L., Luo, J., Dearden, L., Wilkinson, K.A., and Henley, J.M. (2013). SENP3-mediated deSUMOylation of dynamin-related protein 1 promotes cell death following ischaemia. EMBO J *32*, 1514-1528.

Hansson, A., Hance, N., Dufour, E., Rantanen, A., Hultenby, K., Clayton, D.A., Wibom, R., and Larsson, N.G. (2004). A switch in metabolism precedes increased mitochondrial biogenesis in respiratory chain-deficient mouse hearts. Proc Natl Acad Sci U S A *101*, 3136-3141.

Harder, Z., Zunino, R., and McBride, H. (2004). Sumo1 conjugates mitochondrial substrates and participates in mitochondrial fission. Curr Biol *14*, 340-345.

Hardie, D.G., Ross, F.A., and Hawley, S.A. (2012). AMPK: a nutrient and energy sensor that maintains energy homeostasis. Nat Rev Mol Cell Biol *13*, 251-262.

Hasan, M., Koch, J., Rakheja, D., Pattnaik, A.K., Brugarolas, J., Dozmorov, I., Levine, B., Wakeland, E.K., Lee-Kirsch, M.A., and Yan, N. (2013). Trex1 regulates lysosomal biogenesis and interferon-independent activation of antiviral genes. Nat Immunol *14*, 61-71.

Hollenbeck, P.J. (2005). Mitochondria and neurotransmission: evacuating the synapse. Neuron *47*, 331-333.

Honscher, C., Mari, M., Auffarth, K., Bohnert, M., Griffith, J., Geerts, W., van der Laan, M., Cabrera, M., Reggiori, F., and Ungermann, C. (2014). Cellular Metabolism Regulates Contact Sites between Vacuoles and Mitochondria. Dev Cell *30*, 86-94.

Hoppins, S. (2014). The regulation of mitochondrial dynamics. Curr Opin Cell Biol *29*, 46-52.

Hornung, V., Bauernfeind, F., Halle, A., Samstad, E.O., Kono, H., Rock, K.L., Fitzgerald, K.A., and Latz, E. (2008). Silica crystals and aluminum salts activate the NALP3 inflammasome through phagosomal destabilization. Nat Immunol *9*, 847-856.

Houtkooper, R.H., Mouchiroud, L., Ryu, D., Moullan, N., Katsyuba, E., Knott, G., Williams, R.W., and Auwerx, J. (2013). Mitonuclear protein imbalance as a conserved longevity mechanism. Nature *497*, 451-457.

Huang, S.C., Everts, B., Ivanova, Y., O'Sullivan, D., Nascimento, M., Smith, A.M., Beatty, W., Love-Gregory, L., Lam, W.Y., O'Neill, C.M., et al. (2014). Cell-intrinsic lysosomal lipolysis is essential for alternative activation of macrophages. Nat Immunol *15*, 846-855.

Huber, S., Gagliani, N., Esplugues, E., O'Connor, W., Jr., Huber, F.J., Chaudhry, A., Kamanaka, M., Kobayashi, Y., Booth, C.J., Rudensky, A.Y., et al. (2011). Th17 cells express interleukin-10 receptor and are controlled by Foxp3(-) and Foxp3+ regulatory CD4+ T cells in an interleukin-10-dependent manner. Immunity *34*, 554-565.

Huse, M., Lillemeier, B.F., Kuhns, M.S., Chen, D.S., and Davis, M.M. (2006). T cells use two directionally distinct pathways for cytokine secretion. Nat Immunol *7*, 247-255.

Huttenlocher, A., Sandborg, R.R., and Horwitz, A.F. (1995). Adhesion in cell migration. Curr Opin Cell Biol *7*, 697-706.

Ibiza, S., Victor, V.M., Bosca, I., Ortega, A., Urzainqui, A., O'Connor, J.E., Sanchez-Madrid, F., Esplugues, J.V., and Serrador, J.M. (2006). Endothelial nitric oxide synthase regulates T cell receptor signaling at the immunological synapse. Immunity *24*, 753-765.

Ilani, T., Vasiliver-Shamis, G., Vardhana, S., Bretscher, A., and Dustin, M.L. (2009). T cell antigen receptor signaling and immunological synapse stability require myosin IIA. Nat Immunol *10*, 531-539.

Ishihara, N., Fujita, Y., Oka, T., and Mihara, K. (2006). Regulation of mitochondrial morphology through proteolytic cleavage of OPA1. EMBO J *25*, 2966-2977.

Ishihara, N., Nomura, M., Jofuku, A., Kato, H., Suzuki, S.O., Masuda, K., Otera, H., Nakanishi, Y., Nonaka, I., Goto, Y., et al. (2009). Mitochondrial fission factor Drp1 is essential for embryonic development and synapse formation in mice. Nat Cell Biol *11*, 958-966.

Jolly, C., Welsch, S., Michor, S., and Sattentau, Q.J. (2011). The regulated secretory pathway in CD4(+) T cells contributes to human immunodeficiency virus type-1 cell-to-cell spread at the virological synapse. PLoS Pathog *7*, e1002226.

Joshi, R.P., and Koretzky, G.A. (2013). Diacylglycerol kinases: regulated controllers of T cell activation, function, and development. International journal of molecular sciences *14*, 6649-6673.

Junker, C., and Hoth, M. (2011). Immune synapses: mitochondrial morphology matters. EMBO J *30*, 1187-1189.

Kaminski, M.M., Sauer, S.W., Kaminski, M., Opp, S., Ruppert, T., Grigaravicius, P., Grudnik, P., Grone, H.J., Krammer, P.H., and Gulow, K. (2012). T cell activation is driven by an ADP-dependent glucokinase linking enhanced glycolysis with mitochondrial reactive oxygen species generation. Cell Rep *2*, 1300-1315.

Kanfer, G., Courtheoux, T., Peterka, M., Meier, S., Soste, M., Melnik, A., Reis, K., Aspenstrom, P., Peter, M., Picotti, P., et al. (2015). Mitotic redistribution of the mitochondrial network by Miro and Cenp-F. Nat Commun *6*, 8015.

Karamanlidis, G., Lee, C.F., Garcia-Menendez, L., Kolwicz, S.C., Jr., Suthammarak, W., Gong, G., Sedensky, M.M., Morgan, P.G., Wang, W., and Tian, R. (2013). Mitochondrial complex I deficiency increases protein acetylation and accelerates heart failure. Cell Metab *18*, 239-250.

Kasahara, A., and Scorrano, L. (2014). Mitochondria: from cell death executioners to regulators of cell differentiation. Trends Cell Biol *24*, 761-770.

Katajisto, P., Dohla, J., Chaffer, C.L., Pentinmikko, N., Marjanovic, N., Iqbal, S., Zoncu, R., Chen, W., Weinberg, R.A., and Sabatini, D.M. (2015). Stem cells. Asymmetric apportioning of aged mitochondria between daughter cells is required for stemness. Science *348*, 340-343.

Klecker, T., Bockler, S., and Westermann, B. (2014). Making connections: interorganelle contacts orchestrate mitochondrial behavior. Trends Cell Biol *24*, 537-545.

Korn, T., Bettelli, E., Oukka, M., and Kuchroo, V.K. (2009). IL-17 and Th17 Cells. Annu Rev Immunol *27*, 485-517.

Kummerow, C., Junker, C., Kruse, K., Rieger, H., Quintana, A., and Hoth, M. (2009). The immunological synapse controls local and global calcium signals in T lymphocytes. Immunol Rev *231*, 132-147.

Kupfer, A., Swain, S.L., Janeway, C.A., Jr., and Singer, S.J. (1986). The specific direct interaction of helper T cells and antigen-presenting B cells. Proc Natl Acad Sci U S A *83*, 6080-6083.

Lapuente-Brun, E., Moreno-Loshuertos, R., Acin-Perez, R., Latorre-Pellicer, A., Colas, C., Balsa, E., Perales-Clemente, E., Quiros, P.M., Calvo, E., Rodriguez-Hernandez, M.A., et al. (2013). Supercomplex assembly determines electron flux in the mitochondrial electron transport chain. Science *340*, 1567-1570.

Larsson, N.G., Wang, J., Wilhelmsson, H., Oldfors, A., Rustin, P., Lewandoski, M., Barsh, G.S., and Clayton, D.A. (1998). Mitochondrial transcription factor A is necessary for mtDNA maintenance and embryogenesis in mice. Nat Genet *18*, 231-236.

Ledderose, C., Bao, Y., Lidicky, M., Zipperle, J., Li, L., Strasser, K., Shapiro, N.I., and Junger, W.G. (2014). Mitochondria are gate-keepers of T cell function by producing the ATP that drives purinergic signaling. J Biol Chem *289*, 25936-25945.

Legros, F., Malka, F., Frachon, P., Lombes, A., and Rojo, M. (2004). Organization and dynamics of human mitochondrial DNA. J Cell Sci *117*, 2653-2662.

Li, F., Wang, Y., Zeller, K.I., Potter, J.J., Wonsey, D.R., O'Donnell, K.A., Kim, J.W., Yustein, J.T., Lee, L.A., and Dang, C.V. (2005). Myc stimulates nuclearly encoded mitochondrial genes and mitochondrial biogenesis. Mol Cell Biol *25*, 6225-6234.

Li, H., Alavian, K.N., Lazrove, E., Mehta, N., Jones, A., Zhang, P., Licznerski, P., Graham, M., Uo, T., Guo, J., et al. (2013). A Bcl-xL-Drp1 complex regulates synaptic vesicle membrane dynamics during endocytosis. Nat Cell Biol *15*, 773-785.

Li, H., Chen, Y., Jones, A.F., Sanger, R.H., Collis, L.P., Flannery, R., McNay, E.C., Yu, T., Schwarzenbacher, R., Bossy, B., et al. (2008). Bcl-xL induces Drp1-dependent synapse formation in cultured hippocampal neurons. Proc Natl Acad Sci U S A *105*, 2169-2174.

Li, Z., Okamoto, K., Hayashi, Y., and Sheng, M. (2004). The importance of dendritic mitochondria in the morphogenesis and plasticity of spines and synapses. Cell *119*, 873-887.

Liu, X., Weaver, D., Shirihai, O., and Hajnoczky, G. (2009). Mitochondrial 'kiss-and-run': interplay between mitochondrial motility and fusion-fission dynamics. EMBO J *28*, 3074-3089.

Lopez-Otin, C., Blasco, M.A., Partridge, L., Serrano, M., and Kroemer, G. (2013). The hallmarks of aging. Cell *153*, 1194-1217.

Lu, W., Zhang, Y., McDonald, D.O., Jing, H., Carroll, B., Robertson, N., Zhang, Q., Griffin, H., Sanderson, S., Lakey, J.H., et al. (2014). Dual proteolytic pathways govern glycolysis and immune competence. Cell *159*, 1578-1590.

Lloyd-Evans, E., Morgan, A.J., He, X., Smith, D.A., Elliot-Smith, E., Sillence, D.J., Churchill, G.C., Schuchman, E.H., Galione, A., and Platt, F.M. (2008). Niemann-Pick disease type C1 is a sphingosine storage disease that causes deregulation of lysosomal calcium. Nat Med *14*, 1247-1255.

MacAskill, A.F., and Kittler, J.T. (2010). Control of mitochondrial transport and localization in neurons. Trends Cell Biol *20*, 102-112.

Macaskill, A.F., Rinholm, J.E., Twelvetrees, A.E., Arancibia-Carcamo, I.L., Muir, J., Fransson, A., Aspenstrom, P., Attwell, D., and Kittler, J.T. (2009). Miro1 is a calcium sensor for glutamate receptor-dependent localization of mitochondria at synapses. Neuron *61*, 541-555.

MacIver, N.J., Blagih, J., Saucillo, D.C., Tonelli, L., Griss, T., Rathmell, J.C., and Jones, R.G. (2011). The liver kinase B1 is a central regulator of T cell development, activation, and metabolism. J Immunol *187*, 4187-4198.

Malissen, B. (2003). Immunology. Switching off TCR signaling. Science *302*, 1162-1163.

Martin-Cofreces, N.B., Baixauli, F., and Sanchez-Madrid, F. (2014). Immune synapse: conductor of orchestrated organelle movement. Trends Cell Biol *24*, 61-72.

Martin-Cofreces, N.B., Robles-Valero, J., Cabrero, J.R., Mittelbrunn, M., Gordon-Alonso, M., Sung, C.H., Alarcon, B., Vazquez, J., and Sanchez-Madrid, F. (2008). MTOC translocation modulates IS formation and controls sustained T cell signaling. J Cell Biol *182*, 951-962.

Martinez-Martin, N., Fernandez-Arenas, E., Cemerski, S., Delgado, P., Turner, M., Heuser, J., Irvine, D.J., Huang, B., Bustelo, X.R., Shaw, A., et al. (2011). T cell receptor internalization from the immunological synapse is mediated by TC21 and RhoG GTPase-dependent phagocytosis. Immunity *35*, 208-222.

Matsuo, H., Chevallier, J., Mayran, N., Le Blanc, I., Ferguson, C., Faure, J., Blanc, N.S., Matile, S., Dubochet, J., Sadoul, R., et al. (2004). Role of LBPA and Alix in multivesicular liposome formation and endosome organization. Science *303*, 531-534.

McBride, H.M., Neuspiel, M., and Wasiak, S. (2006). Mitochondria: more than just a powerhouse. Curr Biol *16*, R551-560.

Medina, D.L., Di Paola, S., Peluso, I., Armani, A., De Stefani, D., Venditti, R., Montefusco, S., Scotto-Rosato, A., Prezioso, C., Forrester, A., et al. (2015). Lysosomal calcium signalling regulates autophagy through calcineurin and TFEB. Nat Cell Biol *17*, 288-299.

Michalek, R.D., Gerriets, V.A., Jacobs, S.R., Macintyre, A.N., MacIver, N.J., Mason, E.F., Sullivan, S.A., Nichols, A.G., and Rathmell, J.C. (2011a). Cutting edge: distinct glycolytic and lipid oxidative metabolic programs are essential for effector and regulatory CD4+ T cell subsets. J Immunol *186*, 3299-3303.

Michalek, R.D., Gerriets, V.A., Nichols, A.G., Inoue, M., Kazmin, D., Chang, C.Y., Dwyer, M.A., Nelson, E.R., Pollizzi, K.N., Ilkayeva, O., et al. (2011b). Estrogen-related receptor-alpha is a metabolic regulator of effector T-cell activation and differentiation. Proc Natl Acad Sci U S A *108*, 18348-18353.

Mindell, J.A. (2012). Lysosomal acidification mechanisms. Annual review of physiology *74*, 69-86.

Mishra, P., and Chan, D.C. (2014). Mitochondrial dynamics and inheritance during cell division, development and disease. Nat Rev Mol Cell Biol *15*, 634-646.

Misko, A., Jiang, S., Wegorzewska, I., Milbrandt, J., and Baloh, R.H. (2010). Mitofusin 2 is necessary for transport of axonal mitochondria and interacts with the Miro/Milton complex. J Neurosci *30*, 4232-4240.

Mittelbrunn, M., Gutierrez-Vazquez, C., Villarroya-Beltri, C., Gonzalez, S., Sanchez-Cabo, F., Gonzalez, M.A., Bernad, A., and Sanchez-Madrid, F. (2011). Unidirectional transfer of microRNA-loaded exosomes from T cells to antigen-presenting cells. Nat Commun *2*, 282.

Mittelbrunn, M., Molina, A., Escribese, M.M., Yanez-Mo, M., Escudero, E., Ursa, A., Tejedor, R., Mampaso, F., and Sanchez-Madrid, F. (2004). VLA-4 integrin concentrates at the peripheral supramolecular activation complex of the immune synapse and drives T helper 1 responses. Proc Natl Acad Sci U S A *101*, 11058-11063.

Mittelbrunn, M., and Sanchez-Madrid, F. (2012). Intercellular communication: diverse structures for exchange of genetic information. Nat Rev Mol Cell Biol *13*, 328-335.

Mittelbrunn, M., Vicente-Manzanares, M., and Sanchez-Madrid, F. (2015). Organizing polarized delivery of exosomes at synapses. Traffic *16*, 327-337.

Monks, C.R., Freiberg, B.A., Kupfer, H., Sciaky, N., and Kupfer, A. (1998). Three-dimensional segregation of supramolecular activation clusters in T cells. Nature *395*, 82-86.

Morlino, G., Barreiro, O., Baixauli, F., Robles-Valero, J., Gonzalez-Granado, J.M., Villa-Bellosta, R., Cuenca, J., Sanchez-Sorzano, C.O., Veiga, E., Martin-Cofreces, N.B., et al. (2014). Miro-1 links mitochondria and microtubule Dynein motors to control lymphocyte migration and polarity. Mol Cell Biol *34*, 1412-1426.

Mouchiroud, L., Houtkooper, R.H., and Auwerx, J. (2013). NAD(+) metabolism: a therapeutic target for age-related metabolic disease. Crit Rev Biochem Mol Biol *48*, 397-408.

Murphy, M.P. (2009). How mitochondria produce reactive oxygen species. Biochem J *417*, 1-13.

Naon, D., and Scorrano, L. (2014). At the right distance: ER-mitochondria juxtaposition in cell life and death. Biochim Biophys Acta *1843*, 2184-2194.

Neuspiel, M., Schauss, A.C., Braschi, E., Zunino, R., Rippstein, P., Rachubinski, R.A., Andrade-Navarro, M.A., and McBride, H.M. (2008). Cargo-selected transport from the mitochondria to peroxisomes is mediated by vesicular carriers. Curr Biol *18*, 102-108.

Ngo, H.B., Kaiser, J.T., and Chan, D.C. (2011). The mitochondrial transcription and packaging factor Tfam imposes a U-turn on mitochondrial DNA. Nat Struct Mol Biol *18*, 1290-1296.

Nolte-'t Hoen, E.N., Buermans, H.P., Waasdorp, M., Stoorvogel, W., Wauben, M.H., and t Hoen, P.A. (2012). Deep sequencing of RNA from immune cell-derived vesicles uncovers the selective incorporation of small non-coding RNA biotypes with potential regulatory functions. Nucleic Acids Res *40*, 9272-9285.

Okoye, I.S., Coomes, S.M., Pelly, V.S., Czieso, S., Papayannopoulos, V., Tolmachova, T., Seabra, M.C., and Wilson, M.S. (2014). MicroRNA-Containing T-Regulatory-Cell-Derived Exosomes Suppress Pathogenic T Helper 1 Cells. Immunity *41*, 89-103.

Osellame, L.D., Rahim, A.A., Hargreaves, I.P., Gegg, M.E., Richard-Londt, A., Brandner, S., Waddington, S.N., Schapira, A.H., and Duchen, M.R. (2013). Mitochondria and quality control defects in a mouse model of Gaucher disease--links to Parkinson's disease. Cell Metab *17*, 941-953.

Osman, C., Voelker, D.R., and Langer, T. (2011). Making heads or tails of phospholipids in mitochondria. J Cell Biol *192*, 7-16.

Pandey, M.K., Rani, R., Zhang, W., Setchell, K., and Grabowski, G.A. (2012). Immunological cell type characterization and Th1-Th17 cytokine production in a mouse model of Gaucher disease. Mol Genet Metab *106*, 310-322.

Pearce, E.L., Poffenberger, M.C., Chang, C.H., and Jones, R.G. (2013). Fueling immunity: insights into metabolism and lymphocyte function. Science *342*, 1242454.

Pekkurnaz, G., Trinidad, J.C., Wang, X., Kong, D., and Schwarz, T.L. (2014). Glucose regulates mitochondrial motility via Milton modification by O-GlcNAc transferase. Cell *158*, 54-68.

Peters, A., Lee, Y., and Kuchroo, V.K. (2011). The many faces of Th17 cells. Curr Opin Immunol *23*, 702-706.

Pilling, A.D., Horiuchi, D., Lively, C.M., and Saxton, W.M. (2006). Kinesin-1 and Dynein are the primary motors for fast transport of mitochondria in Drosophila motor axons. Mol Biol Cell *17*, 2057-2068.

Piragyte, I., and Jun, C.D. (2012). Actin engine in immunological synapse. Immune network *12*, 71-83.

Pollizzi, K.N., and Powell, J.D. (2014). Integrating canonical and metabolic signalling programmes in the regulation of T cell responses. Nat Rev Immunol *14*, 435-446.

Quintana, A., Pasche, M., Junker, C., Al-Ansary, D., Rieger, H., Kummerow, C., Nunez, L., Villalobos, C., Meraner, P., Becherer, U., et al. (2011). Calcium microdomains at the immunological synapse: how ORAI channels, mitochondria and calcium pumps generate local calcium signals for efficient T-cell activation. EMBO J *30*, 3895-3912.

Quintana, A., Schwindling, C., Wenning, A.S., Becherer, U., Rettig, J., Schwarz, E.C., and Hoth, M. (2007). T cell activation requires mitochondrial translocation to the immunological synapse. Proc Natl Acad Sci U S A *104*, 14418-14423.

Qureshi, O.S., Zheng, Y., Nakamura, K., Attridge, K., Manzotti, C., Schmidt, E.M., Baker, J., Jeffery, L.E., Kaur, S., Briggs, Z., et al. (2011). Trans-endocytosis of CD80 and CD86: a molecular basis for the cell-extrinsic function of CTLA-4. Science *332*, 600-603.

Raposo, G., and Stoorvogel, W. (2013). Extracellular vesicles: exosomes, microvesicles, and friends. J Cell Biol *200*, 373-383.

Ritter, A.T., Asano, Y., Stinchcombe, J.C., Dieckmann, N.M., Chen, B.C., Gawden-Bone, C., van Engelenburg, S., Legant, W., Gao, L., Davidson, M.W., et al. (2015). Actin depletion initiates events leading to granule secretion at the immunological synapse. Immunity *42*, 864-876.

Rizzuto, R., De Stefani, D., Raffaello, A., and Mammucari, C. (2012). Mitochondria as sensors and regulators of calcium signalling. Nat Rev Mol Cell Biol *13*, 566-578.

Robbins, P.D., and Morelli, A.E. (2014). Regulation of immune responses by extracellular vesicles. Nat Rev Immunol *14*, 195-208.

Rowland, A.A., and Voeltz, G.K. (2012). Endoplasmic reticulum-mitochondria contacts: function of the junction. Nat Rev Mol Cell Biol *13*, 607-625.

Rubio-Cosials, A., Sidow, J.F., Jimenez-Menendez, N., Fernandez-Millan, P., Montoya, J., Jacobs, H.T., Coll, M., Bernado, P., and Sola, M. (2011). Human mitochondrial transcription

factor A induces a U-turn structure in the light strand promoter. Nat Struct Mol Biol *18*, 1281-1289.

Saftig, P., and Klumperman, J. (2009). Lysosome biogenesis and lysosomal membrane proteins: trafficking meets function. Nat Rev Mol Cell Biol *10*, 623-635.

Santel, A., and Fuller, M.T. (2001). Control of mitochondrial morphology by a human mitofusin. J Cell Sci *114*, 867-874.

Santidrian, A.F., Matsuno-Yagi, A., Ritland, M., Seo, B.B., LeBoeuf, S.E., Gay, L.J., Yagi, T., and Felding-Habermann, B. (2013). Mitochondrial complex I activity and NAD+/NADH balance regulate breast cancer progression. J Clin Invest *123*, 1068-1081.

Sardiello, M., Palmieri, M., di Ronza, A., Medina, D.L., Valenza, M., Gennarino, V.A., Di Malta, C., Donaudy, F., Embrione, V., Polishchuk, R.S., et al. (2009). A gene network regulating lysosomal biogenesis and function. Science *325*, 473-477.

Satoh, M., and Kuroiwa, T. (1991). Organization of multiple nucleoids and DNA molecules in mitochondria of a human cell. Exp Cell Res *196*, 137-140.

Schulze, H., and Sandhoff, K. (2011). Lysosomal lipid storage diseases. Cold Spring Harb Perspect Biol *3*.

Schwindling, C., Quintana, A., Krause, E., and Hoth, M. (2010). Mitochondria positioning controls local calcium influx in T cells. J Immunol *184*, 184-190.

Sena, L.A., Li, S., Jairaman, A., Prakriya, M., Ezponda, T., Hildeman, D.A., Wang, C.R., Schumacker, P.T., Licht, J.D., Perlman, H., et al. (2013). Mitochondria are required for antigen-specific T cell activation through reactive oxygen species signaling. Immunity *38*, 225-236.

Settembre, C., and Ballabio, A. (2011). TFEB regulates autophagy: an integrated coordination of cellular degradation and recycling processes. Autophagy *7*, 1379-1381.

Settembre, C., De Cegli, R., Mansueto, G., Saha, P.K., Vetrini, F., Visvikis, O., Huynh, T., Carissimo, A., Palmer, D., Klisch, T.J., et al. (2013a). TFEB controls cellular lipid metabolism through a starvation-induced autoregulatory loop. Nat Cell Biol *15*, 647-658.

Settembre, C., Fraldi, A., Medina, D.L., and Ballabio, A. (2013b). Signals from the lysosome: a control centre for cellular clearance and energy metabolism. Nat Rev Mol Cell Biol *14*, 283-296.

Shi, L.Z., Wang, R., Huang, G., Vogel, P., Neale, G., Green, D.R., and Chi, H. (2011). HIF1alpha-dependent glycolytic pathway orchestrates a metabolic checkpoint for the differentiation of TH17 and Treg cells. J Exp Med *208*, 1367-1376.

Smirnova, E., Griparic, L., Shurland, D.L., and van der Bliek, A.M. (2001). Dynamin-related protein Drp1 is required for mitochondrial division in mammalian cells. Mol Biol Cell *12*, 2245-2256.

Solaini, G., Sgarbi, G., Lenaz, G., and Baracca, A. (2007). Evaluating mitochondrial membrane potential in cells. Biosci Rep *27*, 11-21.

Sugiura, A., McLelland, G.L., Fon, E.A., and McBride, H.M. (2014). A new pathway for mitochondrial quality control: mitochondrial-derived vesicles. EMBO J *33*, 2142-2156.

Taguchi, N., Ishihara, N., Jofuku, A., Oka, T., and Mihara, K. (2007). Mitotic phosphorylation of dynamin-related GTPase Drp1 participates in mitochondrial fission. J Biol Chem *282*, 11521-11529.

Tanaka, A., and Youle, R.J. (2008). A chemical inhibitor of DRP1 uncouples mitochondrial fission and apoptosis. Mol Cell *29*, 409-410.

Tannahill, G.M., Curtis, A.M., Adamik, J., Palsson-McDermott, E.M., McGettrick, A.F., Goel, G., Frezza, C., Bernard, N.J., Kelly, B., Foley, N.H., et al. (2013). Succinate is an inflammatory signal that induces IL-1beta through HIF-1alpha. Nature *496*, 238-242.

Taylor, R.W., and Turnbull, D.M. (2005). Mitochondrial DNA mutations in human disease. Nat Rev Genet *6*, 389-402.

Thery, C., Amigorena, S., Raposo, G., and Clayton, A. (2006). Isolation and characterization of exosomes from cell culture supernatants and biological fluids. Curr Protoc Cell Biol *Chapter 3*, Unit 3 22.

Trajkovic, K., Hsu, C., Chiantia, S., Rajendran, L., Wenzel, D., Wieland, F., Schwille, P., Brugger, B., and Simons, M. (2008). Ceramide triggers budding of exosome vesicles into multivesicular endosomes. Science *319*, 1244-1247.

Tubbs, E., Theurey, P., Vial, G., Bendridi, N., Bravard, A., Chauvin, M.A., Ji-Cao, J., Zoulim, F., Bartosch, B., Ovize, M., et al. (2014). Mitochondria-associated endoplasmic reticulum membrane (MAM) integrity is required for insulin signaling and is implicated in hepatic insulin resistance. Diabetes *63*, 3279-3294.

Twig, G., Elorza, A., Molina, A.J., Mohamed, H., Wikstrom, J.D., Walzer, G., Stiles, L., Haigh, S.E., Katz, S., Las, G., et al. (2008). Fission and selective fusion govern mitochondrial segregation and elimination by autophagy. EMBO J *27*, 433-446.

Valdor, R., Mocholi, E., Botbol, Y., Guerrero-Ros, I., Chandra, D., Koga, H., Gravekamp, C., Cuervo, A.M., and Macian, F. (2014). Chaperone-mediated autophagy regulates T cell responses through targeted degradation of negative regulators of T cell activation. Nat Immunol *15*, 1046-1054.

van der Kloet, F.M., Bobeldijk, I., Verheij, E.R., and Jellema, R.H. (2009). Analytical error reduction using single point calibration for accurate and precise metabolomic phenotyping. J Proteome Res *8*, 5132-5141.

van der Windt, G.J., Everts, B., Chang, C.H., Curtis, J.D., Freitas, T.C., Amiel, E., Pearce, E.J., and Pearce, E.L. (2012). Mitochondrial respiratory capacity is a critical regulator of CD8+ T cell memory development. Immunity *36*, 68-78.

van der Windt, G.J., and Pearce, E.L. (2012). Metabolic switching and fuel choice during T-cell differentiation and memory development. Immunol Rev *249*, 27-42.

Varadi, A., Johnson-Cadwell, L.I., Cirulli, V., Yoon, Y., Allan, V.J., and Rutter, G.A. (2004). Cytoplasmic dynein regulates the subcellular distribution of mitochondria by controlling the recruitment of the fission factor dynamin-related protein-1. J Cell Sci *117*, 4389-4400.

Vardhana, S., Choudhuri, K., Varma, R., and Dustin, M.L. (2010). Essential role of ubiquitin and TSG101 protein in formation and function of the central supramolecular activation cluster. Immunity *32*, 531-540.

Varma, R., Campi, G., Yokosuka, T., Saito, T., and Dustin, M.L. (2006). T cell receptor-proximal signals are sustained in peripheral microclusters and terminated in the central supramolecular activation cluster. Immunity *25*, 117-127.

Vernochet, C., Mourier, A., Bezy, O., Macotela, Y., Boucher, J., Rardin, M.J., An, D., Lee, K.Y., Ilkayeva, O.R., Zingaretti, C.M., et al. (2012). Adipose-specific deletion of TFAM increases mitochondrial oxidation and protects mice against obesity and insulin resistance. Cell Metab *16*, 765-776.

Verstreken, P., Ly, C.V., Venken, K.J., Koh, T.W., Zhou, Y., and Bellen, H.J. (2005). Synaptic mitochondria are critical for mobilization of reserve pool vesicles at Drosophila neuromuscular junctions. Neuron *47*, 365-378.

Viader, A., Sasaki, Y., Kim, S., Strickland, A., Workman, C.S., Yang, K., Gross, R.W., and Milbrandt, J. (2013). Aberrant Schwann cell lipid metabolism linked to mitochondrial deficits leads to axon degeneration and neuropathy. Neuron *77*, 886-898.

Villarroya-Beltri, C., Baixauli, F., Gutierrez-Vazquez, C., Sanchez-Madrid, F., and Mittelbrunn, M. (2014). Sorting it out: Regulation of exosome loading. Semin Cancer Biol.

Villarroya-Beltri, C., Gutierrez-Vazquez, C., Sanchez-Cabo, F., Perez-Hernandez, D., Vazquez, J., Martin-Cofreces, N., Martinez-Herrera, D.J., Pascual-Montano, A., Mittelbrunn, M., and Sanchez-Madrid, F. (2013). Sumoylated hnRNPA2B1 controls the sorting of miRNAs into exosomes through binding to specific motifs. Nat Commun *4*, 2980.

Waickman, A.T., and Powell, J.D. (2012). mTOR, metabolism, and the regulation of T-cell differentiation and function. Immunol Rev *249*, 43-58.

Wakabayashi, J., Zhang, Z., Wakabayashi, N., Tamura, Y., Fukaya, M., Kensler, T.W., Iijima, M., and Sesaki, H. (2009). The dynamin-related GTPase Drp1 is required for embryonic and brain development in mice. J Cell Biol *186*, 805-816.

Wang, J., Wilhelmsson, H., Graff, C., Li, H., Oldfors, A., Rustin, P., Bruning, J.C., Kahn, C.R., Clayton, D.A., Barsh, G.S., et al. (1999). Dilated cardiomyopathy and atrioventricular conduction blocks induced by heart-specific inactivation of mitochondrial DNA gene expression. Nat Genet *21*, 133-137.

Wang, R., Dillon, C.P., Shi, L.Z., Milasta, S., Carter, R., Finkelstein, D., McCormick, L.L., Fitzgerald, P., Chi, H., Munger, J., et al. (2011). The transcription factor Myc controls metabolic reprogramming upon T lymphocyte activation. Immunity *35*, 871-882.

Wang, Y., Chen, T., Han, C., He, D., Liu, H., An, H., Cai, Z., and Cao, X. (2007). Lysosome-associated small Rab GTPase Rab7b negatively regulates TLR4 signaling in macrophages by promoting lysosomal degradation of TLR4. Blood *110*, 962-971.

Weinberg, S.E., Sena, L.A., and Chandel, N.S. (2015). Mitochondria in the regulation of innate and adaptive immunity. Immunity *42*, 406-417.

Westermann, B. (2010). Mitochondrial fusion and fission in cell life and death. Nat Rev Mol Cell Biol *11*, 872-884.

Wu, F., Xu, H.D., Guan, J.J., Hou, Y.S., Gu, J.H., Zhen, X.C., and Qin, Z.H. (2015). Rotenone impairs autophagic flux and lysosomal functions in Parkinson's disease. Neuroscience *284*, 900-911.

Wulfing, C., and Davis, M.M. (1998). A receptor/cytoskeletal movement triggered by costimulation during T cell activation. Science *282*, 2266-2269.

Yanez-Mo, M., Siljander, P.R., Andreu, Z., Zavec, A.B., Borras, F.E., Buzas, E.I., Buzas, K., Casal, E., Cappello, F., Carvalho, J., et al. (2015). Biological properties of extracellular vesicles and their physiological functions. J Extracell Vesicles *4*, 27066.

Yao, M., Liu, X., Li, D., Chen, T., Cai, Z., and Cao, X. (2009). Late endosome/lysosome-localized Rab7b suppresses TLR9-initiated proinflammatory cytokine and type I IFN production in macrophages. J Immunol *183*, 1751-1758.

Yi, J.S., Holbrook, B.C., Michalek, R.D., Laniewski, N.G., and Grayson, J.M. (2006). Electron transport complex I is required for CD8+ T cell function. J Immunol *177*, 852-862.

Zeng, H., Yang, K., Cloer, C., Neale, G., Vogel, P., and Chi, H. (2013). mTORC1 couples immune signals and metabolic programming to establish T(reg)-cell function. Nature *499*, 485-490.

Zuchner, S., De Jonghe, P., Jordanova, A., Claeys, K.G., Guergueltcheva, V., Cherninkova, S., Hamilton, S.R., Van Stavern, G., Krajewski, K.M., Stajich, J., et al. (2006). Axonal neuropathy with optic atrophy is caused by mutations in mitofusin 2. Ann Neurol *59*, 276-281.

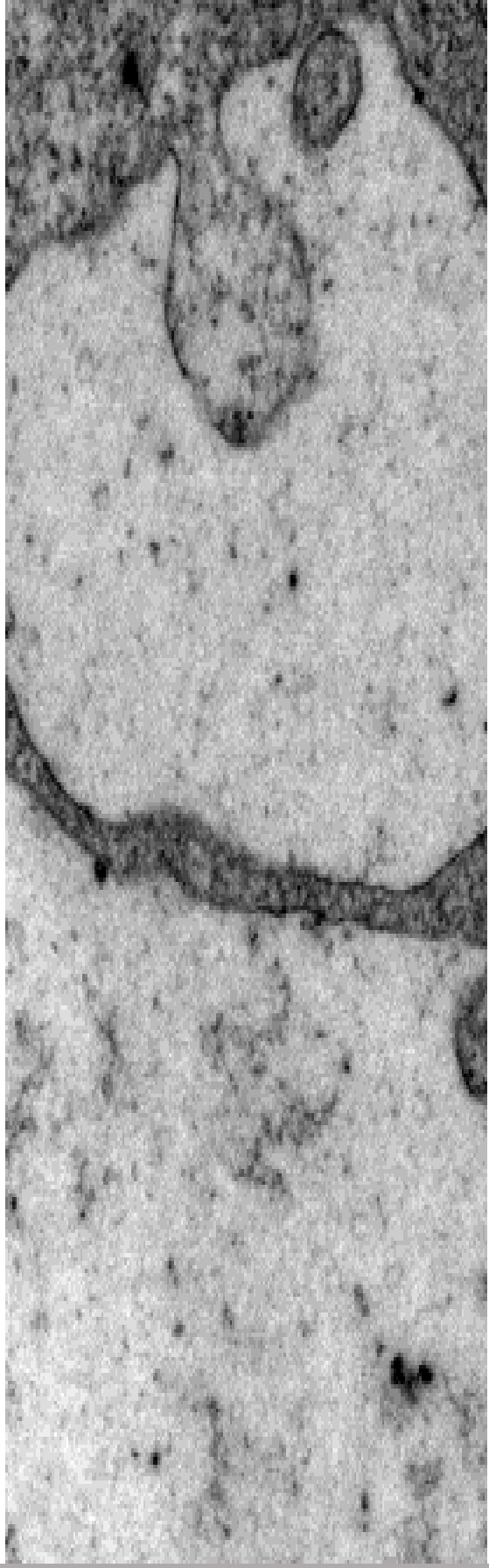

Annexes

8.1 Publications related to this Thesis work:

- **Baixauli F.,** Acin-Perez, R., Villarroya-Beltri, C., Mazzeo, C., Nunez-Andrade, N., Gabande-Rodriguez, E., Ledesma, M.D., Blazquez, A., Martin, M.A., Falcon-Perez, J.M., Redondo, J. M. Enriquez, J. A. and Mittelbrunn, M. Mitochondrial Respiration Controls Lysosomal Function during Inflammatory T Cell Responses. *Cell Metab 2015, Sep 1;22(3):485-98.*

- **Baixauli F**, López-Otín C and Mittelbrunn M. Exosomes and autophagy: coordinated mechanisms for the maintenance of cellular fitness. *Front Immunol. 2014 Aug 20;5:403.*

- Villarroya-Beltri C, **Baixauli F**, Gutiérrez-Vázquez C, Sánchez-Madrid F and Mittelbrunn M. Sorting it out: regulation of exosome loading. *Semin Cancer Biol. 2014 Oct;28:3-13.*

- Martín-Cófreces NB, **Baixauli F,** Sanchez-Madrid F. Immune synapse: conductor of orchestrated organelle movement. *Trends Cell Biol. 2014 Jan;24(1):61-72.*

- **Baixauli F**, Martín-Cófreces NB, Morlino G. Carrasco Y, Calabia-Linares C, Veiga E, Serrador JM, Sanchez-Madrid F. The mitochondrial fission factor dynamin-related protein 1 modulates T cell receptor signaling at the immune synapse. *EMBO J. 2011 Apr 6;30(7):1238-50.*

8.2 Publications unrelated to this Thesis work:

- Villarroya-Beltri C, **Baixauli F**, Mittelbrunn M, Fernández-delgado I, Torralba D, Moreno-Gonzalo O, Enrich C, Guerra S and Sánchez-Madrid F. ISGylation controls exosome secretion by promoting TSG101 lysosomal degradation (submitted).

- **Baixauli F**, Torralba D, Latorre A, Jaso AL, Jorge-Cerrudo I, Garaud J, Villarroya-Beltri C, Chichón FJ, Vázquez J, Enríquez JA, Mittelbrunn M and Sánchez-Madrid F. Exosome shuttle mtDNA that escape immune surveillance (in preparation).

- Mazzeo C, Cañas JA, Zafra MP, Rojas Marco A, Fernández-Nieto M, Sanz V, Mittelbrunn M, Izquierdo M, **Baixauli F**, Sastre J, Del Pozo V. Exosome secretion by eosinophils: A possible role in asthma pathogenesis. *J Allergy Clin Immunol. 2015 Jun;135(6):1603-13.*

- Acín-Pérez R, Carrascoso I, **Baixauli F**, Roche-Molina M, Latorre-Pellicer A, Fernández-Silva P, Mittelbrunn M, Sanchez-Madrid F, Pérez-Martos A, Lowell CA, Manfredi G, Enríquez JA. ROS-triggered Phosphorylation of Complex II by Fgr kinase regulates cellular adaptation to fuel use. *Cell Metab. 2014 Jun 3;19(6):1020-33.*
- Morlino G, Barreiro O, **Baixauli F**, Robles-Valero J, González-Granado JM, Villa-Bellosta R, Cuenca J, Sánchez-Sorzano CO, Veiga E, Martín-Cófreces NB, Sánchez-Madrid F. Miro-1 links mitochondria and microtubule dynein motors to control lymphocyte migration and polarity. *Mol Cell Biol. 2014 Apr;34(8):1412-26.*

- Martín-Cófreces NB, **Baixauli F**, López MJ, Gil D, Monjas A, Alarcón B, Sánchez-Madrid F. End-binding protein 1 controls signal propagation from the T cell receptor. *EMBO J. 2012 Nov 5;31(21):4140-52.*

8.3 Selected Articles